The Concept of "Slow Light" and Nature of Stokes Pulse Delay in Stimulated Brillouin Scattering

Nadezhda Yevgenyevna Kotova

A dissertation submitted for the degree of Doctor of Philosophy

Heriot-Watt University

School of Engineering and Physical Sciences

January 2012

Abstract

This work addresses the nature of the delay experienced by pulsed Stokes radiation when amplified by stimulated Brillouin scattering (SBS), topically referred to as “slow light in SBS”. The term “slow light” refers to the propagation of a light pulse in a medium in which the group velocity of the pulse is considerably lower than the phase velocity of light. A comprehensive review of the literature on “slow light” has revealed a range of inconsistencies in attributing experimentally observed pulse delays to the group velocity effect.

For the case of SBS the controversies are resolved through analytic solutions of the basic coupled SBS equations in both the frequency and time domains. The solutions provide the first mathematically rigorous and physically non-contradictory description of the temporal, spectral and energy characteristics of the Stokes radiation and of the induced acoustic wave in an SBS amplifier. Based on these solutions, a theoretical model of Stokes pulse propagation through a CW-pumped SBS medium is developed, the so called “inertial” model. The solutions are verified experimentally through study of the Stokes pulse dynamics in a set of fibers with different inhomogeneous SBS bandwidths and acoustic wave relaxation times. The results obtained confirm that the delay, shape and amplitude of the output Stokes pulse follow the predictions of the “inertial” model and that, contrary to popular opinion, the phenomenon of group delay, or “slow light”, is irrelevant to the observed delays.

to Svetlana Kotova

Acknowledgements

This thesis is a result of more than three years of work. This was a very challenging time for me and I would like to thank all the people who helped, assisted and encouraged me through this period.

First of all, I would like to express my sincerest gratitude to my supervisors, Dr. Valeri Kovalev and Prof. Robert Harrison. Their commitment to science is evident in the conscientious and rigorous way they carry out their work. I have gained immensely from their insights and I am very grateful for the patient and careful guidance they have given me throughout the course of this work.

I thank the Scottish Universities Physics Alliance for providing the funding for my studies. I thank Dr. Robert Mayer, Prof. Gerald Buller and Dr. Vsevolod Patlan for advice, guidance and useful discussions, Prof. Ajoy Kar for support and help as my administrative supervisor, Prof. Jonathan Knight and Itandehui Gris-Sanchez for providing photonic crystal fibre samples and Dr. Ludmila Iskhakova for elementary analysis of fibre samples. Separate thanks to all the staff in the Physics department of Heriot-Watt University for the warm and friendly environment they created, making the department such a great place to work. Thanks to my office mates Krystian Wlodarczyk and Alberto Campos Zatarain for everyday cheer and support. Finally, many thanks to my family and my friends, Natasha and Piotr, who are always there when I need them.

Table of Contents

ABSTRACT ii

ACKNOWLEDGEMENTS iv

TABLE OF CONTENTS v

LIST OF PUBLICATIONS viii

CHAPTER 1 INTRODUCTION 1

1.1 Background and motivation 1

1.2 Objective of this thesis 6

1.3 Thesis structure 6

CHAPTER 2 MECHANISMS OF PULSE DELAY IN AN OPTICAL MEDIUM. 8

CONCEPT OF "SLOW LIGHT" 8

2.1 Introduction 8

2.2 Propagation of a light pulse in a dispersive media. Phase and group velocity, group index, and pulse delay 9

2.3 Enhanced pulse delay near an optical resonance. "Slow and fast light" 15

2.4 "Slow light" via electromagnetically induced transparency (EIT) 16

2.4.1 Theory of "slow light" via EIT 16

2.4.2 Analysis of key experimental publications 18

2.5 Propagation of a light pulse through a nonlinearly absorbing medium 21

2.6 Conclusions 26

CHAPTER 3 STUDIES OF PULSE DELAYS VIA SBS 27

3.1 Introduction. 27

3.2 Theory of SBS-based "slow light". 28

3.2.1 Equations for Stimulated Brillouin Scattering for the case of constant pump 28
3.2.2 Theory of “SBS slow light” as presented in the literature 30
3.2.3 Weaknesses and shortcomings in the theoretical interpretation of pulse delay via SBS 33
3.3 Experimental realization of SBS-based pulse delay 35
3.4 Further studies: Methods of broadening the SBS gain bandwidth 37
3.4.1 Waveguide-induced broadening of the SBS spectrum 38
3.4.2 Simulation of the effect of waveguide-induced broadening of the SBS spectrum on the group index spectrum 40
3.4.3 Pump-induced broadening of the SBS spectrum 42
3.4.4 Use of discrete pump frequencies 42
3.4.5 Continuous broadening of the pump 45
3.4.6 The problem with pump broadening 47
3.5 Conclusion 48

CHAPTER 4 THEORY OF STOKES PULSE AMPLIFICATION IN A CW-PUMPED SBS MEDIUM 50

4.1 Introduction 50
4.2 Spectral characteristics of waves generated in the SBS interaction 50
4.2.1 Conversion of basic coupled SBS equations to the frequency domain 50
4.2.2 Spectral characteristics of the output Stokes field 55
4.2.3 Spectral characteristics of the generated acoustic wave 56
4.2.4 Modification of the refractive index in SBS 57
4.2.5 Conclusions from section 4.2 60
4.3 Temporal characteristics of the output Stokes field in SBS: Stokes pulse delay and inertia of the acoustic wave 60
4.3.1 An analytical solution of the basic coupled equations in the time domain 61
4.3.2 Dynamics and spectrum of the acoustic wave amplitude 63
4.3.3 Calculations of the output Stokes pulse characteristics 66
4.4 Qualitative explanation of the nature of the delay 70
4.5 Conclusion 71

CHAPTER 5 EXPERIMENTAL STUDIES OF STOKES PULSE PROPAGATION IN CW-PUMPED SBS AMPLIFIER 73

5.1 Introduction 73

5.2 Investigation of Stokes pulse delay behaviour in the quasi-steady state regime of SBS interaction 73

5.2.1 Concept of a test experiment 73

5.2.2 Relations between NA, Γ_B and τ in silica fibres 76

5.2.3 Characterisation of the fibre samples 77

5.2.4 Experimental setup for Stokes pulse delay measurements 80

5.2.5 SBS laser as a generator of Stokes pulses 82

5.2.6 Stokes pulse delay measurements 85

5.2.7 Procedures of experiment 86

5.2.8 Discussion of experimental results 88

5.3 Dynamics of the Stokes pulse in a Brillouin amplifier 90

5.4 Conclusions 94

CHAPTER 6 FINAL CONCLUSIONS 96

APPENDIX 1:ANALYSIS OF SOME PUBLICATIONS ON "SLOW LIGHT" 100

APPENDIX 2: THE PROCEDURE OF OBTAINING EQUATION (5.7) IN CHAPTER 5 110

REFERENCES 113

List of Publications

1. V.I. Kovalev, R.G. Harrison, J.C. Knight, N.E. Kotova. "*Waveguide induced spectral bandwidth enhancement of slow light group index caused by stimulated Brillouin scattering in optical fiber*". Laser and Particle Beams, **26**, 319-322 (2008).

2. V.I. Kovalev, R.G. Harrison, J.C. Knight, N.E. Kotova. "*Slow light in optical fiber using stimulated Brillouin scattering*" Proc. SPIE, v.**7024,** 702415-1-8 (2008).

3. V.I. Kovalev, N.E. Kotova, R.G. Harrison. "*Effect of acoustic wave inertia and its implication to slow light via stimulated Brillouin scattering in an extended medium*", Optics Express, **17**, 2826-2833 (2009).

4. V.I. Kovalev, N. E. Kotova, R. G. Harrison. ""*Slow Light" in stimulated Brillouin scattering: on the influence of the spectral width of pump radiation on the group index"*. Optics Express, **17**, 17317-17323 (2009).

5. V.I. Kovalev, R.G. Harrison, N.E. Kotova. "*Physical mechanism of "slow light" in stimulated Brillouin scattering"*. "Frontiers of Optical Fiber Devices and Applications". Special issue of the journal "Frontiers of Optoelectronics in China", **3(1)**, 22-32, (2010).

6. V.I. Kovalev, R.G. Harrison, N.E. Kotova. "*Physical nature of "Slow light" in stimulated Brillouin scattering"*. In "Frontiers in Guided Wave Optics and Optoelectronics", Ed. by B. Pal, Intech, Croatia, (2010), p.83-104.

7. V.I. Kovalev, N.E. Kotova, R.G. Harrison. *""Slow light" in stimulated Brillouin scattering: on the influence of the spectral width of pump radiation on the group index: Reply*". Optics Express, **18**, 1791-1793 (2010).

8. V.I. Kovalev, N.E. Kotova, R.G. Harrison. *""Slow light" in stimulated Brillouin scattering: on the influence of the spectral width of pump radiation on the group index: Reply"*. Optics Express, **18**, .8055-8057 (2010).

9. N.E. Kotova, V.I. Kovalev, R.G. Harrison. "*Dynamics of the Stokes pulse in a Brillouin amplifier",* submitted to Optics Letters.

10. N.E. Kotova, V.I. Kovalev, R.G. Harrison. "*On the nature of optically controlled delay of a Stokes pulse amplified by stimulated Brillouin scattering in optical fiber",* accepted for publication in Laser Physics.

Science evolves and flourishes when, for firm scientific reasons, traditional understanding is put into question. To suppress this process with the weight of convention is ultimately damaging and, though on occasions it may be uncomfortable, a principal duty of all science is the search for truth. It is hoped that the work presented in this thesis, which challenges conventional understanding of Stokes pulse delay in SBS, is considered by the reader to be justified and correct.

Chapter 1

Introduction

This thesis is in the area of nonlinear optics. It considers the phenomenon of stimulated Brillouin scattering (SBS) as a means of realising optical pulse delays. The work investigates the dynamics and spectral characteristics of the Stokes pulse under SBS amplification.

The research was carried out within the Stimulated Scattering Phenomena Group at Heriot-Watt University. Part of the experimental work was done in collaboration with Centre for Photonics and Photonic Materials, University of Bath, who provided photonic crystal fibre (PCF) samples.

1.1 Background and motivation

The ability to optically control the propagation "speed" of a light pulse in a transparent medium and, correspondingly, the delay of this pulse is a research topic that continues to attract the attention of the scientific community. In the last two decades there has been a particular surge of activity in this area which is topically referred to as "slow light" generation.

This interest is not only motivated by scientific curiosity. Control of the speed of light pulse propagation is, for example, of interest for applications in quantum optics for quantum information processing in achieving long storage time, sufficient to enable quantum operations, so creating building blocks of a quantum processor [1]. Controllable pulse delays have also shown potential applications in nonlinear optics, optical switching and interferometry [2].

However, the main engine of research in this field is the desire to implement optical delay lines for the needs of telecommunication networks. Optical delay lines are believed to have direct applications in signal processing areas such as optical synchronisation and multiplexing, optical equalization, correlation and optical logic gates. Realizing these processes purely in the optical domain might reduce optical-electronic conversion inefficiencies and take advantage of the ultrahigh bandwidth inherent in optics. From a systems perspective, ideally a delay line should possess the following properties: continuous and large tuning range, wide bandwidth, fast reconfiguration speed and it should also preserve the amplitude, frequency and phase of transmitted signals. Devices generating "slow light" are now viewed as strong candidates for achieving such tunable optical delay lines [3].

Obviously the mechanism of light pulse delay relevant to all these applications is a decrease of the pulse propagation speed in an optical medium. This can occur in a medium in which the refractive index n is a function of frequency, $n = n(\omega)$. Consequently the monochromatic wave components that make up the pulse travel at slightly different phase velocities and the coherent superposition of these waves leads to appearance of a pulse the propagation velocity of which is lower or higher than that of the phase velocities of these components. This velocity is referred to as the group velocity, the magnitude of which is determined by the dispersion law of the medium, $n = n(\omega)$.

"Slow light" technology is aimed at reducing and controlling the group velocity of optical pulses. The key feature of "slow light" techniques centers on their ability to introduce a relatively large change in the refractive index seen by the light as it passes through a medium. By making the dispersion of the material sufficiently strong the group velocity can be reduced significantly, to values substantially less than the speed of light in vacuum. Enhancement of the material dispersion naturally occurs in the vicinity of a material absorption or gain resonance, but it can also be achieved with artificially created dispersion profiles such as a transparent window in a lossy background, which has an effect similar to that of a gain spectrum [4].

The first experiments to report observation of pulse delays which corresponded to group velocities substantially lower than the speed of light in vacuum were performed in the mid to late 90s using atomic vapors [5-7]. They made use of the narrow transmission resonance created by the effect of electromagnetically induced

transparency (EIT) in the absorption spectrum of an atomic transition. The combination of large normal dispersion and high transmission provided by the EIT effect secured the impressive results of these experiments, which in fact were responsible for the birth of the terminology “slow light”. Generation of pulse delay via this effect will be considered in more detail in the following Chapter 2.

The EIT method of “slow light” generation was however unsuitable for practical applications, since it was restricted to the particular wavelengths of the atomic transitions and to the delay of only long pulses, the spectral bandwidths of which were sufficiently small to fit the narrow transparency window; besides realization of the EIT effect required quite complicated experimental setups. Consequently research in the field focused on the investigation of resonances of a different nature for realising the “slow light” effect.

One of the proposed techniques was to exploit the resonance associated with the quantum coherent effect commonly called coherent population oscillations (CPO) [8, 9]. CPO can be observed when a strong pump beam and a signal beam of slightly different frequencies interact in a material and cause oscillation of the ground population at the beat frequency of the two input waves. In this process a spectral hole is created at the pump laser frequency of width approximately the inverse of the population relaxation time. This approach was considered advantageous for possible applications since the effect is realised with a simple setup and in solid-state materials. Pulse delays utilizing CPO have been studied in a variety of material systems [8-13]. The early experiments based on ruby, alexandrite and erbium had highly restricted bandwidths on the order of 1 kHz as a consequence of the long population relaxation times of these materials, implying that such materials could only be used to delay pulses of duration not much shorter than 1 ms [14]. Faster population recovery times were achieved in semiconductor structures (quantum wells, quantum dots, semiconductor laser amplifier). However in general high intrinsic absorption inherent to the CPO effect limits its practicality [15].

Pulse delay has also been obtained in specially engineered material structures such as Bragg gratings, photonic crystals (PC), photonic crystal waveguides (PCW) and coupled resonator structures [16-18]. In this class of medium low pulse velocities are a consequence of the large spatial dispersion of dielectric permittivity arising from the high refractive index contrast between materials constituting the structure, which

changes the propagation constant *k*. Qualitatively the delay mechanism is explained as follows. Due to the reflections that occur at the boundary between the materials constituting such structures the light in them propagates in backward and forward directions. Superposition of these waves yields a slowly moving interference pattern, the propagation velocity of which is lower than the phase velocity [18]. In comparison to "slow light" devices based on EIT and CPO, these engineered structures offer a larger bandwidth of operation and more flexibility in terms of operating wavelength, which depends only on the dimensions of the structure. The photonic devices enable room temperature operation, can be quite miniature and thus are suitable for on-chip integration with the telecommunication technologies. However, since the pulse delay essentially occurs due to localization of the electromagnetic field within the device, the delay and the storing of the light are limited in practice by the lifetime of light in the device**.** The lifetime is dominated by intrinsic and extrinsic losses. Another disadvantage of this approach is that continuous tunability of delay is practically difficult because the delay depends on the specific structure of the device [16, 18].

Another approach proposed in the literature to produce "slow light", which has since attracted considerable attention, suggested that the gain resonances arising in stimulated scattering processes, namely stimulated Brillouin and stimulated Raman scattering (SBS and SRS respectively) may lead to modification of the refractive index for signal pulses and thus cause their delay [19, 20].

In SBS light energy is transferred from the higher-frequency light field (i.e., the pump or control field) to the lower-frequency field (i.e., the probe or data Stokes field), by means of interacting with a high-frequency acoustic wave induced in the material**.** This interaction results in amplification of the field at the Stokes frequency, when the latter is detuned from the pump field by the material excitation frequency (i.e., the acoustic frequency). SRS is similar to SBS but instead of the acoustic wave, vibrations in individual molecules are excited**.** The gain bandwidth, which determines the bandwidth of the "slow light" effect in these processes, is determined by the lifetime of the phonons excited in the process (whether acoustic or optical). The Raman gain is much broader than the Brillouin gain, but is also smaller in absolute value [21].

A unique advantage of the stimulated scattering approach which distinguishes it from all the other proposed methods, is that a wide range of media can be used**,** including optical fibres. Further, the resonance can be created at any wavelength within

the optical communications windows by changing the pump wavelength; moreover, the process runs at room temperature, and, when realised in fibres, allows for long interaction lengths and thus low powers for the control beam. These features are very attractive for telecommunication technology and for this reason considerable research effort has been dedicated worldwide in recent years to develop "slow light" devices exploiting these techniques, especially SBS.

Professor Robert Harrison and Doctor Valeri Kovalev, the leaders of the Stimulated Scattering Phenomena Group at Heriot-Watt University, have been working in the field of SBS for over 40 years. When the generation of "slow light" via SBS became widely discussed in the literature it was natural for the group to embark in investigation of this topic.

While the SBS-based method proved itself capable of delaying light pulses, the major problem of this approach for telecom applications was the narrow bandwidth of the SBS resonance. This is ordinarily of the order of ~30-50 MHz in standard silica fibres, whereas for telecom systems gigahertz bandwidths are required for dealing with the real data streams [19]. Several methods of overcoming this problem, based on spectral broadening of the pump were proposed in the literature. These methods will be discussed in detail in Chapter 3. Our group proposed an original alternative approach. Previous studies of the group showed that the waveguiding nature of light propagation in optical fibres broadens the spectrum of SBS inhomogeneously and the broadening can be massive [22, 23], as high as ~15 GHz in high numerical aperture fibres [24]. The idea was to exploit the waveguide-induced SBS broadening effect for the delay of sub nanosecond Stokes pulses. The research proposal based on this idea was supported with funding from EPSRC (Grant No GR/R56105/01).

Correspondingly we started careful theoretical studies of Stokes pulse delay via SBS amplification in optical fibres. Surprisingly this work showed that in fact no modification of refractive index at the Stokes frequencies and therefore no modification of the group velocity of the Stokes pulse in SBS can take place, in essence showing the concept of "slow light" in SBS to be incorrect.

In light of this, for both basic science and potential applications, the critical question to arise from this discovery concerned the true nature of pulse delay in SBS. The primary purpose of the research presented in this thesis is to uncover and

understand through a combined theoretical and experimental study of SBS in optical fibre the mechanism of such Stokes pulse delay.

1.2 Objective of this thesis

The objectives of this thesis are the following:

- Through analysis of the literature, to highlight and explain the inconsistency of SBS-based "slow light".
- To build a theoretical model for the amplification and delay of a Stokes pulse externally injected in a CW pumped SBS interaction. From this provide insight into the temporal and spectral characteristics of the Stokes radiation wave and acoustic wave induced in the SBS process.
- To experimentally investigate the behaviour of the temporal, spectral and energy characteristics, including the delay, of a Stokes pulse amplified via CW pumped stimulated Brillouin scattering in optical fibres by:
    - exploring the CW pump induced delay in a set of fibres with different characteristics,
    - investigating the shape and amplitude of the amplified Stokes pulse.

1.3 Thesis structure

This dissertation is organized into 6 chapters and 2 appendices. The current chapter provides background information about the field of study as well as describing the motivation and main objectives of this work. Chapter 2 presents the classical theory of group velocity/group index which is essential for understanding the phenomenon of "slow light". It also discusses an alternative well known mechanism for pulse delay by means of pulse reshaping in media with saturable absorption or gain. Finally it gives a brief history of "slow light" research and an overview of the key publications in the area. Chapter 3 gives a review of works on "slow light" via SBS, describing the mainstream research and identifying the main problems we discovered in theoretical modelling, interpretation and understanding of the experimental findings in this subject area. Chapter 4 presents the analytic solutions, obtained in this work, of the basic coupled set of equations of the classical SBS theory which describe the temporal, spectral and energy characteristics, of a Stokes pulse amplified in a continuously pumped SBS interaction. These solutions, which are in strict accordance with the physics of SBS, provide rigorous theoretical grounds for identifying the nature of

Stokes pulse delay via SBS amplification. The relevance of these solutions to the phenomenon of "slow light" is discussed. Chapter 5 describes the experiments that were performed for verification of the theoretical prediction made in Chapter 4. Finally Chapter 6 draws conclusion from the work covered in this thesis. Appendix 1 to Chapter 2 contains more detailed analysis of some key publications on "slow light" and Appendix 2 gives some supplementary information on how equation (5.7) in Chapter 5 was obtained.

Chapter 2

Mechanisms of pulse delay in an optical medium.

Concept of “slow light”

2.1 Introduction

Pulse delay and the phenomenon of “slow light” are the central issues of this thesis. As mentioned in the introductory chapter, in dispersive media light pulses propagate with the group velocity, v_g, the value of which can be smaller or higher than the phase velocity of light in the medium, c/n. Because of this, the light pulse can be delayed or advanced compared to when it propagates in a non-dispersive medium. The term “slow light”, in particular refers to the case when the group velocity is considerably lower than c/n. The effect is dramatically enhanced when the spectrum of the pulse is resonant with an absorptive or amplifying transition in the medium.

There is however another mechanism by which a pulse may appear delayed or indeed advanced in resonant type media. This occurs when the absorption or amplification of the pulse non-instantaneously changes under influence of the pulse. This process is commonly referred to as nonlinear absorption or amplification. In this case a pulse transmitted through the nonlinear medium experiences reshaping, and its maximum shifts relative to the maximum of such a pulse when it propagated through a linear medium.

It therefore follows that in the studies of optical pulse delay in resonant systems, which is currently topical in the field of “slow light”, whether absorbing or amplifying, due care must be taken in distinguishing between these physically distinct processes.

Often this has not been the case in the recent literature and as a consequence this has led in some instances to false claims and misinterpretation of experimental findings.

In the following sections we consider in some detail the delay due to the group effect, that is "slow light", we analyze from the perspective of group delay theory some key experiments in the field (in particular EIT based "slow light") and we then consider the delay that can be experienced by the pulse on propagation through a nonlinearly absorbing medium.

2.2 Propagation of a light pulse in a dispersive media. Phase and group velocity, group index, and pulse delay

The concept of group velocity was first introduced by William Hamilton as early as 1839, and a full theoretical treatment of the effect was given by Lord Rayleigh in 1877 [2]. The first experimental observation of light propagation at the group velocity is attributed to Michelson (1884). The effect was observed for optical radiation propagating through a cell filled with CS_2. The ratio of the light velocity in the liquid to that in air was found to be 1.75, whereas the theoretical value based on phase velocity was the refractive index of the liquid, i.e. 1.65 [25].

Let us review the classical treatment of group velocity as it was introduced in the fundamental texts of Jackson [26], Stratton [27], Vingradova [28]. Propagation of a monochromatic plane wave in an optically transparent medium with refractive index n is described by the phase velocity $\upsilon_{ph} = c/n$, where c is the speed of light in vacuum. Phase velocity υ_{ph} is the velocity of a point of constant phase of an electro-magnetic wave (EMW). Strictly monochromatic waves do not however exist in nature. Furthermore to transmit information by an EMW, that is to transmit energy, the monochromatic wave must be modulated. In the linear approximation a modulated wave comprising a continuous and finite bandwidth of optical frequencies gives rise to a pulse. This results from the interference of the monochromatic components.

In a medium without dispersion the phase velocities of different components of the pulse spectrum are equal and the pulse propagates without distortion. In a dispersive medium the propagation velocities of the different monochromatic waves are different. This leads to a change in the phase difference between the components which results in pulse distortion. The velocity of a pulse, which is conventionally defined as

the propagation velocity of its maximum, may differ significantly from the phase velocities of the individual monochromatic components it is made up of, and thus the notion of pulse velocity or group velocity should be defined more accurately. From a mathematical point of view the problem of pulse propagation in a medium requires solving the wave equation

$$\frac{\partial^2 E}{\partial z^2} - \frac{\varepsilon\mu}{c^2}\frac{\partial^2 E}{\partial t^2} - L(E,t) = 0, \tag{2.1}$$

where $L(E,t)$ is some operator that affects the function $E(z,t)$.

Note that below we will consider pulse propagation in optically homogeneous media which means that we put aside the effect of spatial dispersion of the medium's susceptibility on the radiation propagation velocity [29]. Representative examples of optically inhomogeneous media are photonic crystals and materials with Bragg gratings.

The most general form of the operator $L(E,t)$ for an optically homogeneous media is [28, 30]

$$L(E,t) = \frac{4\pi\mu}{c^2}\left[\frac{\partial^2}{\partial t^2}\int_0^\infty \chi(E,\tau)E(t-\tau)\,d\tau + \frac{\partial}{\partial t}\int_0^\infty \sigma(E,\tau)E(t-\tau)\,d\tau\right], \tag{2.2}$$

where $\chi(E,t)$ and $\sigma(E,t)$ are the complex susceptibility and conductivity of a medium, both of which can be dependent on the amplitude of an EMW and on time. It is their dependence on time, t, which results in the frequency dependence of their Fourier transforms, widely known as dispersion. When χ and σ are independent of E the medium is considered to be linear, otherwise it is nonlinear.

Equations (2.1) and (2.2) must be accompanied by boundary conditions. We define the medium to be located in half-space $z \geq 0$ and the input signal at $z = 0$, is

$$E(t, z=0) = E_0(t). \tag{2.3}$$

Let us consider propagation of the pulse (equation (2.3)) through a nonmagnetic ($\mu = 1$) linear optically transparent medium. The spectrum of the pulse is

$$F(\omega) = \frac{1}{2\pi} \int_{-\infty}^{+\infty} E_0(t) e^{i\omega t} dt. \qquad (2.4)$$

Since all its spectral components propagate in the linear medium independent of each other, the solution to the wave equation can be obtained as a superposition of monochromatic waves

$$E(z,t) = \int_{-\infty}^{+\infty} F(\omega) \exp\{-i[\omega t - k(\omega) z]\} d\omega, \qquad (2.5)$$

where $k(\omega) = n(\omega)\omega/c$ is the wavevector and $n(\omega)$ is the frequency-dependent complex linear refractive index of the medium. If we substitute the expression for the signal spectrum from (2.4) into (2.5), the solution of equation (2.1) can be represented as [28]:

$$E(z,t) = \frac{1}{2\pi} \int \int_{-\infty}^{+\infty} E_0(\tau) \exp\{-i[\omega(t-\tau) - k(\omega) z]\} d\omega d\tau. \qquad (2.6)$$

The dispersion law of $k(\omega)$ in the medium is determined by the Fourier transform of operator $L(E,t)$. For example for a linear homogeneous isotropic medium with conductivity σ the dispersion law of $k(\omega)$ takes the form

$$k(\omega) = \frac{\omega}{c}\left(\varepsilon(\omega) + i\frac{4\pi\sigma(\omega)}{\omega}\right)^{1/2} \cong \frac{\omega}{c} n(\omega) + i\alpha(\omega). \qquad (2.7)$$

If in equation (2.7) the refractive index, n, which determines the phase of the propagating wave and the absorption coefficient, α, which affects amplitude of the signal, are both independent of ω, then the solution for the wave equation (2.1) following from equation (2.6) is

$$E(z,t) = E_1(t) e^{-\alpha z} e^{-i\omega\left(t - \frac{n}{c} z\right)} + c.c., \qquad (2.8)$$

where c.c. marks complex conjugate.

For the purposes of describing the group velocity it is essential to consider the dispersion of the refractive index, $n(\omega)$. In this case the required solution of equations (2.1-2) for the signal at $z = 0$ given in the form of equation (2.3) is only possible under some approximations.

Since the group velocity of a pulse is determined by relative change of phases of the spectral components of the pulse and is not affected by absorption, the latter can be neglected for simplicity (only the first term in (2.7) is important). The pulse may then be considered as

$$E_0(t) = A_0(t)e^{-i\omega_0 t}, \tag{2.9}$$

where ω_0 is the pulse central frequency and A_0 is its slowly varying complex amplitude such that $|dA_0/dt| << \omega_0|A_0|$, which means that the spectral width of the signal $\Delta\omega << \omega_0$. When the dependence of the wave vector on ω, $k(\omega)$, varies slowly within the spectral width $\Delta\omega$ it can be expressed by the series expansion,

$$k(\omega) = k_0(\omega_0) + \left(\frac{dk}{d\omega}\right)_{\omega_0}(\omega-\omega_0) + \frac{1}{2}\left(\frac{d^2k}{d\omega^2}\right)_{\omega_0}(\omega-\omega_0)^2 + \ldots \tag{2.10}$$

The field of the pulse at z and t can be written as

$$E(z,t) = A(z,t)\exp\left[i(k_0 z - \omega_0 t)\right], \tag{2.11}$$

where

$$A(z,t) = \frac{1}{2\pi}\int_{-\infty}^{+\infty} A_0(t')dt' \int_{-\infty}^{+\infty} \exp\left\{-i\left[(t-t') - \frac{dk}{d\omega}z\right](\omega-\omega_0) + \frac{i}{2}z\left(\frac{d^2k}{d\omega^2}\right)_{\omega_0}(\omega-\omega_0)^2\right\}d\omega. \tag{2.12}$$

The number of different expansion terms considered in equation (2.10) determines the level of approximation of the dispersion theory. If we take into account only the first term in equation (2.10) we will get the value of phase velocity in the medium for a monochromatic wave of frequency ω_0

$$v_{ph} = \frac{\omega_0}{k_0}. \tag{2.13}$$

In the first approximation of dispersion theory, when $k(\omega)=k_0+(dk/d\omega)|_{\omega 0}(\omega-\omega_0)$, the internal integral in equation (2.12) turns into a δ-function and we have

$$E(z,t) = A_0\left(t - \frac{dk}{d\omega}z\right)\exp\left[i\left(k_0 z - \omega_0 t\right)\right]. \tag{2.14}$$

We can see that in this case the pulse propagates undistorted and the velocity of its propagation is given as

$$\upsilon_g = \left(\frac{dk}{d\omega}\right)^{-1}_{\omega_0}. \tag{2.15}$$

This is what is called the group velocity of the pulse.

It is important to note here that the above theory is derived on the assumption that the medium is non-absorbing/amplifying. However it is possible to show that the same result for group velocity will be obtained if the absorption/amplification of the radiation is not too strong and it is linear and equal for all the spectral components, i.e. for the case when there is no dispersion of the absorption/amplification coefficient and there is no change of amplitudes of individual spectral components relative to one another.

Taking into account that $\upsilon_{ph} = \omega/k = c/n$ and $k = \omega n/c$ we can write down the group velocity in terms of refractive index $n(\omega)$

$$\upsilon_g = c\left[\frac{d(n\cdot\omega)}{d\omega}\right]^{-1}_{\omega_0} = c\left[n(\omega_0) + \omega_0\left(\frac{dn}{d\omega}\right)_{\omega_0}\right]^{-1} = \frac{c}{n_g}, \tag{2.16}$$

where the expression in the brackets is known as the group index, n_g. In the region of normal dispersion, where $dn/d\omega > 0$ and $[n(\omega_0)+\omega_0(dn/d\omega)|_{\omega o}] > 1$, $\upsilon_g <$ c and light pulse propagates slower than light in vacuum (this is so called "slow light"). In the region of anomalous dispersion $[n(\omega_0)+\omega_0(dn/d\omega)|_{\omega o}]$ can be < 1 and then the case of "fast light" $\upsilon_g >$ c is formally realized. It is obvious that if the derivative $dn/d\omega$ is large the group index and group velocity will differ substantially from the phase velocity and its index. The limit for this difference is determined by the validity condition of the series (2.10), $[(dk/d\omega)|_{\omega o}]\Delta\omega << k(\omega_0)$. This gives the estimate for the maximum group index as $n_g << n(\omega_0)(\omega_0/\Delta\omega)$.

Note that this relation shows in particular that a light pulse can, in principle, be stopped, (which means that $n_g \Rightarrow \infty$), only if $\Delta\omega \Rightarrow 0$. This means that the duration of

such a pulse must tend to infinity, which in turn means that the effect is relevant to a monochromatic wave only.

The pulse will propagate undistorted at the group velocity only if $dk/d\omega = const$, so that $d^2k/d\omega^2$ and higher derivatives are negligible. If this condition is not satisfied then the pulse changes its shape in the course of propagation (becomes deformed) and the group velocity loses its precise meaning. Thus $k = k(\omega)$ should change slowly, so that every next term in the expansion series (2.10) is much smaller than the previous; the accuracy with which group velocity can describe pulse propagation is determined by the accuracy with which $dk/d\omega$ is assumed to be constant.

The time delay or the group delay that is experienced by an optical pulse in passing through a material system of length L is given by

$$\Delta T_d = \frac{L}{\upsilon_g} = \frac{L}{c} n_g \tag{2.17}$$

To sum up this section let us emphasise the approximations that were used in deriving the classical concept of the group velocity (group index).

1. Deviation of the group velocity from the phase velocity is not of arbitrary magnitude.
2. The group velocity in the form of Equation (2.16) is introduced to describe pulse propagation in a transparent region of a material where $n(\omega)$ varies linearly within the pulse spectrum.
3. Absorption (or amplification) in the medium has to be not too high and equal for all spectral components of the pulse.
4. The medium's response to a propagating optical field has to be linear.

All these approximations are well satisfied for propagation of low intensity optical pulses, the frequencies of which lie far away from any natural resonances in the medium. The difference between the phase and group velocities in such case is conventionally not more than ~10% [25].

2.3 Enhanced pulse delay near an optical resonance. “Slow and fast light”

Investigations involving the controlling and enhancing of pulse delay increased substantially with the advent of laser when it became possible to study propagation of narrow bandwidth light pulses through media when the carrier frequency of the pulse is in the vicinity of the natural resonance of the media. According to equation (2.16) the fast change of the refractive index with frequency, $dn/d\omega$, at and in the vicinity of a material resonance, as depicted in Figure 2.1, seemed to be a promising mechanism for achieving enhanced delays.

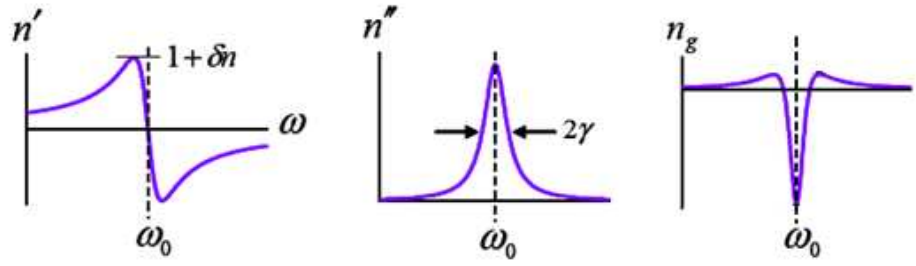

Figure 2.1. Attenuation constant, *n''*, the phase index, *n'*, and the group index, n_g, for a typical spectral resonance (*n''*) with the FWHM 2γ. after [4].

In the late 1960s several groups experimentally investigated the propagation of weak optical pulses through laser amplifying media. A slight increase of pulse delay was observed, which was interpreted as a decrease in the pulse velocity as expected for a linear amplification. The effect however was small because of low available gain [4, 31, 32]. In 1971 Casperson and Yariv [33], were able to achieve a pulse velocity as low as c/2.5 in a xenon amplifier. The delay was attributed to the group velocity effect and the required large value for $dn/d\omega$ was attributed to the high gain and its narrow (Doppler-broadened) linewidth in xenon.

In the early 1980s Chu and Wong, [34], investigated propagation of picosecond laser pulses through a GaP:N crystal as the pulse carrier frequency was tuned through the absorption resonance arising from the bound A-exciton line. Both delay and advancement of the transmitted pulse were observed. In particular, it was concluded that the observed delay corresponded to a group velocity of ~c/40. The authors concluded that a further reduction of the group velocity was possible, but in their case it was limited by the resonantly enhanced absorption of the propagating radiation. Indeed this was an insurmountable limitation of pulse delay methods exploiting rapid change of refractive index in the vicinity of absorption resonances.

Consequently attention turned to nonlinear optical techniques to achieve high dispersion of refractive index simultaneously with a decreased level of absorption of the pulse. The first such technique was electromagnetically induced transparency (EIT). The effect was first realised in atomic vapours**.** Results from the use of this technique for delaying the light pulse were very impressive, demonstrating group velocities several orders of magnitude lower [6] than the speed of light in vacuum. These remarkable findings were responsible for the subsequent proliferation of research in the area and the birth of the topical terminology "slow light" [4, 35]. It is therefore important to consider them in more detail. The theory of the effect and some key experiments are reviewed in the following section.

2.4 "Slow light" via electromagnetically induced transparency (EIT)

2.4.1 Theory of "slow light" via EIT

The technique commonly called EIT [36], in fact is the effect of "hole-burning" in the absorption spectrum of an atomic resonant transition by intense laser radiation, first noted in the mid-sixties [37]. The key idea is that, through using an intense auxiliary electromagnetic field, it is possible to modify the linear dispersive properties of a three-level atomic system in such way that a narrow transparency window appears within an original absorbing resonance [4]. According to Kramers-Kronig relations, such a window must result in a sharp change of the refractive index in a material with normal dispersion in the vicinity of the resonant frequency of this window [38-40]. Calculations made by Harris et al. in [38] revealed that a group velocity of ~c/250 could be achieved in a 10 cm long cell using the resonant transition at λ = 283 nm in Pb vapour. About three years later their theoretical prediction was confirmed experimentally [5, 41].

The scheme of atomic levels (typically known as lambda-scheme) used for EIT is depicted on Figure 2.2. To explore the dispersive properties of such a three-level system one should examine atom field coupling in the vicinity of the resonance and consider the linear susceptibility, $\chi^{(1)}$, experienced by the probe wave. According to [4]

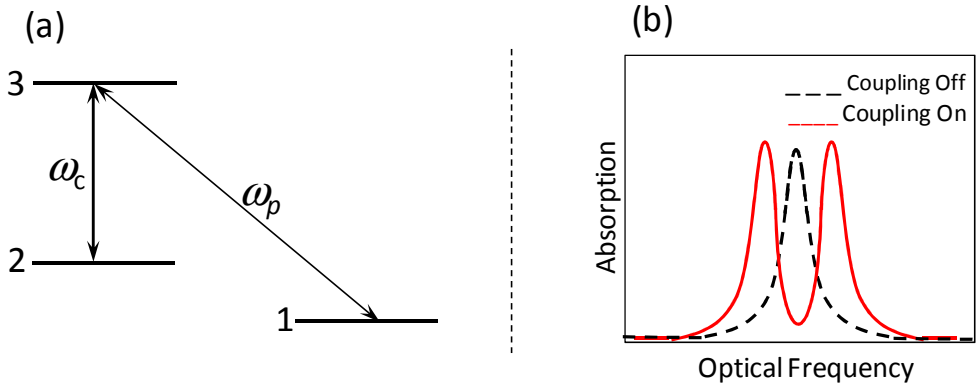

Figure 2.2. (a) Three-level λ-scheme for realizing EIT effect; (b) modification of absorption coefficient of probe field , ω_p, in presence of coupling field, ω_c, after [4]

the susceptibility for the probe wave field in a typical EIT three-level atomic system can be described as

$$\chi^{(1)} = \frac{-iN\mu_{31}^2}{\hbar}\left(\frac{\left[i(\delta-\Delta)-\gamma_{21}\right]}{(i\delta-\gamma_{31})\left[i(\delta-\Delta)-\gamma_{21}\right]+\Omega_c^2/4}\right), \tag{2.18}$$

where μ_{31} and γ_{31} are the electric dipole matrix element and the decay rate between states $|3\rangle$ and $|1\rangle$ (the transition to which the probe frequency is tuned), γ_{21} is the decay rate between states $|2\rangle$ and $|1\rangle$, N is the atomic density, δ is the detuning of the probe field from $|1\rangle$ - $|3\rangle$ transition resonance, Δ is the detuning of the coupling field from $|1\rangle$ - $|2\rangle$ transition resonance, and Ω_c is the Rabi Frequency of the coupling filed.

It follows from equation (2.18) that in an EIT system when $\Delta = 0$ and $\delta = 0$ the group index for a probe pulse at ω_p and absorption coefficients, α_{max} and α_{min}, in the absence and presence of coupling field respectively can be expressed as [4, 42]

$$n_g \cong 8\pi\omega\frac{N\mu_{31}^2}{\hbar\Omega_c^2} = 8\pi\omega\frac{M}{\Omega_c^2}, \tag{2.19}$$

$$\alpha_{max} \cong 2\pi\frac{\omega}{c}\frac{M}{\gamma_{31}}, \tag{2.20}$$

$$\alpha_{min} \cong 8\pi\frac{\omega}{c}\frac{\gamma_{21}M}{\Omega_c^2}, \tag{2.21}$$

where and $M=N\mu_{31}^2/\hbar$ is the parameter of an EIT system. It is important that the same parameter M determines the group index and the absorption coefficients of the system. Since the values of the parameters, which appear in equations (2.19-21) are normally given in publications, it is easy to calculate the values of these equations.

A pulse which does not undergo significant distortion will travel at the group velocity given by

$$\upsilon_g = \frac{c}{n_g} \cong \frac{c|\Omega_c|^2}{8\pi\omega_p M} = \frac{|\Omega_c|^2}{4\alpha_{max}\gamma_{31}}. \tag{2.22}$$

The pulse delay for the EIT can then be written as

$$\Delta T_g = \frac{L}{\upsilon_g} \approx 4\alpha_{max} L \frac{\gamma_{31}}{|\Omega_c|^2}. \tag{2.23}$$

It follows from equation (2.23) that the delay is proportional to the exponential absorption coefficient, $\alpha_{max}L$, and is dependent on radiation intensity through Ω_c.

2.4.2 Analysis of key experimental publications

Now let us consider some of the experimental work. The detailed analysis of the works considered below is presented in Appendix 1. Here we give the main results.

The first intriguing demonstration of very low group velocity belongs to Hau et al. [6]. An optical pulse at wavelength λ = 589 nm with FWHM duration of ~2.5 μs was delayed for ~7 μs in a 229 μm-long cell with sodium atomic vapour at a temperature T = 450 nK which is close to the Bose-Einstein condensation temperature. The observed delay in this experiment corresponds to a group velocity as low as 17 m/s. From the experimental data presented in this paper we can directly estimate the values of n_g, α_{min}, and α_{max}, for the two magnitudes of coupling field intensity, I_c, at which the experiment was performed. These values are presented in the Table 1.

Table 2.1. Values of absorption and group index in [6]: experiment and theory (in brackets).

I_c, mW/cm^2	n_g, x10^6	α_{min}, x10^3 m^{-1}	α_{max}, x10^5 m^{-1}
12	9.2 (27)	9 (21)	2.7 (8.8)
52	1.5 (5.7)	2 (4.5)	2.7 (8.8)

The same values can be calculated using equations (2.19-21) the magnitudes of which are given in Table 1 in brackets. The details of these calculations can be found in Appendix 1.

It follows from Table 2.1 that the measured magnitudes of n_g, α_{min} and α_{max} are lower by a factor of ~3 than those calculated. From an experimentalists' point of view this can perhaps be considered a good agreement. Besides, if in equations (2.19-21) a fitting parameter $\theta = 0.37$ is introduced the difference between experimental and theoretical values will be not more than 20%. However even in this case the magnitude of n_g at $I_c = 52$ mW/cm^2 manifests a difference of more than 20%, in fact being higher than the experimentally measured value by ~40%. Also note that the experimental data presented in the paper supposes that the measurement error is less than 5 %.

A similar level of inconsistency between theory and experimental results can be found in [43]. In this work the delay was observed in a cell of hot Rubidium atoms under EIT conditions. The experimentally obtained delay characteristics are shown in Figure 2.3.

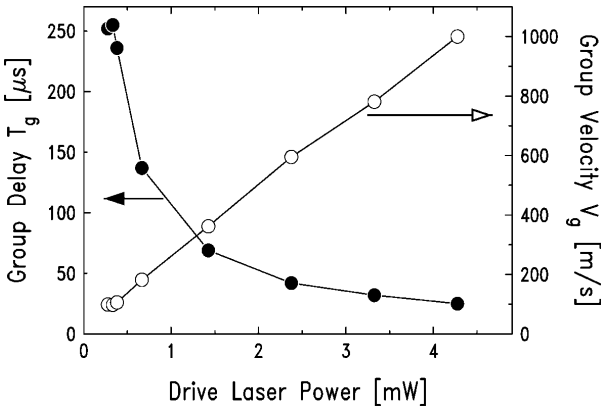

Figure 2.3. Observed group delay (solid circles) and averaged group velocity (open circles) vs the drive laser power, after [43].

Values of group velocity, v_g, from Figure 2.3 can be directly compared with corresponding theoretical values calculated by the authors. For this purpose we only need to find the magnitudes of the Rabi frequencies, Ω, corresponding to the drive laser power in Figure 2.3, since theoretical values of v_g are plotted against Rabi frequency. This is easily done knowing the laser beam diameter (2 mm) and ratio $\Omega = 2\pi(1\cdot\text{MHz})\cdot(I_d)^{1/2}$ (where I_d, the drive laser intensity, is in mW/cm^2) given in the paper. Figure 2.4 shows theoretical dependence of v_g versus $(\Omega/\gamma_r)^2$reproduced from [43]

together with experimental dependency from Figure 2.3 re-plotted against $(\Omega/\gamma_r)^2$, γ_r = 2π(3 MHz) as specified in [43].

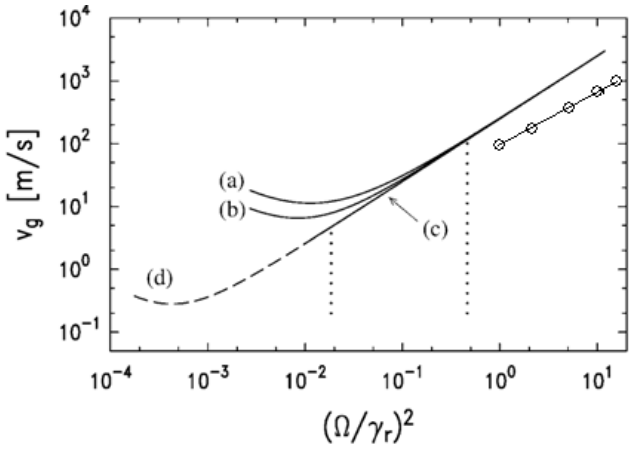

Figure 2.4. Calculated (thicker solid and dashed lines) [43] and, reproduced from Figure 2.3, the experimental (open circles and thin solid line) values of group velocity, v_g, vs drive laser power, which is represented here through $(\Omega/\gamma_r)^2$. Curves (a), (b), and (c) are calculated with Lorentzian, Gaussian, and no Doppler averaging, respectively.

The difference between the two is well pronounced. Actually the authors noted that the experimental data are for the average velocity in the cell, whereas v_g has to be lower toward the output end of the cell because of the reduction of drive laser power due to absorption. According to this, the difference between the two has to increase at lower drive laser powers. However the data in Figure 2.4 shows exactly the opposite effect: the difference is minimal, by a factor ~2.5, at the lowest power and increases to ~4 at the highest power in the experimental range.

A much better agreement between theoretical and experimental values of n_g, α_{min}, and α_{max} can be seen in [5] (see Table 2.2).

Table 2.2 Values of absorption and group index in [5] :experiment and theory**.**

Ω_c, cm^{-1}	n_g	α_{min}, m^{-1}	α_{max}, x10^4 m^{-1}
0.13±0.02	165	4.3 (5.6±0.5)	6 (1.2±0.1)
0.19±0.01	85	2.9 (2.9)	6 (1.2±0.1)
0.4		2.9 (0.8)	6 (1.5±0.1)

However the nature of this agreement is that n_g was taken as the reference point in the analysis in this paper, while in [6] it was the magnitude of M. To some extent this is equivalent to introducing the fitting parameter θ mentioned earlier. The inconsistency becomes evident when we compare the directly measured and calculated magnitudes of α_{max} in the last column of the Table 2.2.

The reader may wonder why such a detailed analysis of these publications has been presented in this review. It is because these papers are highly respected in the scientific community and are the pioneer papers of the "slow light" field. However, as shown above, our analysis has revealed a range of discrepancies in these papers between the experimental data presented and the values calculated using the theory of group velocity. This leaves open the question of whether there are other contributions to the delay in addition to or instead of the group delay effect. One such contribution arises from nonlinearity of absorption/amplification of optical radiation in a medium, which is especially enhanced in the vicinity of material resonances as in the case of EIT. This phenomenon is reviewed in the next section.

2.5 Propagation of a light pulse through a nonlinearly absorbing medium

Here we review pulse transmission through a medium in which its absorption/amplification coefficient is dependent on the radiation intensity. This nonlinear effect, commonly referred to as saturation of the medium's absorption, was the subject of much attention in the 60's after the invention of the laser. This was particularly in regard to the problem of gain saturation in laser amplifiers which limited power scaling of such systems. Also of special interest was research of absorption saturation in resonantly absorbing organic dyes for temporal control of laser radiation, in particular Q-switching [44, 45] and mode-locking [46, 47]. Later, studies of laser induced change of absorption in semiconductors were stimulated not only for their fundamental science [48], but to a great extent by military needs. From then till now this area of nonlinear optics continues to be actively researched throughout laser physics.

In 1963 Frantz and Nodvik [49] presented the theory of pulse propagation and amplification in a laser amplifier accounting for gain saturation. The behavior of a pulse in the system is described by a set of two equations: a partial differential equation for the radiation intensity and a rate equation for the active levels population difference. The general solution of this set of equations was obtained in the form of quite complicated integral equations, and it was noted that these also describe pulse propagation in an absorptive medium. For two specific shapes of pulse, square and Lorentzian, analytic solutions were obtained. These solutions showed that the depletion of population inversion density by the front edge of the pulse results in lower amplification of the trailing edge. In this case the maximum of the amplified pulse

appears at the detector as if its speed was higher than the phase velocity of light. In 1966 Basov et all, [50], investigated experimentally the propagation of a pulse through a laser amplifier for the case in which the intensity of the pulse was high enough to induce gain saturation. They found that the amplifier gave rise to effective pulse advancement, in full agreement with predictions of the Frantz and Nodvik theory[49].

In 1965 Gires and Combaud, [51] investigated propagation of a light pulse in an optically thick saturable absorber. The dynamic transmission equations they used for explanation of the experimentally observed results were the same as in [49]. A quite similar set of equations describes the behavior of a pulse in optical media where the absorption coefficient increases with increase of radiation intensity [52].

In these publications the primary interest was with the peak intensity and shape of transmitted pulse. Selden was the first to consider *the delay* that occurs due to the reshaping of the pulse in the course of its propagation in a saturable absorber [53-55]. He treated the saturation phenomenon as a process involving two energy levels as done in [51]. According to [51] if N_0 is the total number of molecules of the absorber (in this case a dye) per unit volume, n is the number in the excited state at a given instant, and $I(x, t)$ is the photon flux at depth x at time t, the equations for the rate of change of the population in the excited state and the absorption of light in the element dx are

$$\frac{\partial n}{\partial t} = I(x,t)\left(N_0 - 2n\right)\sigma - \frac{n}{\tau_s} \tag{2.24}$$

and

$$\frac{\partial I}{\partial x} = -I(x,t)\left(N_0 - 2n\right)\sigma, \tag{2.25}$$

where σ is the absorption cross section per molecule and τ_s is the lifetime of molecules in the excited state. Using these equations Selden derived an equation for the transmittance of the saturable absorber of a specified length,

$$\frac{d\ln T}{d\tau} + \ln T = 2\beta f(\tau)\left(1 - T\right) + \ln T_0. \tag{2.26}$$

Here T and T_0 are the instantaneous and initial transmittance, respectively, τ is dimensionless time in units of the excited-state lifetime τ_s, $\beta = I_0/I_s$ is the ratio of the incident intensity, $I_{0,}$ to the saturation intensity, $I_s = \sigma\tau_s$ and $f(\tau)$ is the input signal pulse

shape. Taking into account that $\ln T = -\alpha L$, where L is the length of the medium, we can rewrite equation (2.26) in terms of the absorption coefficient α:

$$\frac{d\alpha}{d\tau} + \ln\alpha = 2\beta f(\tau)\left(e^{-\alpha L} - 1\right) + \ln\alpha_0, \tag{2.27}$$

where α_0 is the unsaturated absorption coefficient.

Equations (2.26) and (2.27) describe the dynamic response of a saturable absorber to an incident light pulse $\beta f(\tau)$. It has a straightforward interpretation: the rate of change of optical density $\ln(1/T)$ is proportional to the absorbed power and to the amount by which the density differs from its equilibrium value [54]. The transmitted pulse $U(\tau)$ then takes the form

$$U(\tau) = f(\tau)T(\tau). \tag{2.28}$$

Solving numerically equation (2.26) Selden calculated the shape of a pulse transmitted through the saturable absorber for different values of incident intensity, as represented through β, and for $f(\tau)$ represented as a cosine-squared pulse of duration equal to the saturable absorption decay time. The results of these calculations are shown

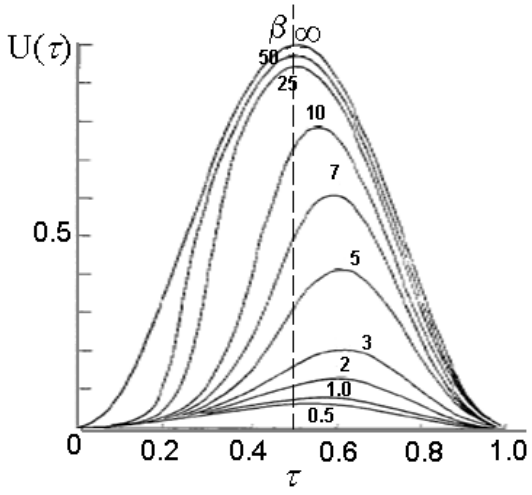

Figure 2.5. Shapes of the pulse transmitted through a saturable absorber as a function of the incident pulse intensity, after [53].

in Figure 2.5. It can be seen that high-intensity $\beta >> 50$ pulses are transmitted with little distortion or attenuation, but those of intermediate intensity $0.5 < \beta < 25$ show a reduction in width, notable attenuation and delay in reaching peak intensity, also it can

be seen that the front edge of the pulse is more distorted than the tail. Using these results Selden determined a quantitative dependency of pulse delay (in units of τ_s) on pulse intensity, which is shown in Figure 2.6 [54].

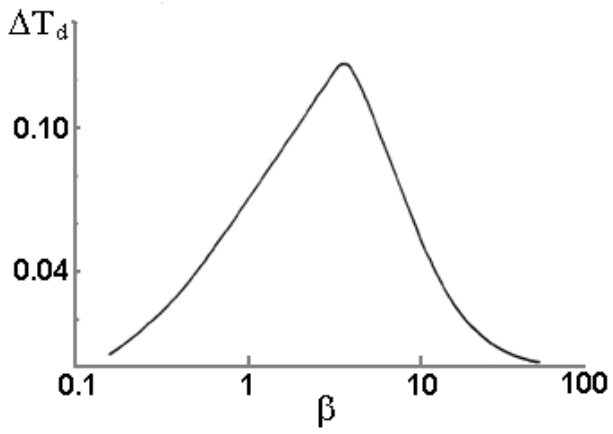

Figure 2.6. Pulse delay as a function of pulse intensity, after [54]**.**

This dependency can be approximated by the expression,

$$\Delta T_d = \tau_s \frac{\beta' \alpha_0 L}{(1+\beta')^3} \tag{2.29}$$

where $\beta' \approx 0.1\beta$.

It can be seen that delay of the pulse is proportional to the lifetime of the excited state, τ_s, which is the reciprocal of the transition bandwidth, $\gamma = 2/\tau_s$, the initial absorption coefficient, α_0, and the length of the medium, L, and is nontrivially dependent on the radiation intensity, $\beta = I_0/I_s$. For the case of amplification, when α_0 is negative, the pulse delay will be also negative, which means the pulse will experience advancement as predicted in [49] and observed in [50].

The absorbing system discussed by Selden demonstrated a reduction of the absorption coefficient under the influence of incident radiation (the effect of photo-bleaching). In addition to this, there are other nonlinear processes, such as multi-photon absorption, in which the absorption coefficient increases with increase of radiation intensity. Such effects will obviously result in an effective advancement of the transmitted pulse maximum, similar to that observed in case of laser gain saturation.

Thus, nonlinear absorption/amplification in a medium also appears to be a mechanism capable of delaying the output pulse, or more correctly, of introducing an effective delay by pulse reshaping. We emphasise that its nature is evidently

completely different from that of group delay: group delay is purely a phase effect, while the delay due to reshaping is an amplitude effect. In principle, these two effects can manifest themselves independently. Clear examples are the classical group delay effect in the region of a medium's optical transparency, and the numerous observations of the pulse reshaping in nonlinear absorbing/gain optical interactions. In the "slow light" case, however, since the radiation frequency is at or in the vicinity of material resonance both delay mechanisms must coexist because even weak probe radiation can induce substantial change of resonant absorption because nonlinearities associated with real transitions in a medium are among the strongest in nature [56, 57].

The presence of nonlinear absorption therefore may be a reason for the inconsistencies we have previously noted in the EIT works discussed above. Of course these publications [5, 6, 43], while being representative, are but a small part of the numerous published works in the subject area of "slow light". Actually among these works can be found results, that are more consistent with the group delay model than those discussed above (see for example [58]). However, there are also others which are wrongly attributed to the "slow light" model, such as [8, 59]. See Appendix 1 for details.

From an applications standpoint — particularly to meet the needs of all-optical telecommunication networks for realizing optical equalizers, data synchronizers and optical buffers — it is of vital importance that the delay is due to the group velocity effect. It is therefore of importance to clearly determine the relative contribution of these two effects to pulse delay in order to correctly understand and interpret experimental findings and from this determine appropriate areas of application. This issue has received very little attention in the literature [60-62], being very much preoccupied with group delay ("slow light") to the exclusion of all or any other mechanism.

The results presented in this Chapter show that the task of distinguishing between the two is, however, non-trivial. This is because the expressions which describe the magnitude of the delay are very similar for both models (see equations (2.23) and (2.29)). Consequently it is often not clear to what extent the delay can be attributed solely to one or other delay effect.

2.6 Conclusions

In this chapter the concept of group velocity as classically represented was reviewed. The approximations, in which the concept was introduced and the conditions which have to be fulfilled to observe pure group delay of light pulses, were highlighted. An alternative mechanism of pulse delay due the nonlinearity of a medium's absorption/amplification was discussed. Since enhancement of group delay under resonance conditions (which is the essence of the "slow light" effect) is unavoidably accompanied by a light-induced change of absorption or amplification of the transmitted pulse, this mechanism must also be considered.

A detailed examination of some of the key publications in the area was given. It showed that many experimental results cannot be unequivocally explained in terms of group delay theory and are in some instances probably the direct consequence of saturable absorption or a mixture of both. In light of this, there is a need for more careful interpretation of the experimental data on pulse delay.

However the particular reason for highlighting these issues here is that much of the "slow light" reasoning in the literature has been subsequently transferred to the idea of "slow light" generation by stimulated scattering phenomena, in particular SBS, which is the central study of this thesis. We will show in the next chapter that the consequences of this are far more serious than those already addressed above, leading to a complete misinterpretation of the physics of pulse delay in these scattering phenomena. This work will in fact show, contrary to popular opinion, that the group velocity delay cannot and does not exist in stimulated scattering phenomena. Rather the delay of the pulse (in this case a Stokes pulse) is a consequence of pulse transformation due to nonlinear interaction in the material. Finally we note that pulse transformation in stimulated scattering is more aligned with pulse reshaping accompanying conventional absorption/amplification saturation in real resonant systems as discussed above, although in stimulated scattering it is a consequence of inertia in a resonant parametric amplification.

Chapter 3

Studies of pulse delays via SBS

3.1 Introduction.

On the tide of excitement associated with realizing low group velocities using such techniques as EIT, and facing the need for new more flexible approaches of creating "slow light", D.Gauthier in 2004 [63], proposed use of the resonant feature of amplification of Stokes radiation in stimulated Brillouin scattering (SBS) for realizing group delay of optical pulses. At the beginning of 2005 first observations of the SBS-induced pulse delay in optical fibres were independently reported by the groups of K. Song et al [19] and Y. Okawachi et al [64]. Since SBS in fibres is a simple, flexible and easy-to-handle effect that can be realized at room temperature, its implementation for pulse delay appeared attractive for applications in telecommunications. Consequently, since 2005 there has been a massive growth of research activity in this area.

Actually, this idea first appeared in Zeldovich's work [65] in 1972. He considered the delay in transmission of a zero duration (δ-pulse) Stokes pulse injected into a medium in which stimulated scattering (SS) is induced with respect to the transmission of this pulse through a linear nondispersive medium in the absence of SS. Conventionally this delay is known as the build up time of the SS interaction [65]. Zeldovich suggested that this time could be equally well interpreted as a consequence of the group velocity effect. In proposing this he made the assumption that the resonant SS gain profile is accompanied by an enhanced normal dispersion of the medium's refractive index for radiation at the Stokes frequency, similar to that which occurs in resonantly excited real atomic/molecular transitions. We note that Zeldovich's

pioneering contribution to this field has not been acknowledged in the later works on the SS-based "slow light".

This chapter provides a review of the main publications in the field of SBS-based "slow light" research performed worldwide over the last several years. Theoretical and experimental aspects of these works are presented. To start with the basic equations of the SBS effect are introduced. Also presented are the derivations from these equations which are used throughout the literature to explain observed Stokes pulse delays. The initial research of our group, carried out during the first stages of studying this phenomenon, is presented. Also the chapter highlights inconsistencies that can be found in the publications on SBS "slow light" which raise questions about the nature of pulse delay in SBS-based "slow light" experiments.

3.2 Theory of SBS-based "slow light".

3.2.1 Equations for Stimulated Brillouin Scattering for the case of constant pump

SBS in an optically transparent medium is conventionally attributed to reflection of incident (pump) radiation by a longitudinal acoustic wave induced in the medium through electrostriction by the interference pattern of that pump and an earlier reflected (scattered) frequency downshifted (Stokes) wave [66]. In the most general case the set of coupled wave equations that describe the phenomenon in a nonabsorbing (α = 0) optical medium comprise nonlinear optical wave equations for the electric fields of the scattered (Stokes), $E_S(r,t)$, and pump, $E_p(r,t)$, waves, and an acoustic wave equation for the variation of the medium's density, $\Delta\rho(r,t)$, [67]. However in many practically important cases the features of SBS can be reasonably well described in the approximation of a constant pump. The number of coupled wave equations then reduces to two: the nonlinear optical wave equation for $E_S(r,t)$, [67],

$$\nabla^2 E_S - \frac{\varepsilon_0}{c^2}\frac{\partial^2 E_S}{\partial t^2} = \frac{1}{c^2}\frac{\partial \varepsilon}{\partial \rho}\frac{\partial^2}{\partial t^2}[\Delta\rho^*(r,t)E_p(r,t)], \tag{3.1}$$

where ε and ε_0 are the permittivity and undistorted permittivity of the medium and c is the velocity of light in vacuum, and the driven acoustic wave equation for $\Delta\rho(r,t)$ [68]

$$\left(\frac{\partial^2}{\partial t^2} - v_S^2\nabla^2 - \Gamma\nabla^2\frac{\partial}{\partial t}\right)\Delta\rho = -\rho_0\frac{\partial\varepsilon}{\partial\rho}\frac{1}{16\pi}\nabla^2\left[E_p(r,t)E_S^*(r,t)\right], \tag{3.2}$$

where v_s, is the acoustic wave velocity in the medium, Γ is the acoustic damping parameter, which is determined by the medium's viscosity and/or thermal conductivity, and ρ_0 is the equilibrium density of the medium, and asterisk, *, marks complex conjugate. The Stokes and pump fields with frequencies ω_S and ω_p and wave-vectors k_S and k_p are conventionally considered to be plane waves counter-propagating along the z direction (the Stokes field in the $+z$ direction and the pump field in the $-z$ direction),

$$E_S(z,t) = \frac{1}{2}\left\{\mathrm{E}_S(z,t)\,exp\left[-i\left(\omega_S t - k_S z\right)\right] + c.c.\right\} \tag{3.3}$$

and

$$E_p(z,t) = \frac{1}{2}\left\{\mathrm{E}_p(z,t)\,exp\left[-i\left(\omega_p t + k_p z\right)\right] + c.c.\right\}, \tag{3.4}$$

where $\mathrm{E}_S(z,t)$ and $\mathrm{E}_p(z,t)$ are the slowly varying amplitudes of the Stokes and pump fields and $\mathrm{E}_p(z,t) = \mathrm{E}_p$ when the pump is the constant amplitude field. The induced density variation wave (acoustic wave),

$$\Delta\rho(z,t) = \frac{1}{2}\left\{\delta\rho(z,t)\,exp\left[-i\left(\Omega t + qz\right)\right] + c.c.\right\}. \tag{3.5}$$

where $\delta\rho(z,t)$ is the slowly varying amplitude of the acoustic wave that is generated in accordance with equation (3.2) at the frequency $\Omega = \omega_p - \omega_S$. It has the wave-vector $q = k_p + k_S$, and co-propagates with the pump wave. Since in this case $\nabla^2 \equiv \partial^2/\partial z^2$, the second and thirds terms on the LHS of equation (3.2) transform to $(v_S q)^2 \equiv \Omega_B^2$ and $\Gamma q^2 \equiv \Gamma_0$.

Since in SBS the density and Stokes field amplitudes vary slowly in both space and time and the acoustic wave attenuates strongly, the wave evolution equations (3.1) and (3.2) for optical and acoustic fields are usually reduced to two well known first order equations for the field amplitudes: the partial differential equation for $\mathrm{E}_S(z,t)$, [67-69]

$$\frac{\partial \mathrm{E}_S}{\partial z} + \frac{n}{c}\frac{\partial \mathrm{E}_S}{\partial t} = -i\frac{\omega_S}{2cn}\frac{\partial\varepsilon}{\partial\rho}\delta\rho^*(z,t)\,\mathrm{E}_p(t), \tag{3.6}$$

and the relaxation equation for $\delta\rho$(z,t),

$$\frac{\partial \delta\rho}{\partial t} + \left(\frac{\Gamma_0}{2} + i\delta\Omega \right) \delta\rho = -i\delta\rho_0 \frac{\partial \varepsilon}{\partial \rho} \frac{\Omega_B}{8\pi v_s^2} \mathrm{E_p}(t) \mathrm{E_S^*}(z,t). \tag{3.7}$$

Here $\delta\Omega = \Omega - \Omega_B$ is the difference between the pump and Stokes fields beat frequency, Ω, and the resonant Brillouin frequency, Ω_B.

It is this set of equations that were used in one of the pioneer papers on SBS "slow light" to theoretically describe the phenomenon [70]. The treatment and reasoning presented in [70] has subsequently been used throughout the literature in this field. In the next section we will reproduce this treatment and also mention an alternative approach for the theoretical description of the "slow light" effect in SBS.

3.2.2 Theory of "SBS slow light" as presented in the literature

In [70] the authors consider the forward-going (+*z* direction) Stokes and backward-going (-*z* direction) pump optical fields. Fourier transformation of equations (3.6) and (3.7) in their work is given as

$$\frac{\partial \tilde{\mathrm{E}}_S}{\partial z} - i(\omega - \omega_{S0}) \frac{n}{c} \tilde{\mathrm{E}}_S = i g_2 \delta\tilde{\rho}^*(z,\omega) \mathrm{E}_p \tag{3.8}$$

and

$$\left(\frac{\Gamma_B}{2} - i(\omega - \omega_{p0} + \Omega_B) \right) \delta\tilde{\rho} = -i \frac{g_1}{\eta} \mathrm{E}_p \tilde{\mathrm{E}}_S^*(z,\omega), \tag{3.9}$$

where the symbol ~ above E_S and $\delta\rho$ denotes Fourier-transforms of E_S(z,t) and $\delta\rho$(z,t) in equations (3.6) and (3.7), $g_1/\eta = [\rho_0(\partial\varepsilon/\partial\rho)\Omega_B]/8\pi v_s^2$ and $g_2 = [\omega_S(\partial\varepsilon/\partial\rho)]/2cn$**,** and Γ_B is denoted as the SBS gain bandwidth. Substituting $\delta\tilde{\rho}(z,\omega)$ from equation (3.9) to (3.8) yields

$$\frac{\partial \tilde{\mathrm{E}}_S}{\partial z} = i(\omega - \omega_{S0}) \frac{n}{c} \tilde{\mathrm{E}}_S + \frac{1/2\, g_0 I_p}{1 - i\, 2\delta\omega/\Gamma_B} \tilde{\mathrm{E}}_S, \tag{3.10}$$

where $g_0 = 4g_1g_2/\eta\Gamma_B$ is the conventional line-centre SBS gain coefficient, $\delta\omega = \omega - \omega_{p0} + \Omega_B$, $I_p = (cn/8\pi)E_p^2$ is the pump intensity, and ω_{p0}, ω_{S0} are the central frequencies of pump and Stokes fields respectively (according to [70]).

Next the authors in [70] consider equation (3.6) to be a wave equation and from this define

$$\frac{\partial \tilde{E}_S}{\partial z} = -i(k(\omega) - k(\omega_{S0}))\tilde{E}_S, \tag{3.11}$$

in which they introduce "the equivalent wave vector for the Stokes wave"

$$k(\omega) = \frac{\omega}{c}n - i\frac{1/2\, g_0 I_p}{1 - i\, 2\delta\omega/\Gamma_B} \equiv \frac{\omega}{c}\tilde{n}_S. \tag{3.12}$$

"The effective complex refractive index" for the Stokes wave then follows as

$$\tilde{n}_S = n - i\frac{c}{2\omega}\frac{g_0 I_p}{1 - i\, 2\delta\omega/\Gamma_B}. \tag{3.13}$$

From equation (3.13) by defining the gain coefficient, refractive index and group index for the Stokes wave as $g_S = -(2\omega/c)\mathrm{Im}(\tilde{n}_S)$, $n_S = \mathrm{Re}(\tilde{n}_S)$ and $n_g = n_S + \omega(dn_S/d\omega)$ they derive their working relations

$$g_S = \frac{g_0 I_p}{1 + 4\delta\omega^2/\Gamma_B^2}, \tag{3.14}$$

$$n_S = n + \frac{c g_0 I_p}{\omega}\frac{\delta\omega/\Gamma_B}{1 + 4\delta\omega^2/\Gamma_B^2}, \tag{3.15}$$

$$n_g = n_{g0} + \frac{c g_0 I_p}{\Gamma_B}\frac{1 - 4\delta\omega^2/\Gamma_B^2}{(1 + 4\delta\omega^2/\Gamma_B^2)^2}. \tag{3.16}$$

It follows from equations (3.14-16) that the gain, g_S, has a Lorentzian-shaped resonance, with a FWHM width Γ_B. This resonance according to [19, 64, 70] will appear in the spectral region $\omega_P - \Omega_B$ in the presence of a continuous-wave pump in the medium. This is schematically illustrated in Figure 3.1(a). Note that if the Stokes pulse is frequency up shifted with respect to the pump by Ω_B, then due to the SBS process the

Stokes pulse energy will be transferred into the field energy at the pump frequency and the pulse will experiences loss, which is shown in Figure 3.1(b).

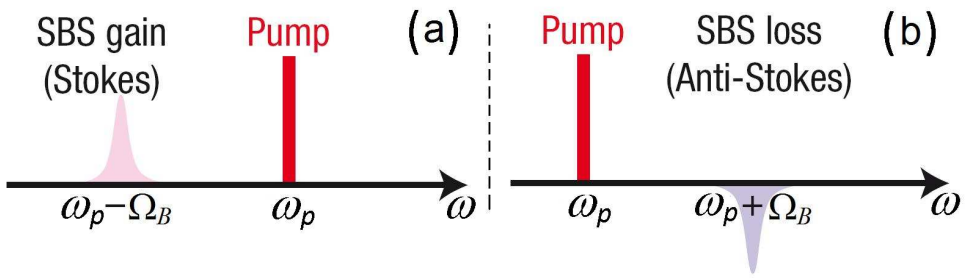

Figure 3.1. (a) Gain contour at Stokes frequencies and (b) loss contour at anti-Stokes frequencies emerging in process of SBS, after [71]**.**

Also from equations (3.14-16) it follows that the gain resonance is accompanied by a corresponding dispersion of the refractive, n_S, and group, n_g, indices. In the vicinity of the gain maximum ($\delta\omega \approx 0$) n_g increases and the group velocity, $v_g = c/n_g$, decreases with increase of I_p. The SBS induced group delay for a light pulse in a medium of length L will then be

$$\Delta T_d \cong \frac{g_0 I_p L}{\Gamma_B} \equiv \frac{G}{\Gamma_B}, \tag{3.17}$$

where G is known as the exponential SBS gain. (This expression is in fact exactly that obtained earlier in Zeldovich's work [65]).

In the first experimental work on "slow light" in SBS, [19], and in practically all the countless later publications (some of them, but by no means all, are referred in the review paper by Thevenaz, [71]) the experimentally measured delays follow this kind of dependence with Γ_B used as a fitting parameter.

In these papers the only major concern was the distortion (broadening) of the output pulse shape, which was first reported in [64]. To account for this the authors of [64] claimed that degree of pulse broadening is expected because of the bandpass filtering of the pulse's spectrum caused by the narrow spectral width of the SBS gain profile. They pointed out that for this reason experimental results could be analyzed in terms of not only absolute delay but also relative delay. In the latter case the delay is measured in units of pulse length (often referred as delay-bandwidth product), which is usually given as

$$\frac{\Delta T_d}{t_{in}} = \left[\frac{B^2 - 1}{16\ln 2}\right]^{1/2} \sqrt{G} \tag{3.18}$$

where B is the pulse broadening parameter, which is introduced as the ratio of the output, t_{out}, and input, t_{in}, pulse durations,

$$B = \frac{t_{out}}{t_{in}} = \left[1 + \frac{16\ln 2 G}{t_{in}^2 \Gamma_B^2}\right]^{1/2} \tag{3.19}$$

In the SBS interaction in standard silica fibres this broadening is especially pronounced because conventionally Γ_B is relatively small, typically 30-50 MHz [72].

An alternative theoretical description of the phenomenon, presented in the first experimental work [19] exploits Zeldovich's idea that the SBS gain for the scattered Stokes radiation is equivalent to conventional material gain (due to population inversion for example). As such the resonant character of frequency dependence (dispersion) of that gain has to be accompanied, according to Kramers-Kronig relations, by the corresponding dispersion of the SBS-induced refractive index for the Stokes radiation. The dispersion of the SBS gain is deduced in [19] from equations for Stokes and acoustic field amplitudes, equations (3.6) and (3.7), in the steady state (StSt) approximation of the SBS theory. The expression obtained for the SBS-induced delay is exactly equation (3.17).

3.2.3 Weaknesses and shortcomings in the theoretical interpretation of pulse delay via SBS

At first glance these theoretical treatments appear sound and convincing. The expression for delay following from them has been adopted and experimentally confirmed in numerous subsequent works, in fact later works just refer to [19, 64, 70] considering the physics of the delay to be established and understood. However these treatments contain a range of inconsistencies.

In [70] the Fourier transformation of equations (3.6) and (3.7) is performed incorrectly. According to the formal mathematics of Fourier transforms the third term on the LHS of equation (3.8) and the RHS of equation (3.11) can appear only if the

slowly varying amplitude of the Stokes field, $E_S(z,t)$, has the form $E_S(z,t)\times \exp[-i[\omega_{S0}t+k(\omega)z-k(\omega_{S0})z)]$. As to equation (3.9), the set of terms in the small curved brackets on the LHS of this equation require the density variation amplitude to be $\delta\rho(z,t)\exp(-i\omega_{S0}t)$ (note that $\omega_{p0} - \Omega_B \equiv \omega_{S0}$) and $\delta\Omega = 0$. These representations mean that the slowly varying amplitudes of the Stokes wave and of the density variation wave have to oscillate at the optical Stokes frequency and the amplitude of the Stokes wave retains the character of a propagating optical wave, which evidently cannot be correct. (The mathematically correct version of the Fourier transforms of equations (3.6-7) is given by equations (4.6-7) in the next Chapter). As such the validity of the expressions for the "effective refractive index", its dispersion at the Stokes radiation frequency and, consequently, the group index as introduced in [70] appear to be in doubt.

As to the theory in [19], as we mentioned, in this work the same equation for the delay, equation (3.17), was deduced using the steady state (StSt) approximation of SBS theory. However, mathematically "steady state" means that the interacting fields are purely monochromatic. As such this approximation cannot be adequate in describing interactions where pulses are involved regardless of their duration. Clearly a monochromatic field by definition has no group velocity and so the concept of group velocity has no meaning in this case.

A similar problem is found in [64], where the authors build their case by describing the spatial growth of a spectral component of the slowly varying amplitude of the Stokes field at frequency ω as

$$E_S(z,\omega) = E_S(0,\omega)e^{g(\omega)I_p z}, \tag{3.20}$$

which displays the usual exponential gain. However, as will be shown in Chapter 4, this kind of expression can only be used for a truly monochromatic Stokes field in the field of a monochromatic pump (this, in essence, is equivalent to the StSt approximation in the theory of SBS, used in [19]), which is not the case for the pulsed interaction of the "delay" experiments.

Another rather serious weakness in [19] and [64, 70] and, by inference, all subsequent work on "slow light" via SBS based on them, is in considering the SBS gain as a conventional material gain, as in media with population inversion. However SBS gain is of a parametric nature, properties of which are fundamentally very different from

those of a material gain. It is only for material resonances that the gain and refractive index of a medium are inseparably interrelated according to the Kramers-Kronig relations, and so the Kramers-Kronig relations are relevant only for material resonances [30, 73]. These relations cannot be applied to SBS (and all other parametric nonlinear interactions), as has been commonly done in the literature on "slow light" since in such interactions a parameter of the system (in optics, the dielectric constant or refractive index) is modulated at some frequency (Ω_B for the case of SBS), which does not coincide with the frequency of either pump or signal to be amplified (ω_p and ω_S in SBS). There are therefore no grounds for the emergence of any measurable "modified effective refractive index at the Stokes frequency" [70] in SBS and the consequent application of the group velocity concept to the Stokes pulses. In Chapter 4 we will discuss in some detail what modification the refractive index experiences at the Stokes frequency in SBS.

At this point we should again emphasize that in all publications on "SBS slow light", the experimentally measured dependencies of Stokes pulse delay on SBS exponential gain follow equation (3.17), the mathematical correctness of which, as derived in [19, 64, 70], is doubtful, as discussed above. This fact itself raises doubt about the correctness of these experimental results.

We believe that the primary reason for this agreement between experiment and theory is that such comparisons have been largely qualitative, mainly in corroborating the delay expression, equation (3.17), through using adjustable parameters to achieve quantitative agreement. As we show (Chapters 2 and 4), delay expressions of this form are not unique to "slow light" and for this reason far more accurate in-depth studies to determine the true nature of SBS pulse delay are necessary. This is taken up in detail in this thesis both theoretically (Chapter 4) and experimentally (Chapter 5).

Let us now analyze in some detail actual experimental realization of SBS in the pulse delay studies.

3.3 Experimental realization of SBS-based pulse delay

In general the experimental setup for observing SBS-induced Stokes pulse delay is standard for all published works (see [19, 64, 74-83] for example). Continuous wave pump radiation is coupled into a fibre under test (FUT) from one end and the Stokes

pulse is launched from the other end. Usually (apart from cases of specially created SBS gain spectra discussed below) the frequency difference between the pump and Stokes field is set to the Brillouin shift Ω_B in FUT. The delay is determined by the difference in the arrival times at the detector of the output Stokes pulse peaks in the presence and absence of the pump. The value of delay is controlled by varying the pump power. One particular example of such a set-up [19] is shown in Figure 3.2.

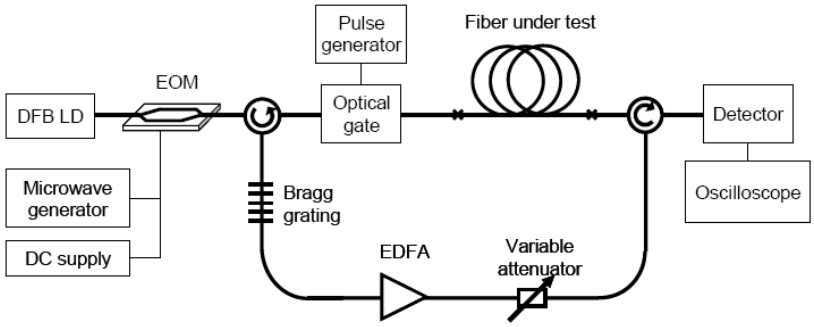

Figure 3.2. Experimental setup for observation of light pulse retardation, used in the first "SBS slow light" experiment [19]. DFB LD is the distributed feedback laser diode; EDFA is the Er-doped fibre amplifier.

In the first experiment by Song, et al. [19], the authors used 12 km of a standard single-mode (SSM) fibre and 6.7 km of a dispersion shifted fibre (DSF) as FUT and varied the pump power from zero to several tens of mW (the estimated maximum gain, G, was up to 30 dB). The FWHM bandwidths of the SBS gain, $\Delta\nu_B = \Gamma_B/2\pi$, in these fibres was given as 35 MHz and 50 MHz (both linear frequencies). It was found that the observed delay follows the dependence given by equation (3.17) with magnitudes of the delay versus gain slopes amounting to ~1.04 ns (in SSM) and 0.73 ns (in DSF) per 1 dB of the gain. The maximal obtained delay was 30 ns for the Stokes pulse with a FWHM of 100 ns [19].

Another pioneering group of Okawachi, et al. [64], reported delays of 25 and 20 ns at G = 11 for 63 and 15 ns long input pulses respectively, (shown on Figure 3.3), in 500 m long SSM (SMF-28) fibre, in which they estimated the FWHM bandwidths of the SBS gain, $\Delta\nu_B$ = 70 MHz. Larger relative delay for a shorter pulse in their experiment was accompanied by more pronounced increase of pulse duration (pulse broadening), B = 1.4 for t_{in} = 15 ns is and B = 1.1 for t_{in} = 63 ns, which are reasonably well accounted for by equation (3.19). Along with this "agreement" the authors noted the difference in the observed delay versus gain slopes for 63 and 15 ns long input pulses (0.53 ns/dB and 0.42 ns/dB) which was not accountable by the theory presented

in their work. Though the disagreement is not big, it is definitely symptomatic. The issue was resolved in their later work, [70], through numerical solution of equations (3.6) and (3.7) only.

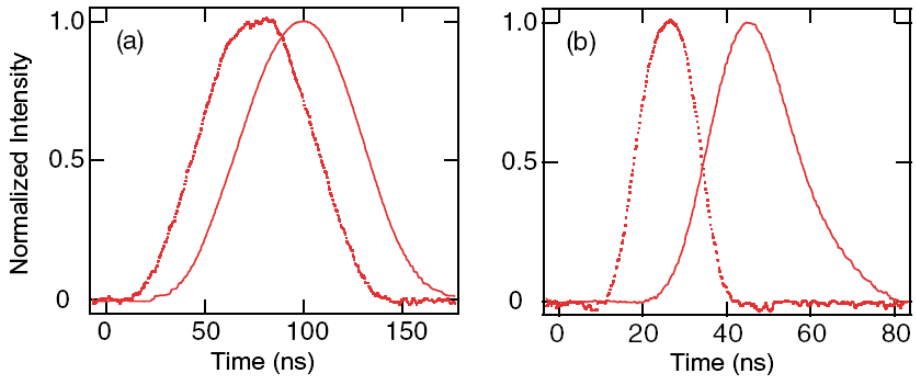

Figure 3.3. Input and delayed output Stokes pulses observed in [70] (a) t_{in} = 63 ns and (b) t_{in} = 15 ns.

A more serious problem in these two works (and actually many similar subsequent publications on "SBS slow light") is, however, that the pump and Stokes radiation sources are far from monochromatic. For the pump sources the spectral width is ~1 MHz (a typical value for DFB laser diode used) in [19] and ~300 kHz in [64]. As such, the mutual coherence lengths of the pump and Stokes fields (correspondingly <150 m and <500 m) are shorter than the lengths of the fibres used (12, 6.7 and 0.5 km). For this reason the conventional formalism of SBS they use, which is developed for coherent interaction of the pump and Stokes radiation along the whole length of the medium, is not fully adequate in describing their experiments.

3.4 Further studies: Methods of broadening the SBS gain bandwidth

Since the issues noted above were not discovered immediately after publication, these papers, [19, 64], and many similar subsequent publications, claimed that the SBS amplification in optical fibres could be a prospective technology for optically controlled delay of optical pulses [71]. The main limitation for its practical applications was supposed to be imposed by the narrow spectral bandwidth of the SBS process and, associated with this, the distortion experienced by the transmitted pulse [64]. As already mentioned, the spectral width of the SBS gain is widely accepted to be of the order 30-50 MHz in usual fibres. This means that the group index contour, which is supposed to be associated with the gain, has even narrower bandwidth, so the delaying effect can only be applied to pulses longer than 40 ns. Thus the SBS process puts a

limit on the minimum duration of the pulse that can be delayed without serious distortion. Since the main proposed application area of the SBS "slow light" devices was telecommunications, where characteristic bandwidths of 10-100 GHz are necessary for high speed data transfer, a substantial effort has been dedicated to overcome this limit [71]. This has become a mainstream pursuit in the field of SBS-based "slow light", aspects of which are discussed below.

As noted at the beginning of this Chapter, the classical SBS bandwidth, the so called homogeneous bandwidth, in bulk solids is mainly determined by the material's viscosity. However, in an optical fibre configuration the situation is substantially different since there are several mechanisms of additional broadening which by their nature render the spectrum inhomogeneous [72]. They include broadening due to the dependence of the Brillouin frequency on the concentration and kind of dopant in the core/cladding, the shape and size of the core, and distribution of mechanical and thermal stresses. Broadening up to ~400 MHz (~10 times the homogeneous SBS bandwidth) was achieved in this way [84]. Some of these effects contribute to the conventionally accepted SBS bandwidth of 30-50 MHz in optical fibres.

3.4.1 Waveguide-induced broadening of the SBS spectrum

At this point it is reasonable to mention earlier work of our group that aimed at a solution of the problem of the narrowness of the SBS gain spectrum. Kovalev and Harrison showed in [22] that the SBS gain spectrum in optical fibre is broadened inhomogeneously due to the waveguiding nature of the fibre, and that the amount of broadening increases for fibres with higher numerical aperture, *NA* [23]. The nature of the broadening arises from the ability of optical fiber to support a fan of beam directions within an angle $2\theta_c$ (Figure 3.4), where θ_c is the acceptance angle of the fiber, defined as

$$\theta_c = \arcsin\left\{1-\frac{n_{cl}^2}{n_{co}^2}\right\}^{1/2} = \arcsin\left[\frac{NA}{n_{co}}\right] \tag{3.21}$$

and $n_{cl,co}$ are the refractive indices of the fiber cladding and core, respectively.

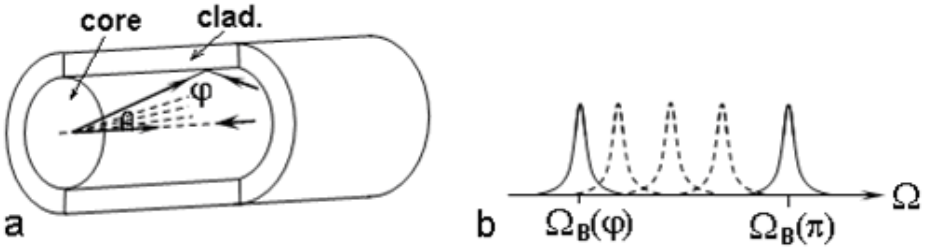

Figure 3.4. Sketch showing the nature of waveguide induced broadening of SBS gain spectrum; (a), schematic of fiber, (b), homogeneously broadened spectral profiles for different angles of scattering, φ [85].

The frequency shift of the Stokes depends on the angle, φ, between the momentum vectors of the pump and scattered radiation through the relation $\Omega_B(\varphi)=4\pi n v_s \sin(\varphi/2)/\lambda$. So the range of $\Omega_B(\varphi)$ in a fiber will be from $\Omega_B(\pi) = 4\pi n v_s/\lambda$ to $\Omega_B(\pi-2\theta_c) = 4\pi n v_s \cos\theta_c/\lambda$. For every $\Omega_B(\varphi)$ there corresponds a homogeneously broadened line of the form

$$\gamma_h(\Omega,\Omega_B) = \left[\frac{\Gamma_0^2}{4(\Omega_B-\Omega)^2+\Gamma_0^2}\right], \tag{3.22}$$

where Γ_0 is the homogenous width of Brillouin spectral line (FWHM). The Stokes spectrum, broadened by guiding, is then the convolution of frequency-shifted homogeneously broadened components, each generated from a different angular component of the pump and Stokes signal (such broadening is inhomogeneous by definition). The shape of the broadened Brillouin linewidth is described by the equation [23],

$$\gamma_i(\Omega,\theta_c) = \frac{\Gamma_0}{2[\Omega_B(\pi)-\Omega_B(\pi-2\theta_c)]}\left[\tan^{-1}\left(2\frac{\Omega_B(\pi)-\Omega}{\Gamma_0}\right)-\tan^{-1}\left(2\frac{\Omega_B(\pi-2\theta_c)-\Omega}{\Gamma_0}\right)\right], \tag{3.23}$$

where θ_c is linked to *NA* through equation (3.21). Figure 3.5 shows $\gamma_i(\Omega,\theta_c)$ for five values of *NA*.

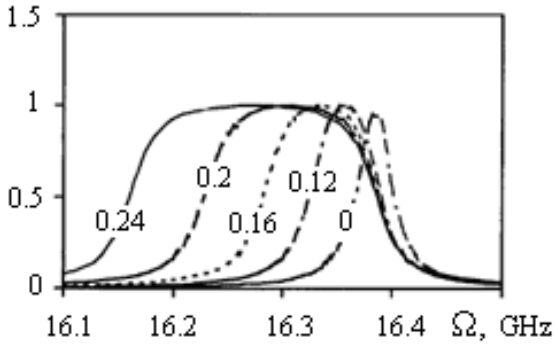

Figure 3.5. Line shape of the Brillouin gain spectrum in optical fiber for several NA values, after [23].

The dependency of FWHM of the broadened spontaneous Brillouin spectrum Γ_B on the *NA* of the fibre is expressed as [23],

$$\Gamma_B \cong \sqrt{\Gamma_0^2 + \Omega_B^2 \frac{(NA)^4}{4n_{co}^4}}. \tag{3.24}$$

Thus the waveguiding effect offers an attractive solution to increase the bandwidth of the SBS gain spectrum with a monochromatic pump. According to Figure 3.5, Γ_B is of ~ 2π(60 MHz) at λ = 1.06 μm for standard single-mode telecom fiber with *NA* = 0.12. With modern photonic crystal fiber technologies it is now readily possible to realise single-mode fiber with much higher *NA*, ~0.8, [86]. For such fiber the estimated broadening is ~2π(2.4 GHz) = 15 GHz. These considerations therefore show that waveguide induced spectral broadening of the gain bandwidth of SBS in optical fiber is potentially massive and readily achievable.

Note that particular attention to this effect is paid here because this information will be used in Chapter 5.

3.4.2 Simulation of the effect of waveguide-induced broadening of the SBS spectrum on the group index spectrum

Following common understanding that the amplification resonance in SBS is accompanied by a corresponding dispersion of the refractive index, we performed numerical simulations of the group index for the SBS spectrum broadened by this waveguiding phenomenon.

In the case of a Lorentzian-shaped SBS resonance with central frequency Ω_B the group index dispersion is described by the expression [64, 87]:

$$n_g(\Omega_B,\Omega) = n - \frac{g_0 I_p \lambda \Gamma_0}{2\pi}\left\{\frac{(\Omega_B-\Omega)}{4(\Omega_B-\Omega)^2+\Gamma_0{}^2} + \omega\frac{4(\Omega_B-\Omega)^2-\Gamma_0{}^2}{\left[4(\Omega_B-\Omega)^2+\Gamma_0{}^2\right]^2}\right\}, \qquad (3.25)$$

where g_0 is the value of the SBS gain coefficient at the exact Brillouin resonance and I_p is the pump radiation intensity. For a continuous range of resonant frequencies, Ω_B, (present due to waveguiding in the fibre core), for which the distribution of their relative amplitudes over the range $\Omega_B(\pi)$ to $\Omega_B(\pi\text{-}2\theta_c)$ is described by some function $F(\Omega_B)$, the spectrum of the "broadened" group index, $n_{gb}(\Omega)$, can be written as the convolution integral,

$$n_{gb}(\Omega) = \int_{\Omega_B(\pi-2\theta_c)}^{\Omega_B(\pi)} F(\Omega_B) n_g(\Omega_B,\Omega)\, d\Omega_B. \qquad (3.26)$$

Results of calculations of the broadened spectrum of the group index for the case when $F(\Omega_B) = 1$ in the range $\Omega_B(\pi)$ to $\Omega_B(\pi\text{-}2\theta_c)$ are presented in Figure 3.6. For the sake of illustration the curves are centred by shifting the limits of integration in such a way that the lower limit is $\omega_1 = \omega_0 - m\Gamma_B/2$ and $\omega_2 = \omega_0 + m\Gamma_B/2$, where m, which is called the rate of broadening, varies from 2 to 100. As seen the width of the profile increases continuously with increasing m. Also it can be observed that the value of group index can stay constant over a broad range of frequencies, especially when $m >$ 60, which is beneficial in overcoming the problem of pulse broadening. However the price for this is a reduction in magnitudes of the group index and of the SBS gain [24].

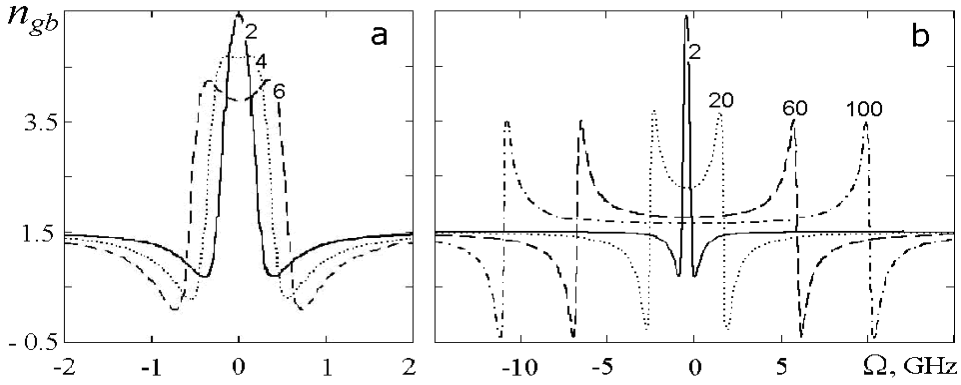

Figure 3.6. Shape of group index, n_{gb}, spectrally broadened due to waveguiding nature of fiber, (a) for m = 2-6, and (b), for m = 2-100, after [24]

This theoretical work was the first step of our group in the study of "slow light" via SBS. The expected following step was to verify this approach experimentally through demonstrating its capability of inducing delay of very short (sub nanosecond) Stokes pulses. However, as detailed earlier in this chapter, a comprehensive analysis of the literature on "slow light" via SBS brought us to the conclusion that there were substantial inconsistencies between the theory used to describe the "slow light" effect as described above, and the actual physics of SBS. For this reason the research of the group was re-oriented to better understand the underlying physics of the phenomenon of Stokes pulse delay. This is addressed in Chapters 4 and 5 which is a principal area of my research.

3.4.3 Pump-induced broadening of the SBS spectrum

The main approach for increasing the bandwidth of the SBS gain spectrum proposed in the literature was based on spectral broadening of the pump radiation. According to common understanding of the SBS phenomenon the SBS exponential gain is proportional to the pump radiation intensity (see equation (3.17)). As such it is expected that the spectral distribution of this gain has to follow that of the pump through the convolution of the natural Brillouin gain spectrum with the pump radiation spectrum [71, 74]. This feature was also used to create specially shaped (customized) SBS gain spectra (see for example [76, 78, 88]). Several methods to achieve this have been proposed, which in principle can be grouped into two, namely the use of a number of different discrete narrowband pump frequencies and controlled continuous broadening of a single frequency pump spectrum.

3.4.4 Use of discrete pump frequencies

One of the first demonstrations [89, 90] of customized gain was realized with the use of bi-chromatic pump field (with components $\omega_p \pm \delta$) to create a gain spectrum consisting of two equal Lorentzian gain lines (with FWHM Γ_B) as shown in Figure 3.7 by two dotted blue contours. The bi-chromatic pump field was obtained via carrier-frequency modulation of CW single-frequency laser field.

In [90] the idea was to obtain the Brillouin gain with a uniform and broadened spectral distribution (dashed red curve in Figure 3.7) by overlap of the individual gain curves and thus achieve a desirable uniform distribution of the group index like that

presented by curve 4 in Figure 3.6 (a) above. The latter was supposed to result in a decreased distortion of the delayed pulses. The authors found that the gain doublet provides a factor of 2 increase in relative delay, though the pulse width used was still of the order of the inverse of the characteristic SBS gain bandwidth in optical fibres. In [89] the authors used the same approach for creation of the dip in the SBS gain profile which has to result in the abnormal dispersion of the medium at the signal frequency and pulse advancement, respectively.

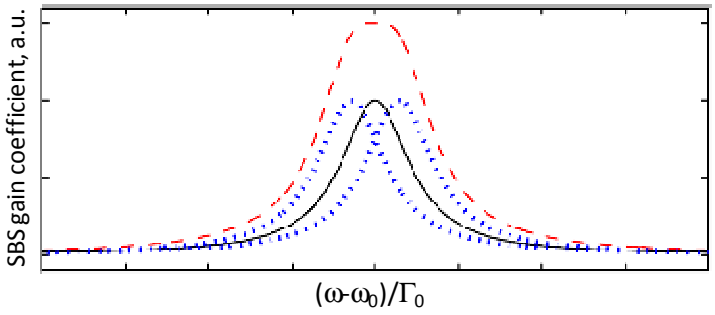

Figure 3.7. Gain contours for single and double Lorentzian lines. Dashed contour is the sum of dotted contours, after [90].

In [83] a bi-chromatic pump was utilized to create a doublet of absorption resonances in the anti-Stokes frequency range to obtain "slow light", that is pulse delay, in the SBS absorption regime. The idea of this experiment mimics that of Camacho [58], mentioned in Appendix 1. According to the authors, the latter is possible, as normal dispersion of refractive index is expected at frequencies situated between the absorption lines; this range of frequencies is referred to as the "slow light bandwidth". The goal of the study was elimination of the delay-dependent amplification of the pulse. In the experiment the pulse carrier frequency was set precisely to the center between the two anti-Stokes absorption resonances. The measured FWHM of a single absorption line in the experiment was 50 MHz, (2 km long highly nonlinear fibre was used as an active medium). The width of the "slow light" bandwidth, B, was adjusted by changing the frequency separation of the pump doublet. The input signal pulses of 9 ns duration were delayed by a maximum of 3 ns. Figure 3.8 shows the delayed pulses and absorption spectra for B ≈ 150 MHz for different values of pump power.

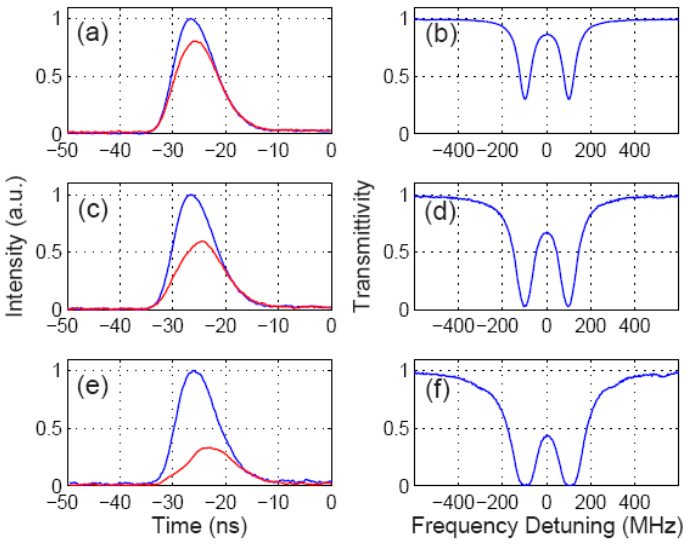

Figure 3.8. (a), (c), (e): Traces of delayed (shown in red) and un-delayed (shown in blue) signal pulses at a pump power of 5 dBm, 10 dBm, and 13 dBm, respectively; (b), (d), (f): Power absorption spectra measured with a CW signal beam at the corresponding pump powers, after [83].

While some improvement of the pulse delay characteristics (magnitude of the relative delay and pulse distortion) was observed in these publications the improvements were below expectations. In a range of similar subsequent experiments various groups attempted to resolve the problems through using more complicated schemes. In particular, in [76] through using a triplet gain the authors showed that the output pulse appeared almost undistorted preserving the same relative delay. In another experiment where a gain triplet was used a 40 ns pulse was delayed by 33 ns, and a reduction of pulse broadening by 30 % was observed in comparison to the case of the single pump. This experimental result is presented in Figure 3.9 [78].

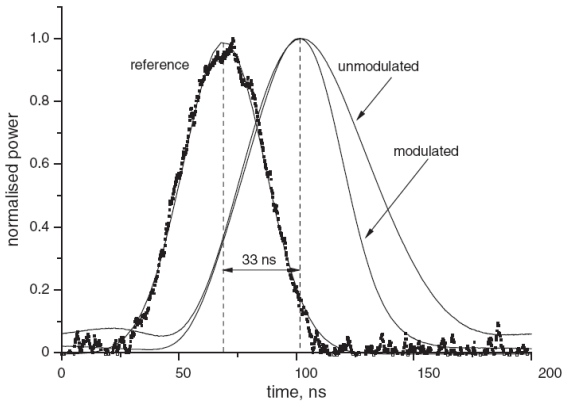

Figure 3.9. Demonstration of pulse broadening reduction in SBS delay process with the use of three-component pump, after [78].

So, use of the set of discrete monochromatic pumps has demonstrated the possibility of some improvement in the performance of the fibre based "SBS slow light devices" through varying the relative amplitude and the separation between pump frequency components. While this approach did not solve the main problem of the SBS based devices, namely narrowness of the bandwidth for real (telecom) applications, these studies created the impression that the dispersive properties of the medium for the Stokes radiation could be tailored by spectral broadening of the pump radiation. For this reason attention was switched to SBS bandwidth enhancement by using continuous broadening of the pump radiation.

3.4.5 Continuous broadening of the pump

In one of the first works promoting continuous pump broadening a smooth broadened SBS gain spectrum with a FWHM of up to 325 MHz was generated by directly modulating the current of the pump laser diode using a pseudo-random bit sequence at 38 Mbit/s [74]. A 6.7-km-long dispersion-shifted fiber with a Brillouin shift, $\Omega_B/2\pi$, of 10.5 GHz and a natural SBS gain bandwidth of ~50 MHz was used. Pulses as short as 2.7 ns were delayed and a maximal delay of 3 ns was achieved. This was a small fraction of the delay achieved using the natural, non-broadened, gain spectrum. However this value was expected, since, according to equation (3.17) the pulse delay is inversely proportional to the SBS bandwidth. The authors also emphasized that the relative delay ($\Delta T_d/\tau_{in} = 1.1$), which is the parameter of interest for real applications, was preserved. We note here that in this work the authors stated that "*to maintain the same absolute delay with extended bandwidth requires the pump power to be raised proportional to the square of the relative spectral broadening and to keep the same normalized delay proportional to the amount of spectral broadening*". All their results are in full agreement with their theory of SBS induced pulse delay.

As a continuation of this work another group [82] modulated the driving current of their pump laser with broadband noise, and broadened the spectrum of pump radiation up to 12 GHz. Delays of 75 ps pulses proportional to *G* were reported (Figure 3.10), and it was concluded that the gain SBS linewidth could be broadened up to the point where the Stokes and anti-Stokes bands start to overlap and mutually neutralize (see Figure 3.11).

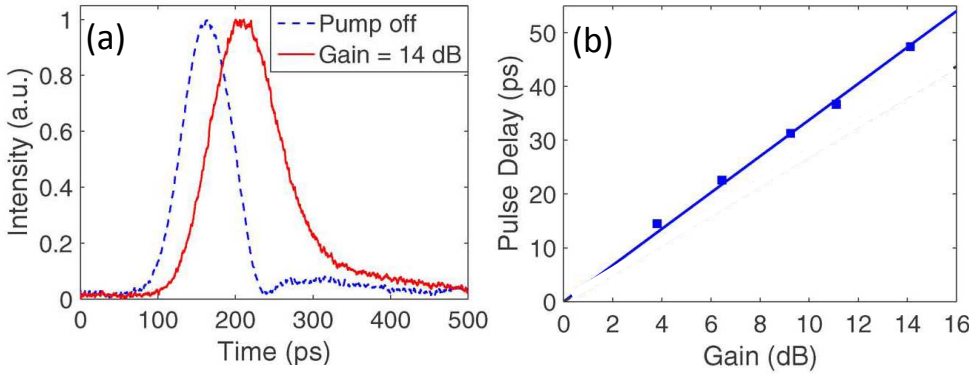

Figure 3.10. Delay of 75 ps pulse in experiment that exploits the SBS gain bandwidth broadened to 12 GHz, after [82].

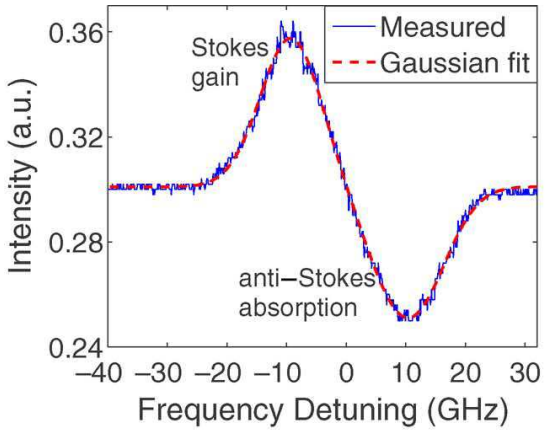

Figure 3.11. Overlap of gain and absorption bands in SBS when wide pump bandwidth is used [82].

This overlapping of absorption and gain spectra at first was considered to be the physical limitation for further extension of the gain spectrum. However as a solution to this problem it was proposed to use an additional pump source separated from the first one by twice the Brillouin frequency shift, Ω_B/π, which is around 20–25 GHz in silica fibres at λ = 1550 nm. The idea was to compensate the loss spectrum in the anti-Stokes frequency region of the lower frequency pump with the gain spectrum of a higher-frequency pump, as shown in Figure 3.12. Such technique of gain-loss compensation was first proposed in [77]. Experimental realization of broadband overcompensation was implemented in [81]. In their experiment the frequencies of the two pump lasers were separated by 21 GHz. Noise-like modulation of 27 GHz bandwidth was applied to each pump source. Each pump propagated in separate fibre to "to avoid the strong four-wave mixing between them". According to the authors the loss spectrum induced by Pump 1 in a 2 km long high-*NA* fibre sample was perfectly cancelled by the gain spectrum induced by Pump 2 in a 6 km DSF sample. The gain spectrum which they

measured is shown in Figure 3.13. Its shape was found to be approximately Gaussian with a linewidth of 27 GHz, and pulses of 37 ps duration were delayed up to 11 ps.

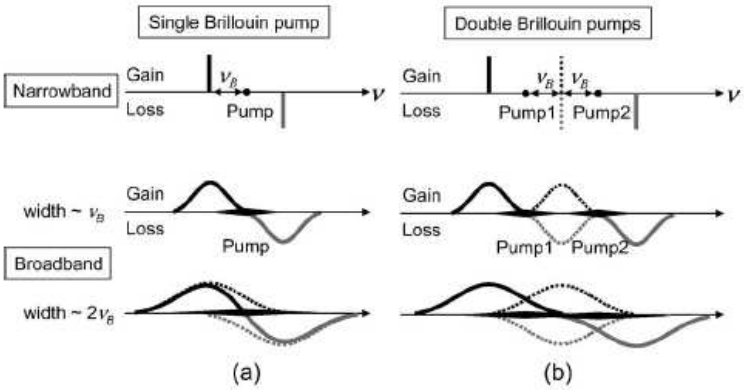

Figure 3.12. Comparison of gain and loss spectra in (a) single and (b) double Brillouin pumps according to narrowband (upper) and broadband (lower) operations, after [81].

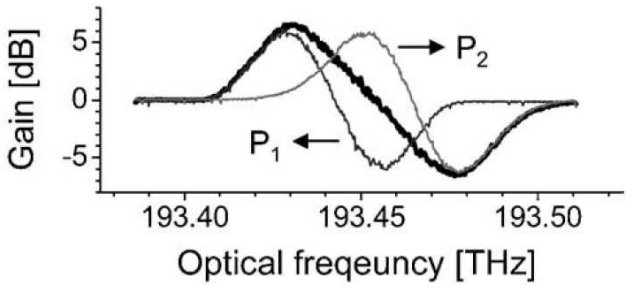

Figure 3.13. Gain-loss spectrum obtained with 27-GHz-modulation of pump sources measured in [81].

It was suggested that with this technique the SBS bandwidth could be further increased by increasing the number of pumps to meet the needs of ultrahigh-data rate optical communications. The only problem discussed on the way of implementing this technique was a substantial increase of the required pump power to maintain the fractional delaying strength when the spectrum of the pump radiation is massively broadened [71].

3.4.6 The problem with pump broadening

At this point it is essential to note the following: the assertion that pump broadening (either discrete or continuous) can be utilized as an effective mean of tailoring the bandwidth of the SBS "slow light" effect is in fact contradicting to the physics of SBS.

1. According to the basic physics of SBS, it is a nonlinear optical interaction. As such the overall spectral width of this interaction cannot be a simple sum of the individual spectral components of pump radiation, as it is supposed in [71, 74].

2. Earlier we highlighted a note in [74] that "to maintain the same absolute delay with extended bandwidth requires an increase in pump power proportional to the square of the relative spectral broadening". This result is a direct consequence of the fact that a broadening of the pump spectrum, $\Delta\nu_p$, leads to the reduction of the SBS gain coefficient, g_B, according to, [72]

$$g_B = \frac{\Delta\nu_B}{\Delta\nu_B + \Delta\nu_P} g_0(\nu_B), \tag{3.27}$$

where $\Delta\nu_B$ is the SBS gain spectral width for a monochromatic pump. Thus for example broadening of a pump power spectrum up to 27 GHz should decrease the SBS gain coefficient by a factor of ~1000, so, to keep a required magnitude of G the pump intensity has to be increased proportionally. Such behaviour has been in fact well known since late sixties, [91], and it has been widely used for suppression of SBS ever since. It seems that this has either been overlooked or ignored in the literature on SBS "slow light".

3. Increase of the pump intensity, as is well known, must unavoidably lead to the appearance of other nonlinear effects. For example the gain, g_R, for stimulated Raman scattering (SRS) in silica fibre, the spectral width of which, $\Delta\nu_R$, is $\geq 10^3$ GHz $\approx 3.10^4\Delta\nu_B$ [20] is ~$0.15g_B$ only [92]. Thus for $\Delta\nu_p > 10\Delta\nu_B$ SRS will overshadow SBS. Also a variety of other nonlinear effects, among which are generation of the harmonics, four-wave mixing self- and cross-phase modulation may appear before SBS in the core of the fiber material when $\Delta\nu_p > 10\Delta\nu_B$ [72]. Therefore attribution of the delays observed in broadband "SBS slow light" to SBS is far from straightforward.

3.5 Conclusion

This chapter has reviewed the milestone works in the field of SBS "slow light". Hopefully it has provided the reader with a feel of how the field was developed, what problems were discovered and what solutions have been proposed. The review has also

drawn attention to some rather serious inconsistencies which we have found on analyzing these works more deeply.

Thus we have found ourselves in a difficult situation. On the one hand there is widespread belief that experimental observations of the pump induced Stokes pulse delay in the SBS interaction results from the group velocity effect, and this interpretation is the correct and only possible explanation of the SBS-induced delay phenomena. This belief is supported by several examples where the performance of SBS-based delay lines were successfully tested in real systems [93-98].

On the other hand the theoretical model is mathematically questionable and the experimental practice of realizing the SBS-induced delay contradicts the physics of the SBS phenomenon. The main contradictory points are the following:

1). incorrect Fourier-transform of the basic coupled equations for the slowly varying amplitudes of the Stokes and acoustic fields and, consequent introduction of effective refractive and group indices for the Stokes radiation; which in fact is negligible;

2). derivation of the expression for pulse delay using the SBS equations in the steady-state approximation, which, by definition, is only valid for fully monochromatic interactions;

3). consideration of the SBS parametric gain as a material gain;

4). use of experimental arrangements (long fibres), for which the conventional coherent SBS formalism does not apply;

5). use of broadening of the pump spectrum as a mean of extending the SBS bandwidth whereas it suppresses the SBS.

In the next two chapters I will give a more physically adequate interpretation and theoretical model of SBS-induced Stokes pulse delay which is fully consistent with the physics of SBS, the results from which will be tested through experiments.

Chapter 4.

Theory of Stokes pulse amplification in a CW-pumped SBS medium

4.1 Introduction

This Chapter presents a rigorous theoretical treatment of the basic coupled equations for the amplitudes of the Stokes field and of the material density variation in SBS and their analytic solutions in frequency and time domains. On the basis of frequency domain solutions we show that the acoustic resonance has next to no effect in enhancing or modifying the natural refractive index and its dispersion in the medium for the Stokes signal. Furthermore the effect of pump broadening on the spectrum of the excited acoustic wave and Stokes pulse is explained. Solutions in the time domain provide the dynamics of Stokes pulse amplification and from this reveal the nature of Stokes pulse delay.

4.2 Spectral characteristics of waves generated in the SBS interaction

4.2.1 Conversion of basic coupled SBS equations to the frequency domain

To start our discussion we recall, from Chapter 3, equations (3.6) and (3.7) for $E_S(z,t)$, and $\delta\rho(z,t)$,

$$\frac{\partial E_S}{\partial z}+\frac{n}{c}\frac{\partial E_S}{\partial t}=-i\frac{\omega_S}{2cn}\frac{\partial \varepsilon}{\partial \rho}\delta\rho^{*}(z,t)E_p(t), \tag{4.1}$$

$$\frac{\partial \delta\rho}{\partial t}+\left(\frac{\Gamma_B}{2}+i\delta\Omega\right)\delta\rho=-i\delta\rho_0\frac{\partial \varepsilon}{\partial \rho}\frac{\Omega_B}{8\pi v_s^2}E_p(t)E_S^{*}(z,t). \tag{4.2}$$

These are the main coupled nonlinear equations that describe the field amplitudes in SBS in the usual slowly varying amplitude approximation and in the limit that the pump signal is not depleted. Here $\delta\Omega = \Omega - \Omega_B$ is the difference between the pump and Stokes fields beat frequency, Ω, and the resonant Brillouin frequency, Ω_B. In Chapter 3 we drew the readers' attention to an incorrect Fourier transform of these equations implemented in one of the first publications of SBS "slow light", which has since been perpetuated throughout the literature in this field. Let us actually perform the Fourier-transform treatment with due care. By definition a Fourier-transform is

$$S[f(t)] = \int_{-\infty}^{\infty} f(t) e^{-i\omega t} dt = F(\omega). \tag{4.3}$$

We will use the following properties of Fourier transforms, [99, 100]

$$S[\frac{d}{dt} f(t)] = i\omega F(\omega), \;\; S[f(t) e^{i\omega_0 t}] = F(\omega - \omega_0), \tag{4.4}$$

$$and \;\; S[f_1(t) f_2(t)] = \frac{1}{2\pi} \int_{-\infty}^{\infty} F_1(\nu) F_2(\omega - \nu) d\nu, \tag{4.5}$$

where $f(t)$ is a function of time, which will be used in the subsequent treatment. Here ω and ν are Fourier transform frequency variables. Fourier transform of Eqs (4.1) and (4.2) then gives

$$\frac{d\tilde{E}_S(z,\omega)}{dz} + i\omega \frac{n}{c} \tilde{E}_S(z,\omega) = -i \frac{\omega_S}{2cn} \frac{\partial \varepsilon}{\partial \rho} \frac{1}{2\pi} \int_{-\infty}^{\infty} \tilde{E}_p(\nu) \delta\tilde{\rho}^*(z, \omega - \nu) d\nu \tag{4.6}$$

and

$$\left(\frac{\Gamma_0}{2} - i(\omega + \delta\Omega) \right) \delta\tilde{\rho}^*(z,\omega) = i\rho_0 \frac{\partial \varepsilon}{\partial \rho} \frac{\Omega_B}{8\pi v_s^2} \frac{1}{2\pi} \int_{-\infty}^{\infty} \tilde{E}_p'^*(\nu) \tilde{E}_S'(z, \omega - \nu) d\nu, \tag{4.7}$$

where symbol ~ above $\delta\rho$ and E_S denotes the Fourier-transform.

By their physical meaning ω and ν are the frequency components of the acoustic, Stokes and pump signals spectra, which are centered around zero for slowly varying amplitudes and around absolute line center frequencies Ω_B, ω_S and ω_p respectively for the fields. In other words Ω_B, ω_S and ω_p are the absolute frequencies of the interacting

fields and ω and ν are the relative frequencies of the Fourier transform, which are zero at Ω_B for the acoustic wave, at ω_S and ω_p for Stokes and pump signals respectively.

First of all we note two differences between these equations and equations (3.8) and (3.9) obtained in [70]. 1). In our equations we prime the Stokes and pump fields within the right hand side (RHS) of equation (4.7), which are responsible for inducing the acoustic wave, to distinguish them from the pump field (the field $\tilde{E}_p(\omega)$ under the integral in equation (4.6)), which is reflected by the acoustic wave, to so generate the new Stokes field described by the RHS of equation (4.6). 2). The frequency variable ω here, we emphasize again, is neither the optical nor acoustic frequency involved in the SBS interaction. We also stress again that $\delta\Omega$ in equation (4.7) is a detuning parameter, which denotes the difference between the frequency, Ω, of the beat pattern of the pump and Stokes fields on the RHS of equation (4.7) and Ω_B. (In the case of non-monochromatic pump and Stokes fields $\delta\Omega$ can be considered as the difference between the central frequencies of their spectra).

As seen, the right-hand sides of equations (4.6) and (4.7) are proportional to the convolution integrals of spectra $\tilde{E}_p(\omega)$ and $\delta\tilde{\rho}^*(z,\omega)$ in equations (4.6) and $\tilde{E}'_P(\omega)$ and $\tilde{E}'_S(z,\omega)$ in equations (4.7) respectively. Equation (4.7) is an algebraic equation, the solution of which gives the expression for the spectral amplitude of the medium's response,

$$\delta\tilde{\rho}^*(z,\omega) = i\rho_0 \frac{\partial\varepsilon}{\partial\rho} \frac{\Omega_B}{8\pi v_s^2} \frac{F_\rho(z,\omega)}{(\Gamma_0/2 - i(\omega + \delta\Omega))}, \tag{4.8}$$

where

$$F_\rho(z,\omega) = \frac{1}{2\pi} \int_{-\infty}^{\infty} \tilde{E}'^*_p(\nu)\tilde{E}'_S(z,\omega-\nu)d\nu \tag{4.9}$$

is the function which determines the spectrum of the driving force for the medium's response.

The Stokes field spectral amplitude is described by the conventional first order differential equation, equation (4.6), the analytic solution of which is [101]

$$\tilde{\mathrm{E}}_S(z,\omega) = e^{-i\frac{\omega n}{c}z}\left[\tilde{\mathrm{E}}_S(0,\omega) + i\frac{\omega_S}{2nc}\frac{\partial\varepsilon}{\partial\rho}\int_0^z F_E(x,\omega)e^{i\frac{\omega n}{c}x}dx\right], \qquad (4.10)$$

where $\tilde{\mathrm{E}}_S(0,\omega)$ is the spectrum of an input Stokes signal at z = 0 and

$$F_E(z,\omega) = \frac{1}{2\pi}\int_{-\infty}^{\infty}\tilde{\mathrm{E}}_{\mathrm{P}}(\nu)\delta\tilde{\rho}^*(z,\omega-\nu)d\nu \qquad (4.11)$$

is the function which determines the spectrum of the source of the generated Stokes field. Equations (4.8-11) describe the spectral features of the SBS-induced material response and Stokes field when both optical fields, pump and Stokes, *are non-monochromatic*.

The spectra of the medium's response and of the Stokes signal are then given by the moduli of $\delta\tilde{\rho}^*(z,\omega)$ and $\tilde{\mathrm{E}}_S(z,\omega)$. In particular the spectrum of the Stokes signal is

$$\left|\tilde{\mathrm{E}}_S(z,\omega)\right| = \left|\left[\tilde{\mathrm{E}}_S(0,\omega) + i\frac{\omega_S}{2nc}\frac{\partial\varepsilon}{\partial\rho}\int_0^z F_E(x,\omega)e^{i\frac{\omega n}{c}x}dx\right]\right| \qquad (4.12)$$

It is easy to see that the equations (4.6) and (4.7) and solutions (equations (4.8-11)) for $\delta\tilde{\rho}^*(z,\omega)$ and $\tilde{\mathrm{E}}_S(z,\omega)$ differ substantially from those usually discussed in textbooks [67, 69, 72]. The nature of this difference is that in the latter the SBS interaction is considered in the steady state approximation, which means that the temporal derivatives in equations (4.1) and (4.2) are set to zero. Physically this means that both input pump and Stokes fields are considered *monochromatic*. Consequently, according to Eqs (4.9) and (4.11) above, the induced acoustic wave and generated Stokes field have to be also monochromatic, and so the equation for the Stokes field and its solution are transformed to the well known textbooks expressions,

$$\frac{d\mathrm{E}_S(z)}{dz} = \left[\frac{g_0\left|\mathrm{E}_p\mathrm{E}_p^*\right|}{2(1-i2\delta\Omega\Gamma_0^{-1})}\right]\mathrm{E}_S(z) \qquad (4.13)$$

and

$$E_S(z) = E_S(0)\exp\left[\frac{g_0\left|E_p E_p^*\right|z}{2(1-i2\delta\Omega\Gamma_0^{-1})}\right]. \qquad (4.14)$$

Here it is again important to remember that $\delta\Omega$ is a detuning parameter, which denotes the difference between the frequency, Ω, of the beat pattern of the monochromatic pump and Stokes fields ($\Omega = \omega_p - \omega_S$) and Ω_B. In these equations $|E_pE_p^*|$ is the pump radiation intensity, and g_0 is the parameter, which is conventionally called the resonant steady state SBS gain coefficient. From equation (4.14) it immediately follows, as is well known, that a monochromatic Stokes field is amplified in the medium with an exponential gain, which is proportional to the intensity of monochromatic pump radiation and the interaction length z.

To appreciate the difference between this textbook description and that described here we must emphasise that the order of three field amplitudes on the RHS of the equation for the Stokes field (equation (4.1) above) is not arbitrary. The sequence of the field multiplication is firmly fixed by the fact that the variation of material's density is induced by the interference pattern of the pump, E_p', and Stokes fields, E_S', (equation (4.2) above) and that the newly generated Stokes field, E_S, results from reflection of the pump field by that induced density variation. The equation for the generated Stokes field E_S is then,

$$\frac{dE_S(z)}{dz} = \left[\frac{g_0(E_p'^* E_S'(z))}{2(1-i2\delta\Omega\Gamma_0^{-1})}\right]E_p, \qquad (4.15)$$

where the field multiple $(E'_p{}^*E'_S(z))$ appears here from the equation for the density variation. The Stokes field on the RHS of equation (4.15) which is responsible for creating the acoustic wave is not the same as the reflected Stokes field on the LHS of this equation, the former of which is distinguished by its prime. The only physical condition when equation s (4.13) and (4.15) can be mathematically the same is when the pump and Stokes fields in these equations are *monochromatic*. This does not however remove the difference in the physical meaning of equation (4.15) and equation (4.13). When such distinction is not made, as in the text-book treatment, one has equation (4.13) and its familiar exponential solution, equation (4.14)**,** which is characterized by the "SBS gain". It is this "gain" that is widely considered to have similar properties to

those of conventional material gain (due to population inversion for example). Consequently such gain, it is claimed, must be accompanied by a corresponding dispersion of the refractive index, which in turn results in modification of the group index [19, 65]. However, there is a detail in this logic which is profoundly inconsistent with this claim. Since $\delta\Omega$ results from the difference of the monochromatic frequencies of the Stokes and pump fields, the spectra of the amplitudes of the generated Stokes field and of the medium's response reduce to δ-functions ($\omega = 0$) and expression ($1 - i2\delta\Omega/\Gamma_0$) is simply a complex number (not a function).

A direct consequence of the generic difference between equations (4.13) and (4.15) is that the solution of equation (4.15) does not necessary give exponential growth of the generated Stokes field, $E_S(z)$. This fact is explicitly demonstrated by the solutions in equations (4.8-11) when pump and/or Stokes fields are non-*monochromatic* which we now consider in the next section.

4.2.2 Spectral characteristics of the output Stokes field

The solution for the Stokes field, equations (4.10) and (4.11), for the case in which either one or both of the fields have nonzero bandwidth demonstrates three important features of the SBS interaction: i) the spectral components of an external input Stokes signal, as shown by the first term on the RHS of equation (4.10), propagates through a non-absorbing medium without gain or measurable loss (its energy loss for creating the acoustic wave is usually negligible), ii) the spectral components of the SBS-amplified Stokes signal (the second term on the RHS of equation (4.10)) are the result of reflection of the pump radiation by the acoustic wave, which is created by the pump and the original Stokes fields (see equations (4.8) and (4.9)), and iii) each spectral component of the amplified Stokes signal arises from a range of spectral components of the non-monochromatic pump and Stokes fields according to equations (4.8-11). It also follows from these equations that the output spectrum of the Stokes signal, $\left|\tilde{E}_S(\omega)\right|$, is the sum of the spectra of the input Stokes signal, $\left|\tilde{E}_S(0,\omega)\right|$, and the convoluted spectrum of the pump field and the medium's excitation, the characteristics which are described by the function $F_E(\omega)$ (see equation. (9)). The latter is the SBS-induced contribution to the Stokes signal, and is determined by which of $\tilde{E}_p(\omega)$ and $\delta\tilde{\rho}^*(\omega)$ is spectrally the broadest.

4.2.3 Spectral characteristics of the generated acoustic wave

Let us now consider spectral characteristics of the medium's response, which are described by $|\delta\tilde{\rho}(z,\omega)|$. According to equations (4.8) and (4.9) they are described by the modulus of the convolution integral, $|F_\rho(z,\omega)|$, multiplied by a Lorentzian shape function of bandwidth Γ_0,

$$|\delta\tilde{\rho}(z,\omega)| = \rho_0 \frac{\partial\varepsilon}{\partial\rho}\frac{\Omega_B}{8\pi v_s^2}\frac{|F_\rho(z,\omega)|}{\sqrt{\Gamma_0^2/4+(\omega+\delta\Omega)^2}}. \qquad (4.16)$$

Examples of the spectra $|\delta\tilde{\rho}(z,\omega)|$ are shown in Figure 4.1 by solid curves for $\delta\Omega$ = 0 (Figure 4.1(a)) and $\delta\Omega$ = 0.1 GHz (Figure 4.1(b)).

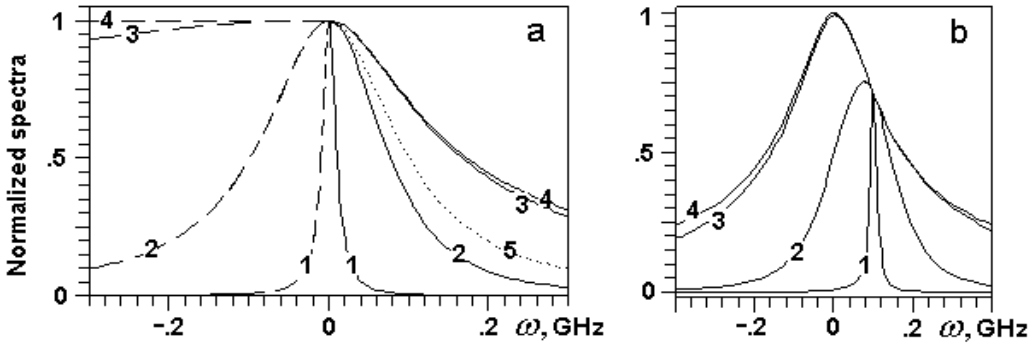

Figure 4.1. (a), LHS and RHS halves of the (symmetrical) spectra of the driving force,$|F_\rho(z,\omega)|$, (dashed) and of the induced acoustic wave, $|\delta\tilde{\rho}(z,\omega)|$, (solid lines) respectively for spectral widths $\delta\omega_\rho$, of $|F_\rho(z,\omega)|$ 0.02(1), 0.2(2), 2(3) and 20(4) GHz, when Γ_0 = 0.2 GHz and $\delta\Omega$ = 0. The dotted line 5 is the Lorentzian-shaped spectrum with Γ_0 = 0.2 GHz; (b), spectra of $|\delta\tilde{\rho}(z,\omega)|$ for the same spectral widths of $|F_\rho(z,\omega)|$ when $\delta\Omega$ = 0.1 GHz.

Figure 4.1(a) is composed of two halves: the LHS depicts the spectra of the driving force, $|F_\rho(z,\omega)|$, (dashed lines) and the RHS shows the corresponding spectra of the induced acoustic wave, $|\delta\tilde{\rho}(z,\omega)|$. It follows from Figure 4.1(a) that when the spectral width (FWHM), $\delta\omega_\rho$, of $|F_\rho(z,\omega)|$ (which results from the convolution of $\tilde{E}_p^{'*}(z,\omega)$ and $\tilde{E}_S^{'}(z,\omega)$ as given in equation (4.9)), is narrower than Γ_0, then the shape, the FWHM width, Γ, and the centre frequency of the medium's response spectrum are determined by $|F_\rho(z,\omega)|$, the central frequency of which is detuned by $\delta\Omega$ as shown by curve 1 in Figure 4.1(b). Nonzero detuning $\delta\Omega$ results also in decreased amplitude of the

medium's response (compare solid curves 1 and 2 of Figures 4.1(a) and 4.1(b)). As $\delta\omega_\rho$ increases, Γ grows, but this growth does not follow the increase of $\delta\omega_\rho$. In particular, $\Gamma < \Gamma_0$ when $\delta\omega_\rho = \Gamma_0$ (compare solid curve 2 dotted curve 5 in Figure 4.1(a)), and when $\delta\omega_\rho >> \Gamma_0$ it saturates at ~$1.7\Gamma_0$ (solid curves 3 and 4 in Figure 1). It also follows from Figure 4.1(b) that the effect of the detuning, $\delta\Omega$, on the features of the medium's response spectrum becomes negligible when $\delta\omega_\rho >> \Gamma_0$ (compare solid curves 3 and 4 in Figure 4.1(b)).

Thus these results show that, when the spectral width of the driving force $\delta\omega_\rho >> \Gamma_0$, the bandwidth of the material response spectrum is predominantly determined by the features of the material and it can never be much greater than that of the medium's resonant response bandwidth (~Γ_0) irrespective of how broad the bandwidth of the broadband pump and/or Stokes emission is/are. This is exactly the feature known from the physics of an externally driven damped oscillator [102]. Equation (4.2) for $\delta\rho$ is just the equation of such an oscillator with the expression on the RHS being the driving force, where $\delta\Omega$ only influences the strength of the medium's response to the drive force at frequency Ω (see Figure 4.1(b)).

4.2.4 Modification of the refractive index in SBS

Now let us consider what changes will be experienced by the refractive index of the material, n, which is $Re[\varepsilon(\omega)]^{1/2}$, in the SBS interaction. This interaction conventionally takes place in an optical transparency region in a medium, which means that both ω_p and ω_S are far away from the frequency of the fundamental material absorption resonance, $\omega_0 \approx 10^{16}$ Hz (see Figure 4.2). In the frame of the atomic model, as a coupled electron decaying oscillator, [103], the shape of this resonance is Lorentzian (see the RHS part of the spectrum in Figure 4.2). Its spectral FWHM width, $2\gamma \approx 10^{15}$ Hz, is determined by the energy losses of the oscillating electron, and its amplitude is determined by the multiple of the oscillator strength, $f(\omega)$, and the density of oscillators (otherwise the medium's density), ρ. It is this resonance that determines the complex dielectric constant of a medium, $\varepsilon(\omega) = \varepsilon'(\omega) + i\varepsilon''(\omega) = D[f'(\omega) + if''(\omega)]\rho$, where D is a coefficient. The real and imaginary parts of $\varepsilon(\omega)$, which are $\varepsilon'(\omega)$ and $\varepsilon''(\omega)$, are not independent but are coupled through the Kramers-Kronig relations [73].

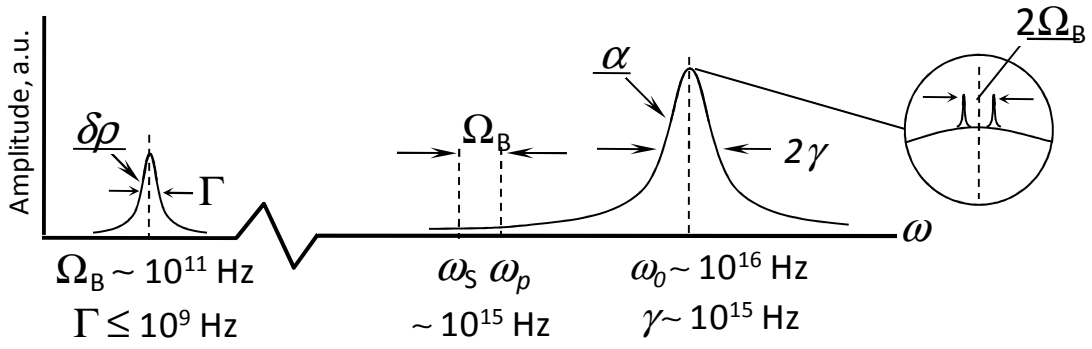

Figure 4.2. The schematic sketch of spectra of the medium's fundamental absorption resonance and of the induced acoustic wave in the SBS interaction.

According to the basic wave equation of SBS describing the Stokes field (equation (3.1)), this field, generated at frequency ω_S, is the pump field at frequency ω_p converted into the Stokes field due to modulation of the dielectric constant by the acoustic wave through modulation of the medium's density, $\delta\varepsilon(\omega) = (\partial\varepsilon/\partial\rho)\delta\rho(\omega) \equiv D[f'(\omega) + if''(\omega)]\delta\rho(\omega)$. The acoustic wave of frequency Ω_B in the SBS interaction is excited in the medium through electrostriction by the beat field of the pump and Stokes waves ($\omega_p - \omega_S = \Omega_B$). According to equation (4.8) an absolute value of the density variation in typical fibre SBS experimental conditions (pump power is of ~(0.1-1)W, fibre length is of ~(0.1-1) km) is less than $\sim 10^{-7}$ g/cm^3 <<< ρ_0, where ρ_0 is the undistorted density. The spectrum of its amplitude and typical magnitudes of its characteristic parameters are given in the LHS spectrum in Figure 4.2. Since $\delta\rho(\omega)$ is a complex function (see equation (4.8)) $\delta\varepsilon(\omega)$ is also complex. Therefore in the SBS interaction we have a medium which is characterised by a conventional complex dielectric constant, $\varepsilon(\omega)$, which is a property of an ensemble of atomic oscillators with resonant frequency ω_0, the concentration of which is modulated at the acoustic frequency Ω_B. By taking the density of the medium for this case as $\rho \cong \rho_0 + \delta\rho(\omega)\exp(-i\Omega_B t)$ we can write

$$\begin{aligned}\varepsilon(\omega) &= D[f'(\omega) + if''(\omega)][\rho_0 + \delta\rho'(\omega) + i\delta\rho''(\omega)] = \\ &= \varepsilon_0(\omega) + D\{f'(\omega)\delta\rho'(\omega) - f''(\omega)\delta\rho''(\omega) + i[f''(\omega)\delta\rho'(\omega) + f'(\omega)\delta\rho''(\omega)]\}.\end{aligned} \tag{4.17}$$

where $\varepsilon_0(\omega)$ is the dielectric constant of the undistorted medium. From examining equation (4.17) one can understand that the SBS induced contribution to the dielectric constant due to density variation is very small. This contribution appears at the beat

frequencies $\omega_0 \pm \Omega_B$ between the acoustic wave, with frequency Ω_B and the resonant frequency ω_0. Using equation (4.17) it is possible to estimate the dispersion of the medium's absorption coefficient, $\alpha(\omega) = (\omega/c)Im[\varepsilon(\omega)]^{1/2}$, and refractive index, $n(\omega) = Re[\varepsilon(\omega)]^{1/2}$, which include the contribution from the SBS interaction. In dielectrics, where conventionally $\varepsilon\,'(\omega) > \varepsilon\,''(\omega)$, these parameters are $\alpha(\omega) \approx \approx (\omega/c)[\varepsilon''(\omega)]/\{2[\varepsilon\,'(\omega)]^{1/2}\}$, and $n(\omega) \approx [\varepsilon'(\omega)]^{1/2}$.

The encircled insert on the LHS part of Figure 4.2 shows the spectrum of the medium's fundamental absorption in the vicinity of ω_0 with the SBS induced spectral peaks located at frequencies $\omega_0 \pm \Omega_B$. It is easy to show that since both $\delta\rho'(\omega)$ and $\delta\rho''(\omega)$ are <<< ρ_0 the magnitude of the SBS induced absorption or gain (conventionally ~10^{-3}-10^{-4} cm^{-1}) is minute compared to the medium's fundamental absorption (≥10^4 cm^{-1} at ω_0) at all frequencies including that at frequencies $\omega_0 \pm \Omega_B$.

Figure 4.3 shows a schematic of the spectra of the square of the medium's refractive index, $n^2 \approx \varepsilon'(\omega)$, and of the refractive index variation, $\Delta n^2 = \delta\varepsilon(\omega) = (\partial\varepsilon/\partial\rho)\delta\rho(\omega)$, induced by the acoustic wave. The former has a typical shape which follows from the Lorentz-Lorenz model with the oscillator attenuation taken into consideration [103]. It follows from this model that $n^2 > 1$ at all frequencies from 0 to ω_0, that $n^2 = 1$ at the frequency ω_0 and that $n^2 < 1$ at all frequencies higher than $\omega_0 + \delta$, where δ is a positive value. The SBS induced variation of dielectric constant contributes to the normal refractive index of the medium mostly at and in the vicinity of frequencies Ω_B and $\omega_0 \pm \Omega_B$. The magnitude of this contribution is small even at these

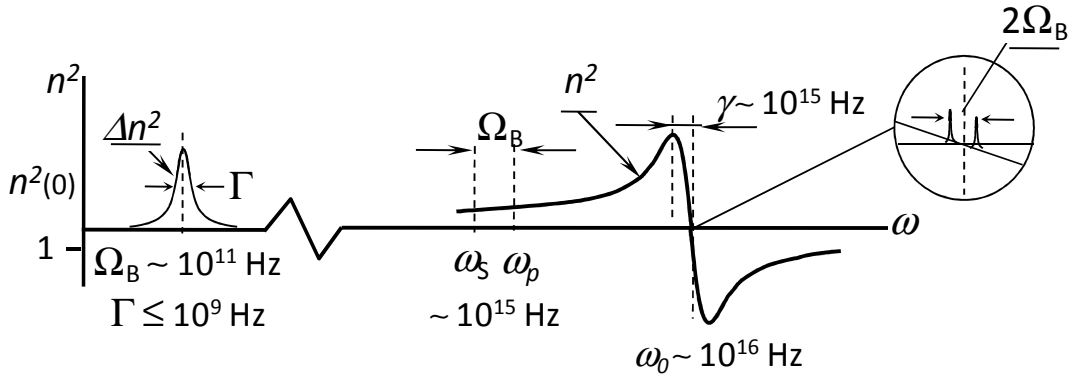

Figure 4.3. The schematic sketch of spectra of the medium's refractive index, n, and of the induced by the acoustic wave refractive index variation, Δn^2.

resonances, and is really negligible at both ω_p and ω_S. It is important to note here that the shape of the spectrum of Δn^2 at Ω_B is radically different from that of n^2 in the vicinity of ω_0. This is a consequence of the imaginary multiple "*i*" in the numerator of the RHS in equation (4.10).

4.2.5 Conclusions from section 4.2

From the studies presented in this section it follows that:

1. Spectral broadening of pump radiation by any reasonable amount greater than Γ_0 results in only a minute increase of the spectral width of the material's resonant response in SBS.

2. The enhancement of the density variation amplitude at the wave resonance (i.e. when the velocity of the interference pattern of pump and Stokes optical waves equals to the velocity of the acoustic wave) has next to no effect in enhancing or modifying the natural group index and its dispersion in the medium for the Stokes signal because of
    a. the small amplitude of its density variation compared to the undistorted medium's density, and
    b. this resonance is far away from the Stokes optical signal frequency to be delayed.
3. Since the SBS-induced changes of refractive index at and around the Stokes frequency are minute, there is no resonant enhancement of the group index and thus delay of the output Stokes pulse cannot be attributed to the enhanced group velocity ("slow light") effect. However since such delays are nevertheless observed experimentally the question arises about the nature of this delay. The underlying physical process that gives rise to Stokes pulse delay in SBS and its theoretical description are addressed in the next section.

4.3 Temporal characteristics of the output Stokes field in SBS: Stokes pulse delay and inertia of the acoustic wave

We start by noting that the dominating approach in the theoretical treatment of Stokes pulse amplification via SBS is based on the use of Fourier transforms, as described in the previous section. This approach has been proven to be efficient in describing spectral, energy and some other characteristics of the SBS interaction. There

is however a fundamental obstacle in applying this technique for describing the temporal dynamics of this interaction through reverting the solutions from the spectral to the time domain. The reason for this is that there is no method for obtaining a uniquely determined solution of the inverse Fourier integral transform in the case of non-monochromatic spectra, because the phase relationship between the monochromatic components is not known. Among the two remaining options for obtaining a result, namely numerical and analytic solution of the set of dynamic equations, equations (4.1) and (4.2), the latter is definitely preferable, where possible, and it is presented below.

4.3.1 An analytical solution of the basic coupled equations in the time domain

Let us start here with the reminder that the gain for Stokes emission in SBS, by its physical nature, is a consequence of reflection of the pump radiation by an enhanced variation of density in a medium, $\delta\rho$(z,t), which is induced by an electrostrictive force resulting from interference of the pump and Stokes emission fields. The evolution of the slowly varying amplitude of the Stokes field, E_S(z,t), in a medium is described by equations (4.1) and (4.2). Since in typical SBS-based Stokes pulse delay experiments the CW pump power is kept below the value at which the SBS interaction begins to cause pump depletion, it remains constant throughout the interaction length (in lossless media). This is also the reason why spontaneous scattering is not taken into consideration. The set of equations (4.1) and (4.2) with appropriate initial and boundary conditions is therefore sufficient for describing the evolution of a Stokes pulse in a medium.

To proceed further it is useful to introduce the new temporal coordinate, $t' = t - zn/c$. We also suppose that the centre frequency of the Stokes pulse spectrum coincides with the resonant Brillouin Stokes frequency, that is $\delta\Omega = 0$. In terms of the new variables equations (4.1) and (4.2) can be rewritten as

$$-\frac{\partial \mathrm{E}_S}{\partial z} = -i\frac{\omega_S}{2cn}\frac{\partial \varepsilon}{\partial \rho}(\rho'(z,t'))*\mathrm{E}_p \tag{4.18}$$

and

$$\frac{\partial \rho'}{\partial t'} + \frac{1}{\tau}\rho' = -i\rho_0\frac{\partial \varepsilon}{\partial \rho}\frac{\Omega_B}{8\pi v^2}\mathrm{E}_p\mathrm{E}_S^*(z,t'). \tag{4.19}$$

It is remarkable that this set of equations has an analytic solution, which can be obtained using Reimann's method [104-106]. We consider a typical Stokes pulse delay experiments in optical fibre, in which the duration of the pulse is much less than its transit time in the medium and the pump is CW monochromatic radiation. If there are no acoustic waves in the medium before a Stokes pulse enters, and $E_S(t' \leq 0) = 0$, $E_S(z=0,t') = E_{S0}(t')$ and $E_p(z,t') \equiv E_p = \text{const}$, the solutions of equations (4.18) and (4.19) for the Stokes field and the density variation are, [107],

$$E_S(z,t') = E_{S0}(t') + \frac{gI_p z}{\tau}\int_0^{t'}\left(e^{-\frac{t'-\vartheta}{\tau}}\right)\left[I_1\left(\sqrt{2gI_p z\frac{t'-\vartheta}{\tau}}\right)\Big/\left(\sqrt{2gI_p z\frac{t'-\vartheta}{\tau}}\right)\right]E_{S0}(\vartheta)d\vartheta \quad (4.20)$$

and

$$\rho'(t') = -i\rho_0\frac{\partial\varepsilon}{\partial\rho}\frac{\Omega_B}{8\pi\tau v^2}E_p\int_0^{t'}\left(e^{-\frac{t'-\vartheta}{\tau}}\right)I_0\left(\sqrt{2gI_p z\frac{t'-\vartheta}{\tau}}\right)E_{S0}^*(\vartheta)d\vartheta. \quad (4.21)$$

Here $I_p = |E_p|^2$ is the pump radiation intensity in [W/cm^2], g is the SBS gain coefficient in [cm/W], and $I_{0,1}(X)$ are the Bessel functions of imaginary argument X, and g is the SBS gain coefficient,

$$g = 10^7\frac{\omega_S^2\rho_0\tau}{4nc^3v_s}\left(\frac{\partial\varepsilon}{\partial\rho}\right)^2\ [cm/W]. \quad (4.22)$$

Equation (4.20) displays three important features of the SBS interaction:

i) the externally prepared input Stokes signal (the first term on the RHS of equation (4.20)) propagates through a non-absorbing medium without any additional delay, gain or measurable loss (its energy losses for creating the acoustic wave is usually negligible),

ii) the SBS-generated output Stokes signal (the second term on the RHS of equation (4.20)) is a result of reflection of the pump radiation by the acoustic wave, which is created by the pump and the original Stokes fields according to equation (4.21), and

iii) since the contribution of the input Stokes signal to the second term on the RHS of equation (4.20) is integrated in time from its beginning ($t' = 0$) to the given moment t', the first and second terms are generically incoherent.

Following iii) the Stokes radiation intensity, $I_S(t) \sim |E_S(t)|^2$, at the medium's output is the sum of corresponding intensities,

$$\mathrm{I}_S(L,t') = \mathrm{I}_{S0}(L,t') + \left| \frac{G}{\tau} \int_0^{t'} \left(e^{-\frac{t'-\vartheta}{\tau}} \right) \left[I_1\left(\sqrt{2G\,\frac{t'-\vartheta}{\tau}} \right) \Big/ \left(\sqrt{2G\,\frac{t'-\vartheta}{\tau}} \right) \right] \mathrm{E}_{S0}(\vartheta)\, d\vartheta \right|^2 \qquad (4.23)$$

It is interesting to compare solutions for the spectral amplitudes of the Stokes field and density variation (equations (4.8-11)) and the dynamic solutions (equations (4.20) and (4.21). The only direct similarity between the two is that the solutions for the Stokes field consists of two terms, the first of which is the input Stokes pulse transmitted without any amplification, delay and distortion. The second terms in equations (4.10) and (4.20) and the terms in equations (4.8) and (4.21) are obviously different. More importantly, equations (4.20-21) do not follow from equations (4.8-11)**.** The latter is a clear manifestation of the fact noted above that there is no method for obtaining a uniquely determined solution of the inverse Fourier integral transform in the case of non-monochromatic spectra.

4.3.2 Dynamics and spectrum of the acoustic wave amplitude

It is important to remember that with the direct Fourier transform the spectral characteristics naturally follow from the solutions in time domain. To see this let us consider in more detail the solution for the density variation given by equation (4.21). This consideration will help us to understand the underlying nature of the Stokes field behaviour described above. Though equation (4.21) is quite complicated it may be simplified in the limit of small gain, $G < 1$, so that the Bessel function $I_0(\mathrm{x})$ can be set to unity. While this approximation does not allow us to describe gain narrowing of the SBS spectrum typical for higher G [108], it still captures reasonably well the trends in the temporal and spectral features of ρ', which determine those of the SBS gain and modified refractive index.

Consider the input Stokes pulse, the time-dependent intensity envelope of which is given by

$$\mathrm{I}_S(z=0,t) = \left|\mathrm{E}_S(z=0,t)\right|^2 = \mathrm{I}_{S0}(3.5t/t_p)^2 e^{-3.5t/t_p} \qquad (4.24)$$

where I_{S0} is the intensity at the peak of the input Stokes pulse and t_p is its FWHM duration. The shape of such pulse is shown in Figures 4.4 and 4.5 (curves for $G = 0$) and it is a good approximation for pulses actually used in experiments [109]. Such a

shape is more appropriate to theoretical modeling compared to the Gaussian, which is traditionally used in the literature, because it has zero amplitude at $t = 0$. When $I_0(x) = 1$, the integral in equation (4.21) can be taken for $E_{S0}(t)$ given by equation (4.24). It results in the following analytic expression for $\rho'(t)$,

$$\rho'(t) = A\left\{\frac{2}{(2b-\tau)^2}\left[2\tau b\left(e^{-\frac{t}{\tau}} - e^{-\frac{t}{2b}}\right) + (2b-\tau)te^{-\frac{t}{2b}}\right]\right\}, \qquad (4.25)$$

where $b = t_p/3.5$, and $A = -i\rho_0 \frac{\partial\varepsilon}{\partial\rho}\frac{\Omega_B}{8\pi v^2} E_p E_S^*(0)$. The spectral characteristics of the acoustic wave amplitude follow from the Fourier transform of equation (4.25),

$$\rho'(\omega) = A\sqrt{\frac{2}{\pi}}\frac{4\tau b}{(2b-\tau)^2}\left[\tau\frac{1+i\tau\omega}{1+(\tau\omega)^2} - 2b\frac{1+i2b\omega}{1+(2b\omega)^2}\right] + \sqrt{\frac{2}{\pi}}\frac{8b^2}{(2b-\tau)}\left[\frac{1+i4b\omega-(2b\omega)^2}{[1+(2b\omega)^2]^2}\right]. \qquad (4.26)$$

The temporal dynamics of the induced acoustic wave amplitudes and their spectra together with those of the Stokes pulse initiating the SBS interaction for several values of t_p/τ are shown in Figure 4.4. Depending on the ratio of t_p/τ different characteristic types of SBS interaction are initiated, which can be seen in Figure 4(a): curves 1 give an example of quasi-steady state interaction when $t_p/\tau >> 1$, curves 3 demonstrate transient type interaction when $t_p/\tau << 1$, and curves 2 are for an intermediate case when $t_p/\tau \cong 1$. Figure 4.4(b) is composed of two halves, (as in Figure 4.1 above): Stokes pulse spectra are shown on the left hand side and mediums' response spectra are on the right hand side.

In the first case of a long Stokes pulse, that is $t_p/\tau >> 1$, the shape of the acoustic wave pulse shown in Figure 4.4(a) as the solid curve 1 almost reproduces the shape of the input Stokes pulse (dotted curve 1). The spectrum of the excited acoustic wave in this case, Figure 4.4(b), reproduces the spectrum of the input Stokes pulse, shown by the solid and dashed curves 1 respectively. These are both narrower than FWHM of the Lorentzian-shaped spectrum, Γ_0, corresponding to $\tau = 18$ ns (dotted curve 5). This is to be expected since equation (4.2) is in essence the equation for the amplitude of a driven damped oscillator; for such a system the spectrum of the induced oscillations is fully determined by the spectrum of the driving force when it is narrower than reciprocal decay time of the oscillator.

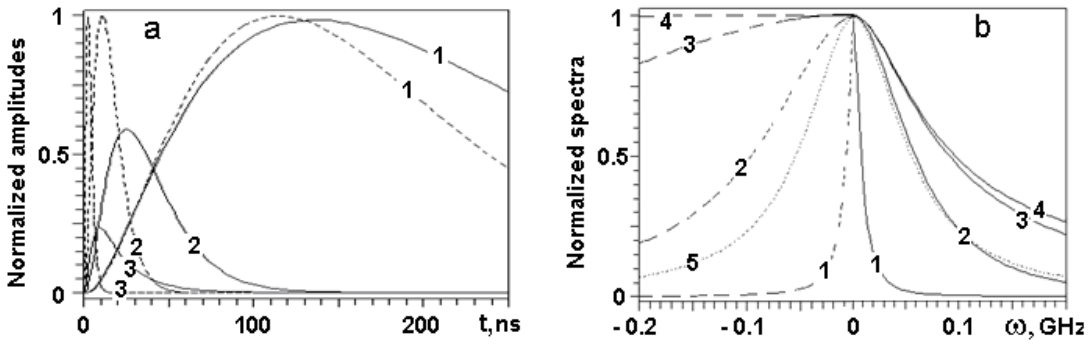

Figure 4.4. (a) Dynamics and (b) spectra of the normalised acoustic wave amplitude (solid lines) for Stokes pulses of the shape given by equation (4.24) (dashed lines) with t_p = 200(1), 18(2), 4(3) and 0.5 ns(4), τ = 18 ns. (the dynamics for t_p = 0.5 ns is not shown on the timescale of Figure 4.4(a)). The dotted line 5 in (b) is the Lorentzian-shaped spectrum with τ = 18 ns. Note, curves in (b) show half spectra of the pulses at LHS and of corresponding to them medium's response at RHS.

In the case of shorter Stokes pulses, $t_p/\tau \leq 1$, (dashed curves 2 and 3 in Figure 4.4 (a)) their spectral width is broader than Γ_0, (dashed curves 2 and 3 and also curve 4 for t_p = 0.5 ns pulse in Figure 4.4(b)). As seen the dynamics of the medium's response (solid curves 2 and 3 in Figure 4.4(a)) and its spectra (solid curves 2, 3 and 4 in Figure 4.4(b)) differ substantially from those of the Stokes pulses and their spectra. In the temporal domain the maximum amplitude of the induced $\delta\rho(t)$ decreases with decrease of pulse duration and a long tail appears after a Stokes pulse, which decays exponentially with a decay time of $\sim\tau$. The spectra of $\delta\rho(t)$ in these cases are narrower, increasingly so for shorter pulses, than the spectra of the driving force (input Stokes pulse). Their width is then determined predominantly by the reciprocal decay time of the oscillator as is to be expected for a damped oscillator, which is driven by a broad-band force.

There are several important conclusions from this consideration.

1. The spectra of the material response in SBS (the SBS-induced acoustic pulse), which are obtained through the Fourier transform of equation (4.2) itself and through the Fourier transform of the analytic solution of the set of dynamic SBS equations, equation (4.21), are qualitatively undistinguishable. This confirms the fact that, while the inverse Fourier transform cannot give a uniquely determined solution, the forward one can.

2. The amplitude of the SBS-induced acoustic pulse always follows the amplitude of the Stokes pulse with a delay which is due to inertia. Consequently, scattering of the CW pump off the acoustic wave and, thus growth of the amplitude of the generated Stokes field, is delayed with respect to the input Stokes pulse. This effect is illustrated in the next section.

3. Reduction of the amplitude of the induced $\delta\rho(t)$ with decrease of pulse duration results in its reduced amplification (as shown in Figure 4.7(c) for G_{ef} below).

4.3.3 Calculations of the output Stokes pulse characteristics

Now let us consider the Stokes pulse dynamics. The input Stokes signal can be taken as in the previous section (see equation (4.24)). Since the SBS exponential gain, G, in the fiber is supposed to be below the SBS threshold, this, according to [110], limits G to ≤ 12 for our consideration of standard silica fibers of > 0.1 km length. Figures 4.5 and 4.6 show the calculated relative output Stokes pulse powers, $P_S(t) = |E_S(t)|^2 S$ (S is the effective area of fiber mode cross section), amplitudes and shapes for four input pulse durations, t_p, and different G. Curves for $G = 0$ show the shape of input pulses. Here the decay time of the acoustic wave, $\tau = 2/\Gamma_0$, in silica is taken to be $\tau = 18$ ns which corresponds to pump radiation wavelength ~1.55 μm. We emphasize that the decay time of the acoustic wave, which is determined by the viscosity of fused silica [111], is used in these calculations rather than the SBS spectral width. This is because the latter depends on intrinsic characteristics of the fiber (core/cladding design, doping type and concentration, numerical aperture, etc. and the ambient environment (mechanical, thermal and electromagnetic fields (see Chapter 3), all of which can result in substantial variation of the resonant Brillouin frequency, Ω_B. However they do not appreciably affect the viscosity of the medium.

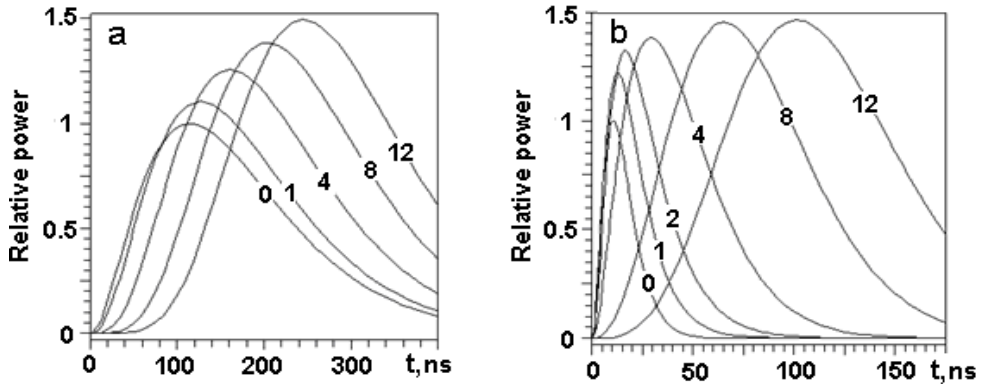

Figure 4.5. Output Stokes pulse shapes for (a), t_p = 200 ns (>>τ) and G = 0 (1), 1(0.42), 4(0.026), 8(0.0006), and 12(0.000012) and (b), for t_p = 18 ns (=τ) and G = 0(1), 1(0.9), 2(0.6), 4(0.2), 8(0.09), and 12(0.00026), where numbers in brackets are the output amplitude magnification factors. The numbers on curves are *Gs*.

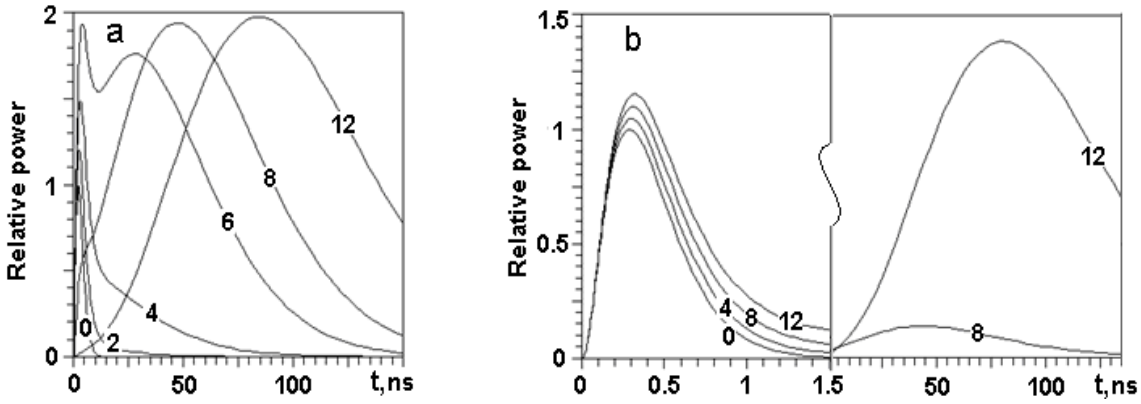

Figure 4.6. Output Stokes pulse shapes for a), t_p = 4 ns (<τ) and G = 0(1), 2(1), 4(1), 6(1), 8(0.2), and 12(0.007), and (b), for t_p = 0.5 ns (<<τ) and G = 0(1), 4(1), 8(1), and 12 (1 at the first peak and 0.3 at the tail). LHS of (b) is temporally stretched to show profiles.

From the calculated shapes of output Stokes pulses presented in Figures 4.5 and 4.6 we can find the dependencies of the induced delay of the output Stokes pulse, its duration and peak power, which is estimated to be $P_{S0}e^{G_{ef}}$, where G_{ef} is the effective SBS exponential gain, on G. It can be seen that all of the quantities increase with G, but the rates of the growths depend substantially on the ratio of pulse duration to acoustic wave decay time, t_p/τ, as shown in Figure 4.7.

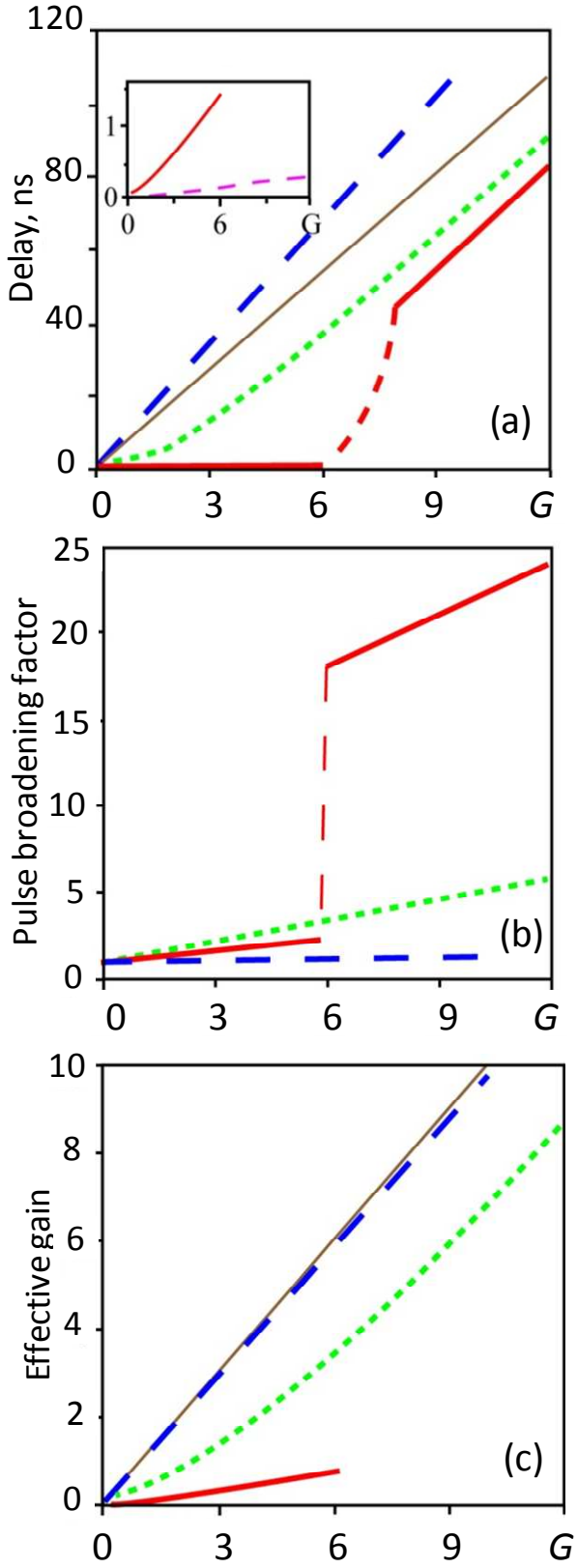

Figure 4.7. (a), Delay, (b), broadening factor, and (c), effective exponential gain at peak of the output Stokes pulse vs gain G for pulse durations t_p = 200 (dashed blue), 18 (dotted green), 4 (thick solid red in the main graph and in the insert), and 0.5 ns (dashed pink in the inset). Thin solid lines in a) and c) are $\Delta T_d = 9G$ ns and $G_{ef} = G$ dependencies respectively.

For a long input Stokes pulse, t_p = 200 ns that is t_p/τ = 200/18 >> 1, the output pulse, on increase of G, remains similar in form (Figure 4.5(a)), and is increasingly delayed following $\Delta T_d/G \cong 11$ ns as shown by the thick dashed line in Figure 4.7(a). The duration of the output pulse compared to that of the input is slightly broadened with increase of G (see dashed line in Figure 4.7(b)), and G_{ef} decreases very slightly compared to G (dashed line in Figure 4.7(c)).

Additional calculations for longer pulses (t_p > 18 ns) have shown that the slope of $\Delta T_d(G)$ may coincide with $\Delta T_d \cong \pi G/2 \cong 9G$ ns, which is shown by the thin solid line in Figure 4.7(a), but this happens only when $t_p/\tau \cong 3$ and >100. For t_p/τ < 3 the slope of $\Delta T_d(G)$ falls below the value $\Delta T_d \cong 9G$ ns. From these calculations it follows that $\Delta T_d(G)$ depends on the pulse duration and this dependence can be interpolated by the equation

$$\Delta T_d \cong \eta G\tau/2, \tag{4.27}$$

where η is an empirical parameter which has a functional dependence on the ratio t_p/τ, which is shown in Figure 4.8.

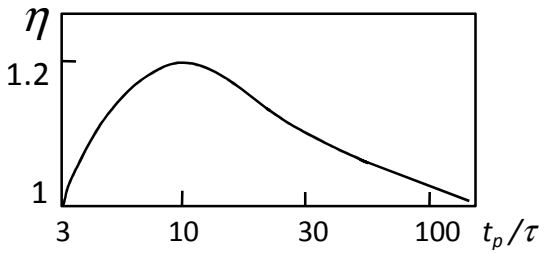

Figure 4.8. Dependence of η on the ratio t_p/τ.

For t_p = 18 ns (Figure 4.7(b)), that is t_p/τ = 1, ΔT_d for the output pulse again increases with G though not linearly; at lower G (0 to ~2) with slope $\Delta T_d/G \cong 3$ ns, and at higher G (> 2) with the slope $\Delta T_d/G \cong 9$ ns (dotted line in Figure 4.7(a)). The pulse broadening in this case increases substantially with G, by a factor ≥ 5 at G > 10 (dotted line in Figure 4.7(b)) and G_{ef} decreases notably, by a factor of ~3 at lower G to ~1.5 at $G \geq 10$ (dotted line in Figure 4.7(c)).

For the short pulses, $t_p \leq 4$ ns (Figure 4.6), that is for $t_p/\tau < 1$, significant new features appear. For $G < 4$ the output pulses approximately retain their shape with only a slight increase of ΔT_d with G ($\Delta T_d/G \cong 0.1$-0.15 ns for t_p = 4 ns and $\Delta T_d/G \cong 0.03$ ns

for t_p = 0.5 ns, as is shown in inset of Figure 4.7(a), solid and dashed lines respectively). In both cases G_{ef} for the leading peak decreases substantially, by a factor ~10. For G between 4 and 6 there is a substantial growth of the power in the tail of the pulses and for $G > 8$ the maximum of the pulse shifts to the tail (see Figures. 4.6(a) and 4.6(b)). This is because of the long decay of the acoustic wave excited by the short Stokes pulse interacting with the CW pump. The dependence of ΔT_d on G for $G > 8$ then follows the linear relation $\Delta T_d \cong (9G - 25)$ ns (thick solid line in Figure 4.7(a)). The pulse broadening factor is then ~20 for t_p = 4 ns (solid line in Fig. 4.7(b) at $G > 6$) and ~200 for t_p = 0.5 ns.

It is rewarding to note that our analytical results presented in Figure 4.7 show dependencies of pulse delay and broadening on G which demonstrate trends quite similar to these obtained numerically in [70, 112] and experimentally in [64] in the small signal limit for pulses of durations $t_p > \tau$ and $t_p < \tau$ in the SBS interaction in silica fibres at λ = 1.55 μm.

4.4 Qualitative explanation of the nature of the delay

Let us now summarise the important points of the previous section, in which we have considered the temporal behaviour of the generated Stokes field and acoustic wave and from this deduced the nature of Stokes pulse delay.

As we have seen, the Stokes pulse at the output of the SBS interaction region is a sum of the reflected pump, Stokes frequency shifted, and of the transmitted input Stokes pulse, the latter of which propagates through the medium without amplification and does not acquire any phase shift in the process.

As can be seen from Figure 4.4(a) the acoustic field in SBS always appears with a delay in regard to an input Stokes pulse due to its inertia. Consequently scattering of the pump off the acoustic grating and thus growth of the amplitude of the output Stokes field, begins with a delay.

Thus the mechanism of the delay for an output Stokes pulse in an SBS interaction is the following: as the input pulse propagates through the medium it triggers the processes of inducing the acoustic wave, which subsequently leads to the reflection of the pump to Stokes radiation. At the output of the SBS interaction region the reflected pump is simply added to the propagating input Stokes pulse. Since the

reflected/scattered Stokes signal does not start to contribute to the output pulse instantly, but with delay determined by the relaxation time of the acoustic wave, the maximum of the output pulse becomes effectively delayed. This is the mechanism of the delays observed experimentally.

Thus, by its physics, pulse delay in SBS is in some way analogous to the delay experienced by a pulse on passing through a saturable absorber/gain, the phenomenon discussed in Chapter 2. In both cases the delay is the result of a shift of the pulse peak and thus is an amplitude rather than phase effect. In this sense it can be compared with the delay which is introduced by a mechanical shutter (Figure 4.9).

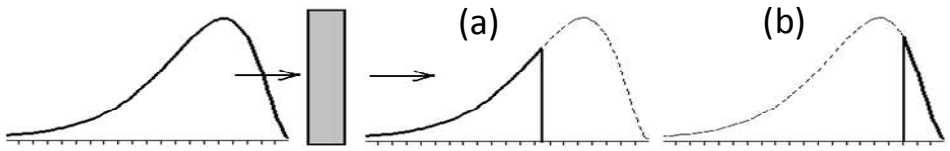

Figure 4.9. Schematic of the effect of effective delay (a)/advancement(b) introduced by the mechanical shutter.

Saturation of the transition and the inertia of acoustic wave excitation act as a "shutter" in saturable media and SBS respectively. However there is a certain difference between these effects, and it is important to highlight it. In the first instance the input pulse experiences a reshaping, and consequent pulse peak shift, because of non-equal change of the amplitudes of its leading and trailing edges due to its resonant interaction with the material. However, in SBS the shift of the pulse peak occurs due to the incoherent addition of the generated Stokes field to the input pulse and so the output pulse is of completely different nature to the input pulse.

We also note that the empirical expression for the pulse delay in the SBS equation (4.27), obtained from our theoretical modelling by its nature coincides with the expression for pulse delay in saturable absorbers, which follows from Selden's calculations (equation (2.29) in Chapter 2). Both of them contain the product of length of the medium, absorption/gain coefficient and lifetime characterising the interaction.

4.5 Conclusion

In this chapter we showed that spectral broadening of the pump radiation by any reasonable amount results in only minute increase of the spectral width of the material's

resonant excitation in SBS (only up to ~$1.7\Gamma_0$). The maximum of this resonance is centred at the Brillouin frequency, Ω_B, consequently the resonantly enhanced dispersion of refractive index is also centered at this frequency and is all but negligible at the Stokes frequency. In other words, the acoustic resonance has next to no effect in enhancing or modifying the refractive index of the material at Stokes frequencies. This, together with the fact that SBS is a parametric process, testifies that Stokes pulse delays cannot be attributed to the decrease of group velocity, and consequently cannot be interpreted as observation of "slow light".

The delay of an output Stokes pulse in the SBS interaction is predominantly a consequence of the phenomenon of SBS build-up, which arises from the inertia of the medium in responding to the optical fields.

The next chapter describes the experiments that were performed to confirm the predictions of theoretical studies in this chapter.

Chapter 5

Experimental studies of Stokes pulse propagation in CW-pumped SBS amplifier

5.1 Introduction

The subject of the experimental studies presented in this chapter is the verification of the results and conclusions of the theoretical modelling of Stokes pulse propagation in a CW pumped SBS amplifier. Specifically major attention is paid to the SBS-induced delay and shape of the output Stokes pulse. The data obtained is compared with calculations based on the models of inertia of acoustic wave excitation (see Chapter 4) and the group velocity effect, otherwise known as "slow light" (see Chapter 3). A major problem is with unambiguous identification of the nature of the Stokes pulse delay. To this end it is important to find such parameters on which the dependencies of the delay are specific and essentially different for the two models. Below, two approaches are used to verify the nature of the delay. One is based on the study of the delay of the Stokes pulse and the other on inspection of its temporal form.

5.2 Investigation of Stokes pulse delay behaviour in the quasi-steady state regime of SBS interaction

5.2.1 Concept of a test experiment

As shown in Chapter 3 the concept of "SBS slow light" in optical fibres attributes the delay of a Stokes pulse to a reduction of the pulse group velocity. Pulse delay in this concept is described by the equation

$$\Delta T_d \cong G / \Gamma_B, \tag{5.1}$$

where $G = g_0 I_p L$ is the SBS exponential gain, g_0 is the SBS gain coefficient, I_p is the pump intensity, L is the length of the medium and Γ_B is the FWHM spectral width of the SBS gain profile [64, 70]. When this expression was first obtained by Zeldovich [65], the only mechanism responsible for spectral broadening of the SBS gain in bulk solid media was that associated with the medium's viscosity. As such Γ_B in equation (2) in [65] was generally the same as the homogeneous bandwidth $\Gamma_0 = 2/\tau$, where τ is the acoustic decay time. However as was shown in Chapter 3, in the literature on "SBS slow light" various means of increasing this bandwidth are exploited. All of them, by their nature, lead to inhomogeneous spectral broadening while the homogeneous width associated with the acoustic decay time, τ, may not be affected. In spite of this the induced delay is still described by equation (5.1) but with Γ_B being the inhomogeneous spectral bandwidth of SBS and the magnitude of delay is independent of the pulse duration.

In contrast to this, the theoretical modelling presented in Chapter 4 shows that the delay of a Stokes pulse in the SBS interaction occurs exclusively because of the build-up time of the acoustic wave, which in turn is determined exclusively by the acoustic decay time, τ, otherwise the homogeneous bandwidth $\Gamma_0 = 2/\tau$. The expression for the delay of an input Stokes pulse of duration $t_p > \tau$ which follows from this modelling (see Chapter 4, section 4.3.3) can be approximated as,

$$\Delta T_d \cong \eta G \tau / 2, \tag{5.2}$$

where η is a parameter, that is dependent on the ratio t_p/τ as shown in Figure 4.8. Remembering that $\Gamma_0 = 2/\tau$ equations (5.1) and (5.2) at first glance look similar, especially in the case of homogeneous broadening, that is when $\Gamma_B = \Gamma_0$. However even in this case equation (5.2) is certainly not the same as equation (5.1) since equation (5.2), which was inferred from results of the "inertial" theory, explicitly shows the delay to depend on t_p through the parameter η. The most pronounced difference between the equations is, however, expected when the SBS gain spectrum is broadened inhomogeneously (when $\Gamma_B \neq \Gamma_0$). Since the difference between Γ_B and Γ_0 can be substantial, [24], the difference between delay following from equations (5.1) and (5.2) is expected to be experimentally measurable even regardless of the magnitude of η in

equation (2). As such this opens up an effective way to experimentally verify the physical mechanism of SBS-induced Stokes pulse delay.

As described in Chapter 3 (section 3.5.1) it has been shown theoretically [22] and confirmed experimentally [23] that Γ_B is functionally dependent on the *NA* of fibre due to the effect of waveguiding of optical radiation in the fibre. This dependence is described by the expression, [23],

$$\Gamma_B \cong \sqrt{\Gamma_0^2 + \Omega_B^2 \frac{(NA)^4}{4n_{co}^4}} \tag{5.3}$$

where Ω_B is the Brillouin shift and n_{co} is the refractive index of the core material. As seen, in the limit that *NA* = 0, which describes bulk media, equation (5.3) gives $\Gamma_B = \Gamma_0$, as expected. As *NA* increases the second term in the square root may considerably exceed the first term so Γ_B may vary over a massive range (from ~50 MHz for *NA* ≅ 0.11 up to ~15 GHz for *NA* ≅ 0.8 in silica fibres [24]. It is by far the dominant mechanism of broadening, and was so chosen as the parameter for variation in our experiment. Equation (5.1) then directly follows as

$$\frac{\Delta T_d}{G} \cong \frac{1}{\Gamma_B} = \frac{1}{\sqrt{\Gamma_0^2 + \Omega_B^2 \frac{(NA)^4}{4n_{co}^4}}} [\text{ns}], \tag{5.4}$$

while we re-write equation (5.2) in terms of Γ_0 as

$$\frac{\Delta T_d}{G} \cong \eta \frac{\tau}{2} = \frac{\eta}{\Gamma_0} [\text{ns}]. \tag{5.5}$$

So the experimental results have to be compared with the dependencies (5.4) and (5.5). Equation (5.4) is the expression for delay according to the group velocity ("slow light") model, from which we may expect that the delay will decrease with increase of the *NA* of the fibre. By contrast, according to the "inertial" model (equation (5.5)), the delay is independent of *NA*. One or other of these trends should therefore underlie our experimental observations and this is the key to determining which is a more correct description, equation (5.4) or equation (5.5). The exercise is however non-trivial because of the interdependence of Γ_B (and so *NA*) and τ (= $2/\Gamma_0$) in fibres. This is discussed in the next section.

5.2.2 Relations between NA, Γ_B and τ in silica fibres

In standard fibres variation of *NA*, which determines Γ_B, can be realized by doping its core and/or cladding. For standard silica-based fibres the most common dopants for the core and cladding are GeO_2 and SiF_4 respectively. Their major role is in changing the refractive index difference, $\Delta n = n_{co} - n_{cl}$ between the core and cladding to obtain a desirable value of *NA*. In the case, when the cladding is not doped, Δn depends on the GeO_2 molar concentration, ρ, mol% through the expression $\Delta n(\rho) = n_{co}(\rho) - n_{co} \cong 0.0009 n_{co}\rho$ [113], and $NA(\rho)$ can be approximated as

$$NA(\rho) \cong \sqrt{2n_{co}\Delta n(\rho)} \approx 0.062\sqrt{\rho}. \tag{5.6}$$

Since doping of silica also alters its mechanical properties, it changes other SBS fibre parameters in equations (5.4) and (5.5), namely Ω_B and τ. The dependency of these parameters on ρ can be obtained from [113, 114]. The focus of these works was the detailed investigation of the influence of dopant concentration on the SBS linewidth, Γ_B, in different fibres. Using this data we have found that the dependencies of Ω_B and τ on ρ, at λ = 1.06 μm can be approximated by the expressions $\Omega_B(\rho) = (16.2 - 0.09\rho)$ [GHz], and

$$\tau = \frac{2}{\Gamma_0} = \frac{1}{\pi(2\rho + 35)} [\text{ns}]. \tag{5.7}$$

Details of the derivation of equation (5.7) are given in Appendix 2.

It follows from equation (5.6) that using the values of *NA*, specified by the fibre manufacturer, one can determine the values of ρ, and from this Γ_B, and τ, according to equations (5.3) and (5.7) for the fibres used in an experiment. For standard fibres ρ is therefore the underlining control parameter and it is easy to see from the dependencies described above that $\Delta T_d/G$ decreases with increase of ρ for both equations though their forms are definitely different.

Another way to vary *NA* of a fibre is micro-structuring of its cladding, i.e. using photonic crystal fibre (PCF) design. In this case variation of *NA* can be realised without doping the core. Since in usual PCF the core is undoped (pure silica, ρ= 0) there is no dopant-caused change in τ and Ω_B in the core material when *NA*, and so Γ_B, are varied.

Consequently in such PCF $\Delta T_d/G$ will decrease with growth of *NA* according to equation (5.4), whereas according to equation (5.5) it has to remain constant. Since this is qualitatively different kind of behaviour compared to behaviour in standard fibres, the use of PCF provides an extra opportunity for experimental verification of our theoretical results.

5.2.3 Characterisation of the fibre samples

In our experiment a set of standard fibres and PCFs was investigated. The parameters of the samples are given in Table 5.1.

Standard fibre samples. In most of the standard fibres investigated, except the FS-SC sample, the *NA* (which ranged from 0.12 to 0.31) was varied (according to the manufacturers specification) by varying the concentration ρ of GeO_2 in their core from 3.7 to 25 mol%. This data was obtained using the dependency of *NA* on ρ as discussed earlier (section 5.2.2). For the FS-SC sample with *NA* = 0.24 the data on the fibre design was not available from the manufacturer. For this reason the elementary composition of the core and cladding of this sample was investigated by Dr. Iskhakova in IOFAN, Moscow, Russia. This study showed that *NA* = 0.24 in this fibre is obtained by doping the core with ρ of GeO_2 of ~9 mol% and the cladding with ρ of SiF_4 of 0.7 mol%. Values of $1/\Gamma_B$ and τ were calculated using equations (5.3) and (5.7). The values of Brillouin frequency shift Ω_B (which also changes with the dopant concentration as noted above), used in the calculation of $1/\Gamma_B$ are also represented in the

Table 5.1. Characteristics of investigated fibre samples.

Fibre type	Dopant	Sample code	*NA*	ρ, mol%	Ω_B, GHz	$1/\Gamma_B$, ns	τ, ns
Standard	GeO_2 in the core	SM1322	0.12	3.7	15.8	2.3	7.5
		SM1000	0.13	4.4	15.8	2.1	7.3
		SMF28	0.14	5.1	15.7	1.9	7.0
		ND716	0.16	6.7	15.6	1.5	6.6
		SM1500	0.31	25	13.9	0.48	3.7
	GeO_2 in the core + SiF_4 in the cladding	FS-SC	0.24	9	15.4	0.73	6
PCF	pure silica core	PCF2	0.26	0	16.2	0.61	9
		PCF3	0.34	0	16.2	0.36	9

table. Most of the standard fibres used in this experiment were the same as in experiments that earlier established the waveguide induced broadening of the SBS spectrum [23].

PCF samples. The characteristics of the PCF samples used are given in the last two lines of Table 5.1. Use of the PCF is especially beneficial for our experiment as they have high NA and undoped core, so the difference in equation (5.4) and (5.5) should be quite pronounced. PCF samples for our experiment were produced by the group of Professor Jonathan Knight, Centre for Photonics and Photonic Materials of the Bath University. The main characteristics of the PCF fibre samples, namely core diameter, losses and estimated values of *NA*, were specified by the manufacturers based on the characteristics of the pre-form of fibre samples. Since *NA* is a critically important parameter in our experiment we conducted our own measurements to verify the *NA* values of the samples.

The layout of the experimental setup for *NA* measurement is shown in Figure 5.1. The procedure consisted of measuring the intensity distribution of the radiation emitted from the end of the fiber with the photodetector connected to the digital oscilloscope. Radiation from the Nd:YAG laser was launched into the fiber under test via the coupling lens with $NA = 0.4$. The size of the laser beam incident on the coupling lens was adjusted with the telescope to fill the aperture of the lens. The detector was stepped linearly across the far-field intensity distribution at a distance y from the fibre end and the intensity was monitored and measured with the oscilloscope. The detector had an aperture which limited its receiving area to ~0.2 mm^2. The length of test samples was ~2-3 m. An IR sensor was used to monitor the leakage of radiation to the cladding. It was found that at a distance of about 25 cm from the input fibre end no radiation from the cladding could be detected with the sensor. Thus it was assumed that at the output fibre end the radiation guided through the core was dominant. The measured magnitudes of the intensity were multiplied by $cos\theta$ to take into account the angle incidence of output radiation on the detector. Then the values obtained were normalised to the maximum value and plotted against the angle θ. The *NA* of the fibre was taken as $NA = sin\theta_m$, where θ_m is the angle at which the intensity decreases to 5% from its maximum value. This measurement procedure conforms to the "method B" of *NA* measurements specified in the British Standard BS EN 3745-302:2002 [115].

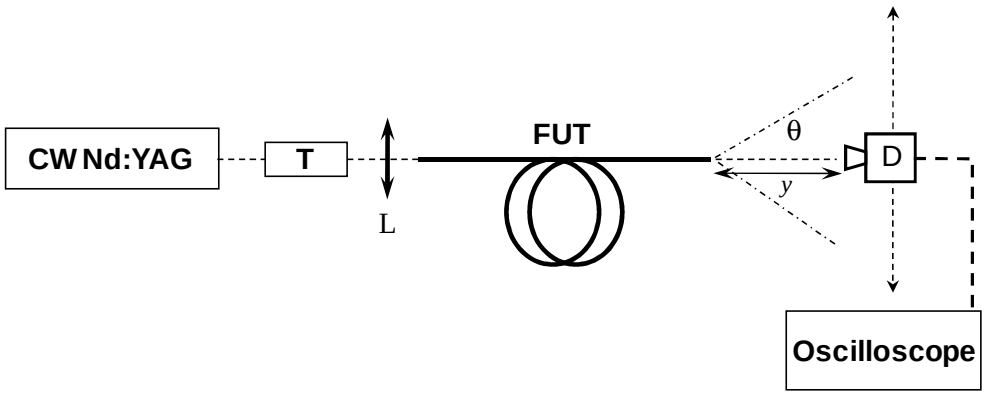

Figure 5.1. Schematic of experimental setup for NA measurements. FUT – fibre under test, T – telescope (beam expander), L – coupling lens, *NA*=0.4, D-photodetector BPX-65.

To verify this technique the *NA* of a standard fibre, namely FS-SC, was measured. The FS-SC fibre sample has an *NA* = 0.24 and core diameter of 3 μm, and thus it is single mode at λ = 1.06 μm. The typical radiation diagram for this sample is shown on Figure 5.2. It can be seen that radial intensity distribution for it has smooth approximately Gaussian shape. The value of *NA* obtained through the measurement (*NA* = 0.24 ± 0.03) agrees well with the value of 0.24 provided in that fibre's specification, which testifies to the validity of our technique for *NA* measurement.

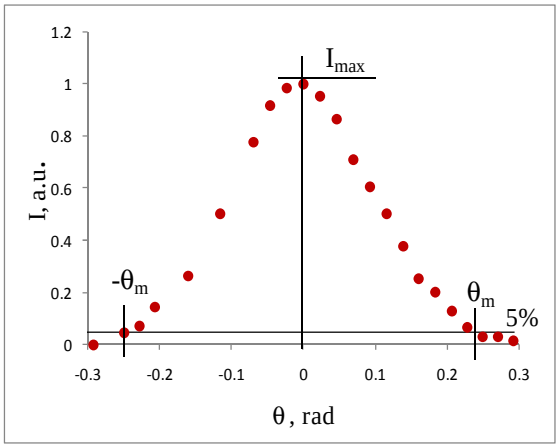

Figure 5.2. Typical angular intensity distributions obtained for FS-SC fibre.

Several measurements of intensity spatial distribution were performed for each of the PCF fibre samples PCF2 and PCF3. Typical radiation diagrams are presented in Figure 5.3. The intensity distributions for PCF samples (core diameters are 4 and 6 μm for PCF2 and PCF3 respectively) are not as smooth as for FS-SC fibre, which is due to the fact that the fibres are not single mode at λ = 1.06 μm. The values of *NA* obtained from these measurements were 0.26 ± 0.04 and 0.34±0.04 which correspond the values estimated by manufacture (0.25 and 0.35 for PCF2 and PCF3 respectively).

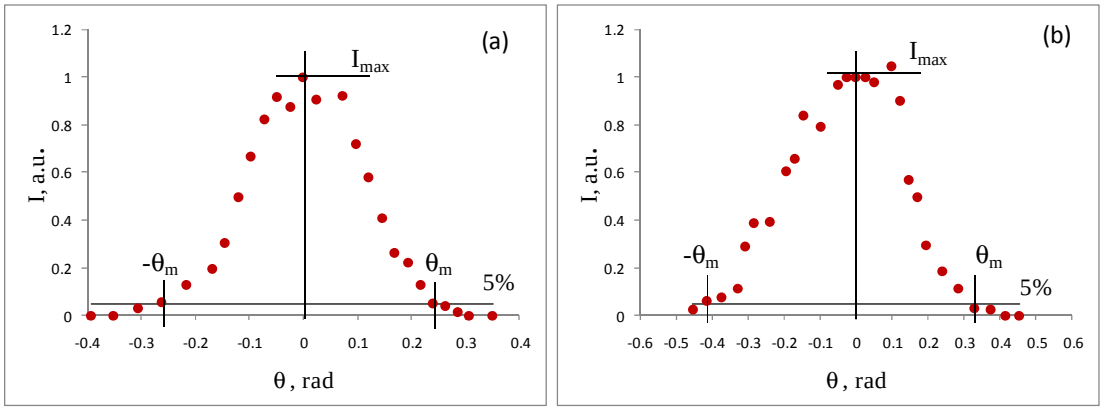

Figure 5.3. Typical angular intensity distributions obtained for (a) PCF2and (b) PCF3 fibre samples.

5.2.4 Experimental setup for Stokes pulse delay measurements

The experimental setup for our study of the Stokes pulse delay is shown in Figure 5.4. A single longitudinal and fundamental transverse mode CW Nd:YAG (λ = 1.06 μm) laser with a variable continuous wave (CW) output power of 0-2 W and spectral bandwidth of ~ 40 kHz was used as a pump source [116]. The laser comprised a Nd:YAG rod (103 mm x 4 mm length x diameter) placed in a ring cavity. The rod was pumped by a CW Krypton arc lamp and both were inside a commercial laser head (Spectron Laser Systems, SL900). A Faraday rotator and a half-wave plate, placed in the cavity, provided unidirectional laser operation. This, along with a Fabry-Perot etalon, allows for single longitudinal mode operation. Operation of the laser on a TEM_{00} mode was achieved by placing a 1 mm diameter aperture inside the cavity. The laser was optically isolated from the external experimental setup by inserting a Faraday isolator (FI) in the path of the beam. This prevented feedback to the pump laser from the setup which otherwise caused temporal instabilities and large fluctuations in the output power and also longitudinal mode hopping (initiation of lasing of another longitudinal mode(s)).

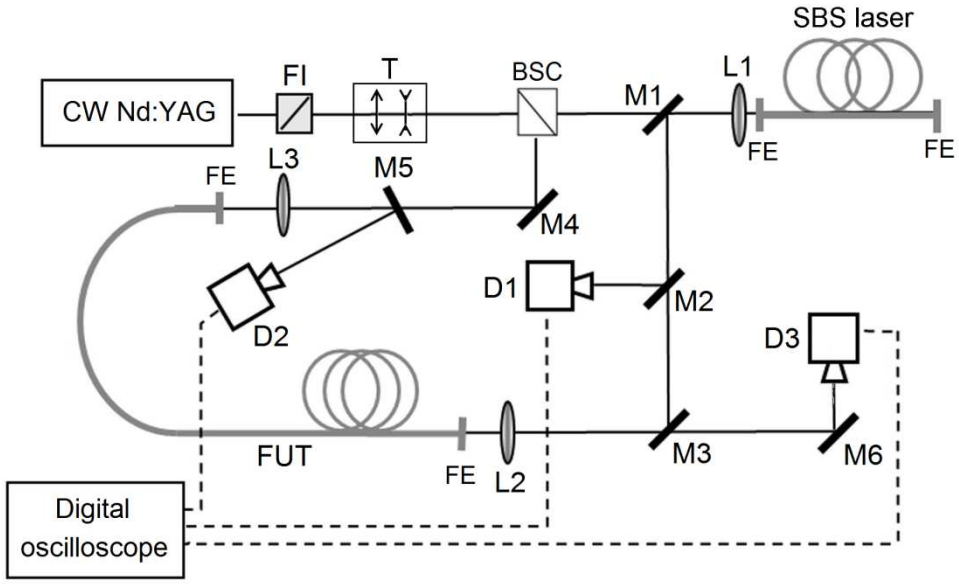

Figure 5.4. Schematic of the experimental setup: M1 - M6 – mirrors, L1 - L3 – lenses with *NA* = 0.4 and f = 6.3 mm, D1 - D3 – photodetectors BPX-65, BSC – beam splitter (50/50), FI – Faraday isolator, T-telescope, FE – fibre ends, FUT – fibre under test.

The output beam was divided by a 50/50 beam splitter (BSC). One pump beam was sent into a fibre that served as an active medium for the SBS laser, which was used as the source of Stokes pulses. The cavity for this SBS laser was provided by the fibre ends (FE) cleaved perpendicular to fibre axis with a natural reflectivity $R \cong 3.5$ %. The other pump beam was used to pump the fibre under test (FUT) in which amplification of the Stokes pulses was realised. The generated Stokes pulses and the pump beam were launched into the FUT via lenses L2 and L3 respectively. The telescope (T), consisting of convex and concave lenses of diameter 2.4 cm with f = 15 cm and f = 10 cm respectively, was used to adjust the size of the laser beam incident on the coupling lenses L2 and L3 to maximize the coupling efficiency**.** The pump power and thus the value of *G* in the FUT were varied by changing the position of the fibre end relative to the focus of lens L3. By this method the pump power in the FUT was varied while keeping the level of pump power in the SBS laser fixed. The active media for both the SBS laser and the FUT were made from the same fibre sample to ensure that the Stokes pulse spectrum matched the SBS gain spectrum of the FUT. All optics was antireflection coated for $\lambda = 1.06$ μm.

The detection system consisted of photo-detectors D1 - D3 (BPX-65 with the 3 ns rise-time) connected through amplifiers to a digital oscilloscope LeCroy 9354L (sampling rate of 2 GHz). D1 and D2 monitored the temporal and power characteristics

of the input and output Stokes pulses and D3 monitored the pump power in the FUT. The signals from photodiodes were amplified by linear amplifiers (Comlinear CLC 100) with the gain of ~100. The data from LeCroy 9354L was recorded to a floppy disk and then transferred to a PC for further signal processing and analysis.

5.2.5 SBS laser as a generator of Stokes pulses

An important element of our experimental setup is the source of Stokes pulses. A natural choice was to use an SBS fibre laser as a pulse generator because it is an easy solution to create a system, in which the spectrum of the generated Stokes pulses would match the SBS gain spectrum of the test fibre, provided they are made from the same fibre sample.

The fact that a fibre based SBS laser emits a periodic sequence of pulses, typical of mode-locking was discovered in [117]. The reason for such behaviour is that the SBS gain spectrum in optical fibres is broadened inhomogeneously [22]. Due to this multi longitudinal mode operation in fibres that are sufficiently long sets in from the threshold for laser oscillation. These modes are phase-locked resulting in the generation of a periodic sequence of pulses**,** the repetition frequency of which is equal to the reciprocal of the round trip time through the fibre and is referred to as the fundamental oscillation frequency, FOF. The duration of the emitted pulses, t_p, is inversely proportional to the spectral width of oscillation. The latter is determined by the physical properties of the fibre but also depends on pump power and length of the SBS fibre laser [118]. In particular it was found there that a gradual decrease in the duration of generated pulses on increase of the pump power is interrupted by transitions to the higher harmonics of FOF. Over the transition between periodic oscillations at successive harmonics of FOF the Stokes emission is unstable and irregular exhibiting fluctuating amplitude spiking which were earlier interpreted as the SBS chaos [119, 120]. Further increase of pump power leads to a decrease of the pulse amplitude and increase of a constant amplitude (CA) component in the Stokes laser emission, which ends up in the pure CA emission mode [118].

This complicated character of the fibre SBS laser dynamics requires careful control and optimisation of its parameters for the needs of our test experiment. To this end several representative fibre samples of those to be used in the experiment on pulse delay were thoroughly studied as Stokes pulse generators. Special attention was paid to

the effect of the *NA* of the fibre on the duration of generated pulses, t_p, since the spectrum of the SBS gain bandwidth increases with increase of fibre *NA* due to waveguide induced broadening, and t_p is expected to be shorter in higher *NA* fibres**.**

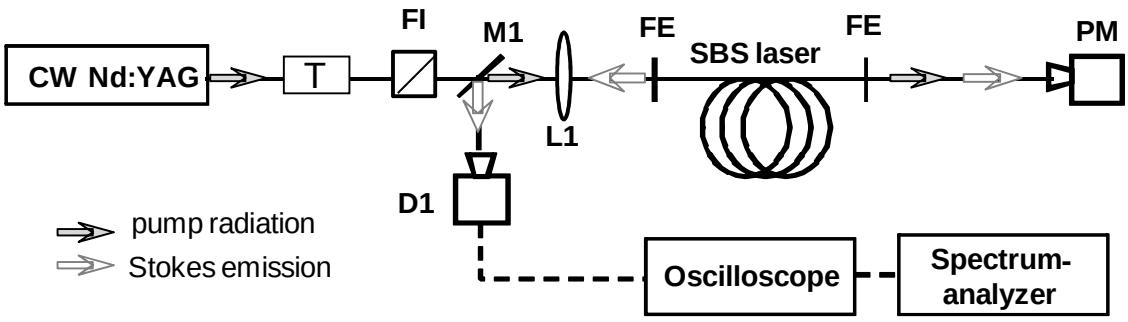

Figure 5.5. Experimental setup for investigation of the characteristics of a fibre SBS laser: FI – Faraday isolator, FE – fibre ends, L1- coupling lens with *NA* = 0.4 and f = 6.3mm, M1 – beam-splitting mirror, R = 10%, D1 – photodetector, PM – power meter, T – telescope.

The experimental setup for investigating the characteristics of the fibre SBS laser is shown in Figure 5.5 It was assembled with the same elements as those used for the SBS laser in the main experimental scheme, shown in Figure 5.4. The additional elements used in these measurements were the RF spectrum analyser (model HP 8554B) and a power meter (PM) Coherent 210 which registered the power of pump radiation transmitted through the test fibre. The power reflectivity of the SBS laser cavity mirrors, R = 3.5%, was determined by the Fresnel reflection from the surface of silica with n = 1.45.

Three fibre samples were investigated. These were a standard single mode (SSM) fibre, high numerical aperture (HNA) fibre, and a photonic crystal fibre (PCF). Parameters of the fibres such as length, L, core diameter, d_c and *NA*, along with the SBS bandwidth, Γ_B, estimated using equation (5.3), threshold power for onset of SBS laser oscillation, P_{th}, and duration of the generated pulses, t_p, are given in Table 5.2.

Table 5.2. Parameters of investigated SBS fibre laser samples.

Fibre	*NA*	d_c, μm	L, m	Estimated Γ_B, MHz	P_{th}, mW	t_{p_min}, ns
SSM	0.11	7.7	200	60	65	250
HNA	0.24	3	200	220	70	110
PCF	0.28	5	50	300	140	40

In each tested fibre, SBS lasing was achieved and the train of output Stokes pulses were recorded at different levels of pump power, P, above P_{th}. Figure 5.6 shows the oscilloscope traces and spectra of SBS laser emission when the pump power slightly (~10%) exceeded the P_{tr}. It can be seen that the spectrum of excited Stokes emission broadens and the pulse shortens with increase of the *NA* of the fibres. Careful examination of Figure 5.6 shows that not all of the registered modes are mode-locked and so contribute to the pulse formation: in fact three to five of these modes with the highest amplitude are actually contributing to the observed pulses.

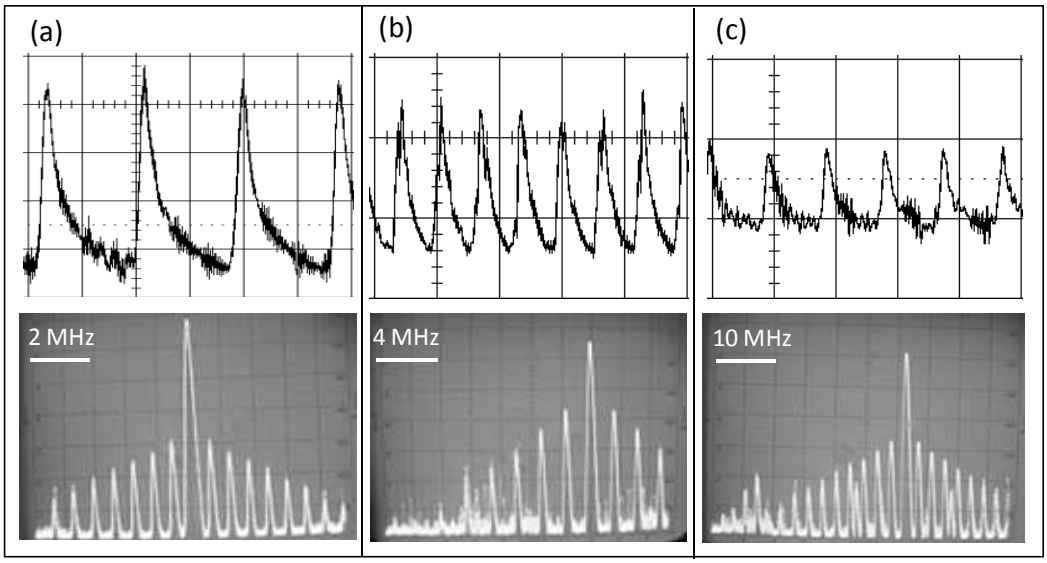

Figure 5.6. Dynamics and spectra of the generated Stokes emission in investigated samples: (a) SSM, (b) HNA, (c) PCF. The times scale is 1 μs/div for (a) and (b), and 0.5 μs/div for (c). Spectra are represented in log scale. Obtained pulse durations are 320 ns, 220 ns and 80 ns respectively

Increase of the pump power allowed us to obtain shorter pulse durations in each fibre sample, consistent with the observation in [118]. In the SSM sample a shortening of pulses was observed when P was increased from P_{th} to ~$1.5P_{th}$. Further increase of P led to gradual elongation of the pulses and then the transition to generation of the pure CA emission. HNA and PCF samples exhibited oscillation at higher harmonics of FOF before switching to the CA regime. The ratio of the pump power P, at which the shortest pulses were obtained, to P_{th} were ~1,5 ~3 and ~3.5 for the SSM, HNA and PCF fibres respectively. The pulses with the shortest durations are shown on Figure 5.7 and the magnitudes of pulse durations are given in the last column of Table 5.2.

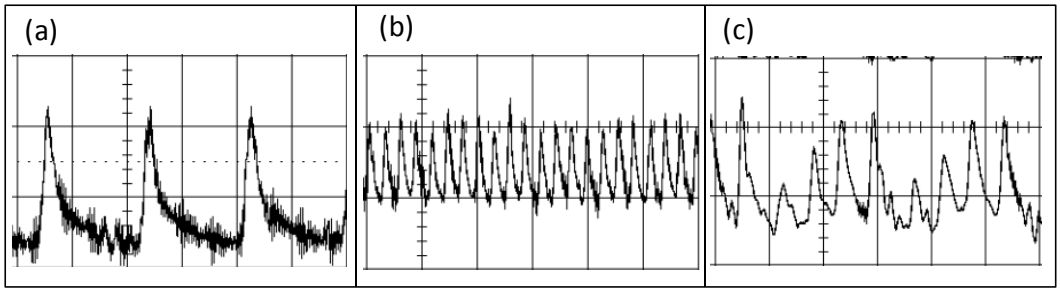

Figure 5.7. Shortest pulse durations for each investigated fibre sample. The time scale is 1 μs/div for (a) and (b) and 0.2 μs/div for (c). Obtained pulse durations are 250 ns, 110 ns and 40 ns respectively.

5.2.6 Stokes pulse delay measurements

Now we move to the description of our experiment on Stokes pulse delay. In the experiments on pulse delay using the set up presented in Figure 5.4 both the active media for the SBS laser and the fibre under test (FUT) were made, as already mentioned, from the same fibre sample to ensure that the Stokes pulse spectrum matched the SBS gain spectrum of the FUT. With each fibre sample particular attention was devoted to formation of stable and reproducible trains of Stokes pulses in the fibre SBS laser. Taking into account the features of the SBS laser described in the previous section the laser fiber length and the level of pump power in it were adjusted to achieve the shortest possible pulses. This was done to increase the accuracy of delay measurement since accuracy decreased with increase of pulse duration, (as the procedure involved registration of the pulse peak position, the peak is more pronounced for shorter pulses). The length of the FUT was not of principal importance and in the majority of cases was determined by the available length of the fibre sample. Lengths of the SBS lasers and FUTs are given in the Table 5.3 together with the durations of generated pulses. As can be seen from the Table 5.3 the pulse durations varied from 80 to 250 ns, well exceeding the τ in the tested fibres (see Table 5.1) so the SBS interaction occurred under conditions conventionally known as quasi steady state.

Table 5.3. Lengths of SBS laser and FUT and durations of pulses from the SBS laser.

Sample code	*NA*	L_{gen}, m	L_{FUT}, m	t_p, ns
SM1322	0.12	90	300	110
SM1000	0.13	95	65	120
SMF28	0.14	50	200	150
ND716	0.16	125	100	170
SM1500	0.31	80	120	80
FS-SC	0.24	60	110	90
PCF2	0.26	100	140	140
PCF3	0.34	150	100	250

5.2.7 Procedures of experiment

For each fibre sample, the trains of input and output Stokes pulses were recorded at different levels of pump power in the FUT. Typical oscilloscope traces are shown in Figure 5.8. Digitized traces were processed to reduce the noise and so increase the accuracy of pulse peak identification.

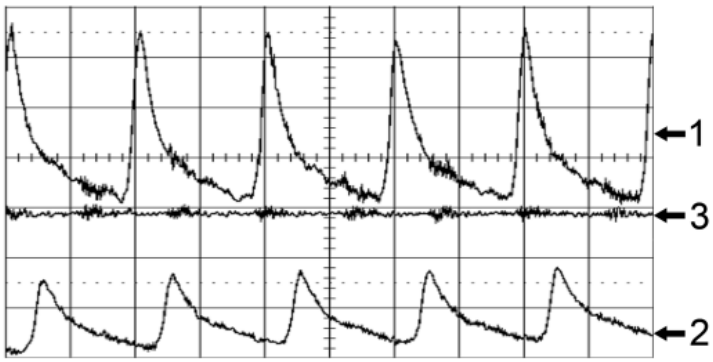

Figure 5.8. Typical oscilloscope traces of input (1) and output (2) Stokes pulses in FUT. Trace (3) is the signal from D3 monitoring the pump power; time scale is 500 ns/div.

Noise reduction was realised through time domain processing of the data obtained. The method was implemented as a simple command-line utility in Object Pascal, which was provided by Dr. Vsevolod Patlan. The algorithm performs a piece-wise polynomial approximation by means of a least-square fit of data points in the moving window. The program is controlled by two parameters, the polynomial order and number of point in the window. Figure 5.9 shows the result of processing for a window of 50 points and a polynomial order of 2. The approach seems feasible since the useful signal under evaluation is relatively slow changing and can easily be described by simple a polynomial function. Unlike filtering by moving averaging, this

method does not introduce any visible signal distortion. From the processed data the positions of the input and output pulse peaks and their amplitudes were obtained to determine the delay and amplification of each output pulse.

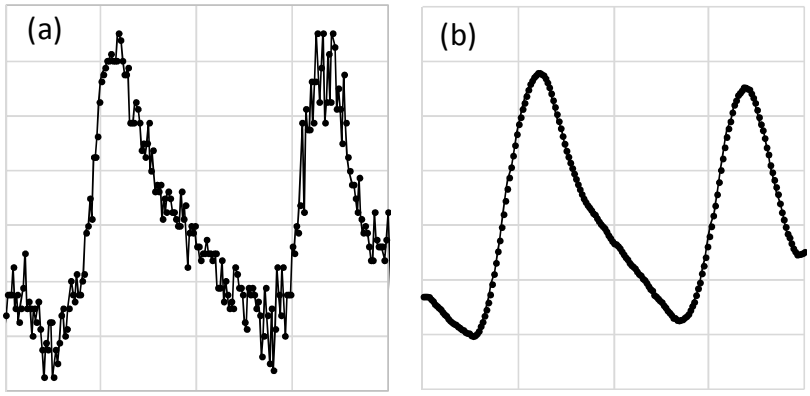

Figure 5.9. Fragment of digitized pulse train. (a) before processing, (b) after processing.

The transit time through the FUT, *T,* for the pulse was determined as the time-interval between the maxima of the output and input pulses. From this, $\Delta T_d(G)$ was obtained as the difference in the transit times with the pump, $T(G)$, and without it, T_0: $\Delta T_d(G) = T(G) - T_0$. The exponential gain, G, in the FUT was determined as $G = \ln(A_A/kA_S)$, where A_A is the amplitude of the amplified output Stokes pulse, A_S is the amplitude of input Stokes pulse and k is a coefficient which characterises the coupling efficiency of a Stokes pulse to, and attenuation in, the FUT. This method of determining G is justified for the quasi steady state regime (see results of calculations in Chapter 4, Figure 4.7.). The attenuation coefficient was determined as $k = A_{Sout}/A_{Sin}$ where A_{Sout} and A_{Sin} are the amplitudes of the output and input Stokes pulses from and into the FUT in the absence of the pump.

The fibre ends of the FUTs were cleaved perpendicular to the fibre axis. The threshold exponential gain for initiation of lasing from a spontaneously scattered signal is therefore $G_{\text{th}} = 2(\alpha L - \ln R) \approx 7$ [121]. However when seeded with an external Stokes pulse the generation in the SBS laser may start at even smaller values of G ($G \approx 6$ [122]). For this reason in our experiments G was kept below ~5. For the fibre sample with $NA = 0.13$ a maximal gain of $G \approx 3{,}5$ was determined by the length of the FUT and available pump power.

From four to seven measurements of ΔT_d were taken at each value of pump power. From this data the mean value of ΔT_d and its standard error were determined

and then plotted against their corresponding values of G. The gradient of the $\Delta T_d(G)$ dependency and its error were found by the weighted least squares fit method [123]. Figure 5.10 shows the experimentally obtained data points for delay ΔT_d together with the fitted linear dependencies/gradients (solid lines) and gradient error (dashed lines) for the four fibres investigated.

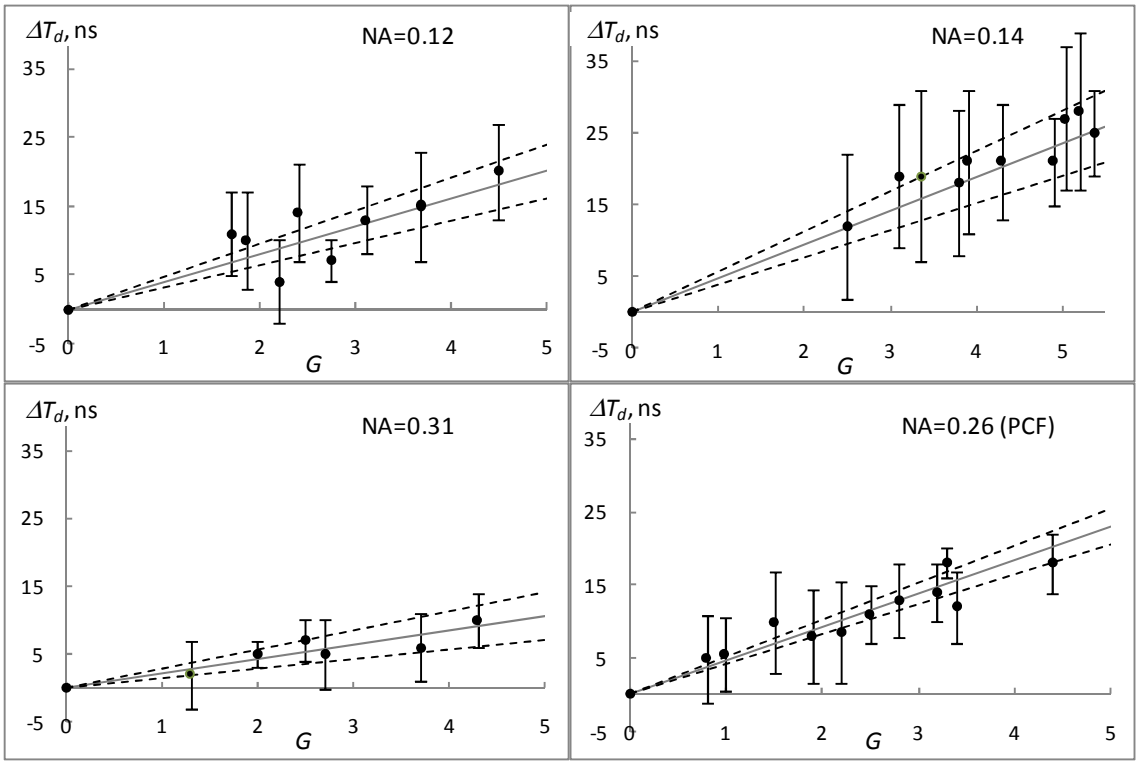

Figure 5.10. Dependency of pulse delay on G for four of the investigated fibre samples. Solid line shows the trend-line of $\Delta T_d(G)$ dependency and dashed line show the standard error of the trend.

5.2.8 Discussion of experimental results

The values of the gradients $\Delta T_d/G$ and their errors for the tested fibres are summarised in Table 5.4.

The gradients $\Delta T_d/G$ plotted against their corresponding values of NA and ρ of the tested fibres are shown in Figures 5.11 (a) and (b) respectively. Standard fibres are represented by squares, PCF are shown by circles and the triangles show the fibre with NA = 0.24 with the doped cladding.

Table 5.4. Gradients of $\Delta T_d/G$ dependency.

Sample code	*NA*	$\Delta T_d/G$, ns	$\delta(\Delta T_d/G)$, ns
SM1322	0.12	4.0	0.8
SM1000	0.13	4.0	0.7
SMF28	0.14	4.7	0.9
ND716	0.16	4.2	0.9
SM1500	0.31	2.1	0.7
FS-SC	0.24	3.4	0.4
PCF2	0.26	4.6	0.5
PCF3	0.34	4.5	0.9

The theoretical dependencies, namely those described by equations (5.4) and (5.5) are plotted in both figures as blue solid lines (labelled $1/\Gamma_B$) and pairs of green dashed (labelled $\eta\tau/2$) and dashed-dotted lines (corresponding to $\eta\tau/2 \cong 5\eta$ ns) respectively. The latter lines comprise pairs because in our experiments the ratio of t_p/τ ranges from ~15 to ~30 resulting in a variation of η (see equation (4.27) and Figure 4.8 in Chapter 4) between ~1.1 and ~1.2 which is represented correspondingly by the lower and upper lines.

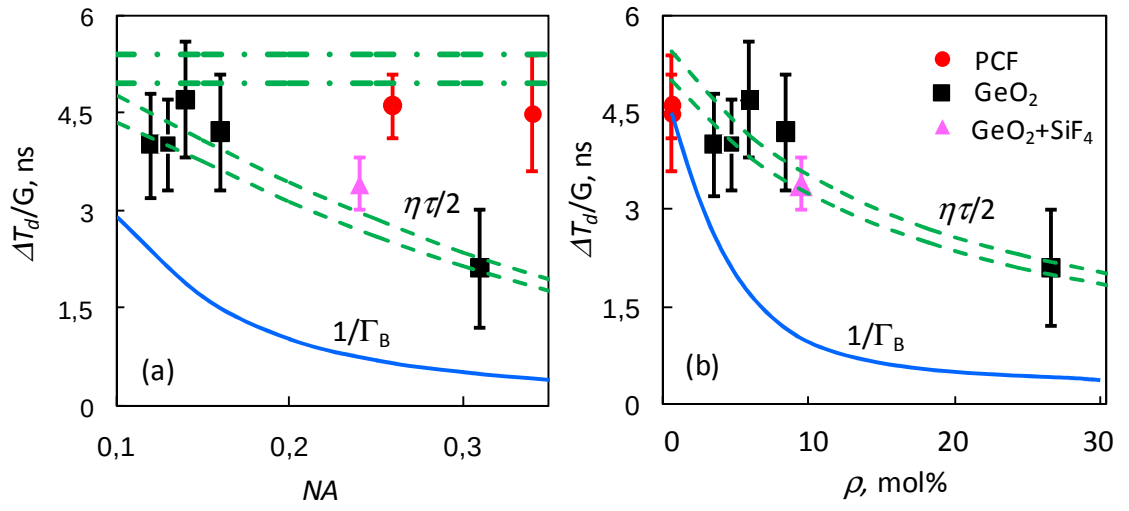

Figure 5.11. Experimental and theoretical dependencies of $\Delta T_d/G$ on *NA* (a) and ρ (b). Solid line in both graphs show the prediction of the "slow light" concept ($1/\Gamma_B$), dashed and dash-dotted green lines represent the range predicted by the "inertial" model, dash-dotted line is $\tau/2$ dependency.

First of all it is easy to see that all experimental points lie well above the $1/\Gamma_B$ dependency predicted by the "slow light" model, equation (5.4). Now let us examine the data for standard fibres (squares and triangle). As seen the experimental data show $\Delta T_d/G$ to monotonically decrease with increase of both *NA* (Figure 5.11(a)) and ρ

(Figure 5.11(b)). It is immediately obvious that these are in pleasing agreement with the prediction of the "inertial" model being substantially displaced from the behaviour predicted by the "slow light" model which, for example, in Figure 5.11(b) is lower by a factor of two at ρ = 3-4 mol% and up to a factor of four at ρ = 25 mol%. So while both models predict a decrease in $\Delta T_d/G$ with increase in *NA* and ρ, the experimental data is in convincing agreement with the "inertial" model.

The extension of our experimental data to those obtained using PCF provides another important test of our findings since for this type of fibre *NA* is varied by fibre design and not the doping. Accordingly, as discussed above, for PCF one expects that for the "slow light" model, equation (5.4), $\Delta T_d/G$ will decrease with increase in *NA* whereas for the inertial model, equation (5.5), $\Delta T_d/G$ will be independent of *NA*. The latter theoretical dependency is plotted as the horizontal pair of dashed-dotted lines in Figure 5.11(a), which, as discussed above, encompass the variation of η in equation (5.2) (or equivalently equation (5.5)). The experimental data points for the PCF's, as shown in Figure 5.11(a) show the delay to be independent of their *NA* that is they, within experimental error, are in quite good agreement with the prediction of the "inertial" model. Referring now to Figure 5.11 (b), since the core of PCFs is undoped the magnitudes of the measured $\Delta T_d/G$ in these samples evidently appears as a single (big red) point at $\rho = 0$.

The results presented in this section provide good evidence that the delay of the Stokes output pulse in the SBS amplifier is proportional to the decay time of the acoustic wave, τ, in the fibre, which is the reciprocal of the homogeneous width of the SBS spectrum Γ_0. It is not affected by any kind of additional (inhomogeneous) broadening of the SBS spectrum as expected from the model of "slow light". These findings therefore confirm the prediction of our theory, developed in Chapter 4, in which the Stokes pulse delay is attributed exclusively to the inertia of exciting the acoustic wave in the medium.

5.3 Dynamics of the Stokes pulse in a Brillouin amplifier

Another means to test our "inertial" model of Stokes pulse delay is by investigating the shape of the Stoke pulses at the output of the SBS interaction region. According to the "slow light" concept the shape of the output pulse should be similar to

that of the input pulse. Conventionally, observed temporal broadening of the output pulse is usually attributed to the narrow spectral width of the SBS gain bandwidth [64]. Actual changes to the shape of pulse do not follow from such consideration, which, in fact, can only predict the change in the width of the pulse. Contrary to this, the theory presented in Chapter 4 describes not only the delay of the Stokes pulse but also pulse shape and changes it undergoes under SBS amplification. In particular equation (4.23) in Chapter 4 gives an analytic expression for the temporal dependence of a Stokes pulse intensity when the pulse propagates though the CW pumped SBS medium. Thus comparison of experimental pulse shapes with the pulse shapes following from theoretical model provides a further means of validating the "inertial" model.

The experimental setup used for investigation of the Stokes pulse dynamics was similar to that described in the previous section (see Figure 5.4). The experiment was performed with the fibre sample with NA = 0.12. The lengths of SBS generator and FUT were 85 and 300 m respectively. The SBS laser generated pulses with duration of 150 ns. Since, according to the theory presented in Chapter 4, the difference between the shapes of input and output pulses is expected to be more pronounced with decrease of pulse duration a high frequency $LiNbO_3$ amplitude modulator (AM) (JENOPTIC, model AM1060HF) was inserted on the way of the SBS laser beam between mirrors M1 and M2 to create shorter pulses. The modulator was driven by a pulse generator HP 8133A (3 GHz bandwidth). In this case the highest possible pump power was used for pumping the SBS laser, which provided a high level of the CA component in the output signal [118]. In this configuration we were able to obtain a well reproducible train of ~20 ns Stokes pulses.

Typical oscilloscope traces are shown in Figure 5.12. The trains of input and output Stokes pulses for pulse durations 150 ns and ~20 ns were recorded at different levels of pump power in the FUT. The experiment was conducted with pump powers in the FUT that provided relatively small G, up to ~ 2.5. In this case the amplitudes of the transmitted pulses with and without amplification are of comparable values and the difference in pulse shapes is more pronounced. Consequently the contribution to the output Stokes pulse from the pump reflected off the acoustic wave could be easily identified. Trains of output Stokes pulses transmitted through the FUT without the pump were used to determine the transit time through the fibre and the level of attenuation/coupling losses in it. Digitized traces were processed to reduce the noise. Input and output pulse shapes were obtained from the processed data.

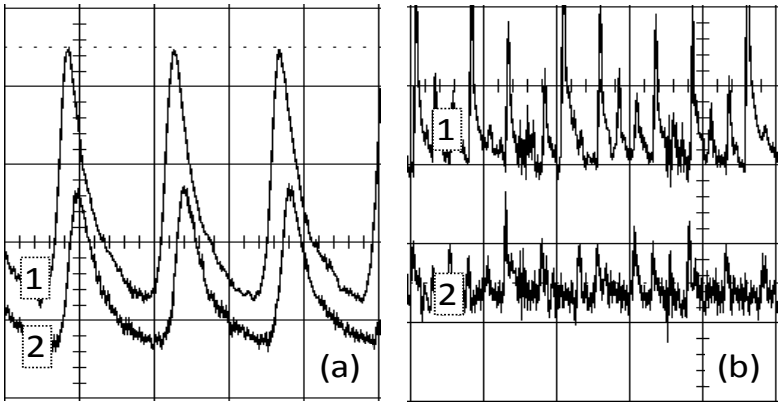

Figure 5.12. Typical oscilloscope traces of input (1) and output (2) Stokes pulses in FUT for t_p = 150 ns (a) and 20 ns (b), the time scale is 500 ns/div.

Figures 5.13 and 5.14 show the measured pulse shapes, represented by solid curves, together with calculated ones, shown by dashed curves, for input pulse durations 150 ns and 20 ns correspondingly. Input Stokes pulses transmitted without SBS amplification, output Stokes pulses and their differences are denoted with indexes 1, 2 and 3 respectively. For each pair of transmitted input and amplified pulses obtained at different pump levels a calculation was performed to find the value of *G* for each case. The amplitudes of pulses in Figures 5.13 and 5.14 are normalised to the amplitudes of transmitted input Stokes pulses. The intensity of the Stokes pulse at the fibre output $I_S(L,t) \propto |E_S(L,t)|^2$, was calculated using equation (4.23) for an input Stokes pulse (curves denoted by 1s), the time dependent intensity of which was modelled by equation (4.24) for an input Stokes pulse (denoted by curves 1), the time dependent intensity of which was modelled by the expression, which closely models the experimental pulse shape (compare solid and dashed curves 1 in Figures 5.13 and 5.14). Curves 3 are the contributions to the Stokes output of pump reflected off acoustic wave, which are described by the second term on the RHS of equation (4.23). We have found that for each *G* the calculated curves 2 and 3 give the best fit with the experimental data in both amplitude of the signals and pulse shapes at $\tau \cong 5$ ns. Deviations between the measured and calculated shapes of output Stokes pulses, which are most pronounced at the tails of pulses in Figure 5.14, correlate with those of the input pulses; they are simply a consequently of imperfect modelling of the form of the input pulse by equation (4.24).

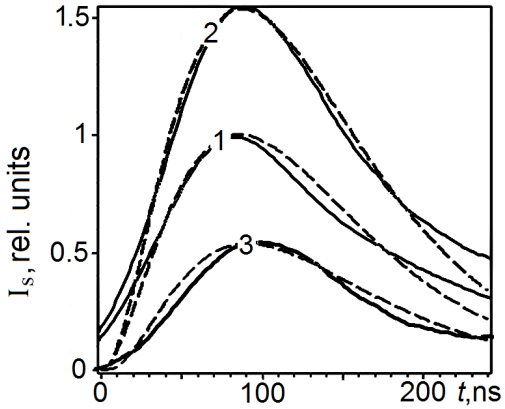

Figure 5.13. Experimental (solid curves) and theoretical (dashed curves) dynamics of the incident (1) and output Stokes pulses (2) and of their difference (3) for t_p = 150 ns, τ = 5 ns and G = 1.1**.**

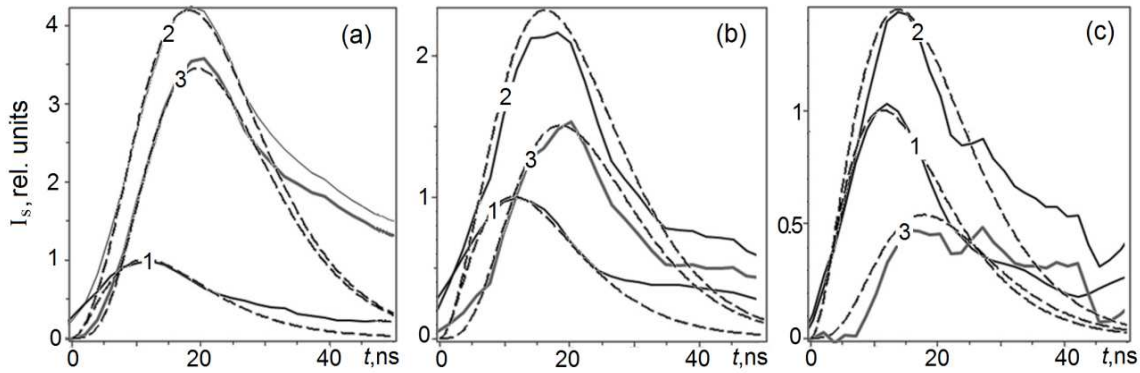

Figure 5.14. Experimental (solid curves) and theoretical (dashed curves) amplitudes and dynamics of the incident (1) and output Stokes pulses (2) and of their difference (3) for t_p = 20 ns, τ = 5 ns and G = 2.4 (a), 1.75 (b) and 1.2 (c).

Evidently these experimental findings are further evidence in support of the correctness of the "inertial" model which describes even details of the output Stokes pulse dynamics. These are confirming, in particular, that this pulse consists of the transmitted input Stokes pulse, and a Stokes frequency shifted pump wave reflected by the induced acoustic wave. The former propagates through the medium without amplification while the latter starts to contribute to the Stokes output pulse not instantly but with a delay determined by the time required to build up the acoustic wave. The shape, amplitude and delay of the output Stokes pulse are fully consistent with this physical representation.

5.4 Conclusions

In this chapter two approaches for experimental verification of the conclusions following from the theoretical modelling presented in Chapter 4 were proposed. The first one exploits the difference between the dependencies of pulse delay on SBS amplification for the two physically distinct models of delay: the "group velocity" concept in which the delay depends on the SBS bandwidth regardless of the broadening nature and the concept of "acoustic wave inertia", in which delay is determined by the acoustic wave relaxation time. For this method the numerical aperture, *NA*, of the fibre and the doping concentration, ρ, of the fibre core were found to be ideal control parameters as they provide a way of controllable change of the SBS bandwidth and acoustic wave relaxation time. Another approach is based on detailed comparison of calculated and measured dynamics of the output Stokes pulse.

The experimental set up suitable for the proposed studies was designed, constructed and aligned. A set of various fibre samples appropriate for the proposed experiments were prepared and thoroughly characterised. Techniques for data acquisition and processing were developed and calibrated.

The results of the experimental studies are as follows:

1. The Stokes pulse delay versus the SBS exponential gain tracks the change of acoustic wave relaxation time in the fibre core, thus validating the "inertial" model, which attributes the delay to the build up time of the acoustic wave.

2. The shapes and amplitudes of the output Stokes pulse measured at different SBS exponential gains have explicitly shown that it is the sum of the unamplified transmitted input pulse and the pump field, reflected and Stokes frequency shifted off the acoustic wave induced in the medium. Because the latter is delayed due to the time taken for the acoustic wave to build up, the observed delay in the Stokes output pulse appears as a shift of the pulse maximum with respect to the transmitted input Stokes pulse. The Stokes pulse shapes and amplitudes obtained were found to be in remarkably good agreement with our theoretical predictions thus providing further evidence in support of "inertial" model.

Thus the experimental findings presented in this Chapter provide good evidence of the validity of the theoretical model developed in this work, revealing the nature of the

Stokes pulse delay to be due to the build up time of the acoustic wave and not to the group velocity effect, otherwise “slow light”.

Chapter 6

Final conclusions

The work presented in this thesis has investigated the nature of the delay experienced by pulsed Stokes radiation when transmitted through a SBS-amplifying medium, topically referred to as “slow light” in SBS. In the course of this work the following studies were performed and results obtained.

1. The classical concept of the group velocity was reviewed and the conditions under which the effect may be observed were highlighted.

2. The effect of “slow light” was introduced as the propagation of a light pulse in a medium in which its group velocity is considerably lower than the phase velocity of light in that medium. It was shown that the effect is especially pronounced in the vicinity of a medium’s absorption or amplification resonance. The methods and optical media currently being studied for obtaining this effect were introduced and the theoretical and experimental works that gave birth to this research topic were reviewed.

3. Analysis of a set of key publications in this subject area revealed that, in some instances, attributing the observed pulse delays to the effect of group velocity is not straightforward.

4. An alternative effect, which may contribute to the observed delay, namely saturation of gain/absorption, was analyzed. Since this effect is unavoidable in resonant interactions of light with matter, the conclusion was drawn that special care must be taken in interpreting experimental results as “slow light”.

5. In the course of reviewing publications on “slow light” via SBS, inconsistencies in the interpretation of the experimentally observed delay through the group velocity

effect, along with contradictions with the basic physics of SBS were revealed, exposing a quite serious misunderstanding of the nature and physics of SBS by the “slow light” community.

6. The core of the work presented in this thesis represents analytic solutions of the basic coupled SBS equations obtained for SBS amplification in both the frequency and time domain. Based on these solutions, a theoretical model of Stokes pulse propagation through a CW-pumped SBS media was developed, the so called “inertial” model.

7. This model led to the following conclusions:

- The signal at the Stokes frequency at the output of the SBS interaction region is a sum of the input Stokes pulse and the Stokes frequency shifted pump field reflected off an acoustic wave, which is excited in the process by the interference pattern of the pump and input Stokes signals.

- In general, the reflected pump (generated Stokes signal) is incoherent with respect to the input Stokes pulse that induces the interaction. The reason for the incoherence is the non-stationary and non-local response of the medium to the driving force, which is the interference pattern of the pump and input Stokes signals.

- The input Stokes signal field in an SBS amplifier neither experiences gain, in its conventional understanding as the negative absorption in a material, nor an SBS-induced phase shift. As such the phenomenon of “slow light” which is, by its very nature, a phase-related effect cannot exist in SBS.

- The delay in the arrival of the output Stokes pulse, as registered in experiments, is the consequence of a delayed growth of the Stokes field amplitude which occurs because the reflected (CW) pump signal contribution to the Stokes output is not immediate but delayed as determined by the build up time of the acoustic wave. Thus, since the delay is due to delayed growth of the acoustic wave amplitude, it is an amplitude-related effect, which has nothing to do with the phase-related group delay effect.

8. The results and conclusions of these theoretical studies were verified by a series of experiments.

- Investigations of the Stokes pulse delay were made in a set of fibers to determine its dependence on the inhomogeneous SBS bandwidth and on the acoustic wave relaxation (or build up) time. The experiment exploited the fact that the former is determined by the numerical aperture of the fibre while the latter is determined by the fibre core composition. It was found that the Stokes pulse delay tracks the change of acoustic wave relaxation time in accordance with the "inertial" model, and does not follow the inhomogeneous bandwidth of the SBS spectrum as expected from the "slow light" model.

- The dynamics of the output Stokes pulses were studied at different SBS amplification levels. This study revealed that the shape and amplitude of the output Stokes pulse are fully consistent with the predictions of the "inertial" model and showed for the first time that the input Stokes pulse is not amplified in the SBS interaction.

These experiments are consistent with the "inertial" model of Stokes pulse delay in the SBS interaction.

Thus the work presented in this thesis provides insight into the physics of Stokes pulse propagation in an SBS amplifier and resolves currently widespread misunderstandings in the field. It follows from the theoretical and experimental studies presented that the concept of "slow light" via SBS is unsound on both physical and mathematical grounds. On the contrary, the "inertial" model, which is based on a direct analytic solution of the dynamic SBS equations, is adequate and fully describes the phenomenon of Stokes pulse delay in SBS. As far as applications are concerned, this work has revealed that the suitability of the Stokes pulse delay in SBS for optical communications is doubtful because the output pulse is not a truly delayed input pulse as required in such applications. However, we believe, the effect may be exploited as a means for reshaping and amplification of pulses in systems where this is required.

Evidently this work challenges the foundation of current understanding of Stokes pulse delay in SBS as being a manifestation of the group velocity effect and in so doing provides a physically different interpretation of the phenomenon. It is interesting to note that similar inconsistencies have been found in "slow light" studies exploiting other approaches (see Chapter 2). "Slow light" via CPO is an example which was considered by Selden [60] and Zapassky and Kozlov [61, 62]. They concluded that delays in that case are well explained with the theory of saturable absorbers. Not

surprisingly the authors of these publications have found themselves in a marginalized position, somewhat similar to ours, in the sense of rejection of our studies by the SBS "slow light" scientific community. I therefore think it appropriate to end this thesis with a quote from one of their publications [124].

"In recent years the range of mechanisms for obtaining "slow light" has got substantially wider, experiments became simpler and authors started to approach the analysis of the experimental results without appropriate criticism, explaining every observable delay by decreased group velocity of the pulse". "We arrive at a situation when the credibility of many works on "slow light" is questionable. The problem is not in the quality of the experiment but in the inadequacy of the logic adopted for justification of the experimental findings. The situation is worsened when obvious physical mistakes made in these works are systematically "unobserved" and publications containing these mistakes do not receive critical reviews in the literature". "It is true that many, if not most, of the works involved in the "slow light" field, irrespective of their novelty and degree of reliability, are published in the most prestigious journals and automatically acquire high rating, whereas any attempts to express doubt in regard to credibility of these works in the same publishing editions faces firm opposition. This situation evidently harms the prestige of science in general and specifically the acknowledgement of true achievements in this area of physical optics".

Appendix 1: Analysis of some publications on "slow light"

In this appendix we present the analysis of some key publications in the field of "slow light" generation. We pay special attention to the experiments based on the EIT phenomenon and also consider works exploiting other effects. The reason why we decided to perform such analysis was that in the course of investigating pulse delay via SBS we discovered the nature of the effect to be misinterpreted throughout the literature. The delay is attributed to the group velocity effect, whereas in reality it is a consequence of pulse reshaping experienced by the pulse on propagation through the material. In light of this it was a matter of scientific curiosity to explore to what extent the theory of group velocity can explain the delays observed through other effects.

We start with the work of Hau et al [6] which reported group velocities as low as 17 m/s. They studied the delay of an optical pulse at wavelength λ = 589 nm with FWHM duration of ~2.5 μs on propagation through a 229 μm-long cell with the ultra cold sodium atomic vapour. The experiment was performed for the two values of intensity of the coupling field I_c: I_{c1} = 12 mW/cm^2 and I_{c2} = 52 mW/cm^2. The experimentally observed pulse delay for T = 450 nK and I_c = 12 mW/cm^2 is shown in Figure A1.1(a). Figure A1.1(b) represents calculated transmission and refractive index dispersion profiles for the same temperature and I_{c2} = 52 mW/cm^2. Finally Figure A1.2 shows the speed of light pulse versus vapour temperature.

From this experimental data one can directly estimate the values of the group index n_g and absorption coefficients α_{min} and α_{max} in the presence and absence of the coupling field at T = 450 nK for I_{c1} and I_{c2}. Data in Figure A1.2 gives values of n_g. Next, in Figure A1.1 (a) the amplitude of the reference pulse is ~30 a.u. and the amplitude of the delayed pulse is ~4 a.u., so, the transmission of the cell in the presence of the coupling field with intensity of I_{c1} is $exp(-\alpha L)$ = 4/30 = 0.13. Since the length of

the medium, L, is ~230 μm, this gives α_{min} of ~9000 m^{-1} at I_{c1}. From Figure A1.1 (b) it follows that the maximum of the cell transmission at I_{c2} is ~0.65, which gives α_{min} of ~2000 m^{-1}. The estimated probe pulse transmission coefficient in the absence of the coupling field according to the authors, is $exp(-\alpha L) = exp(-63)$. This corresponds to $\alpha_{max} \approx 2.7.10^5$ m^{-1}. These values are presented in Table A1.1.

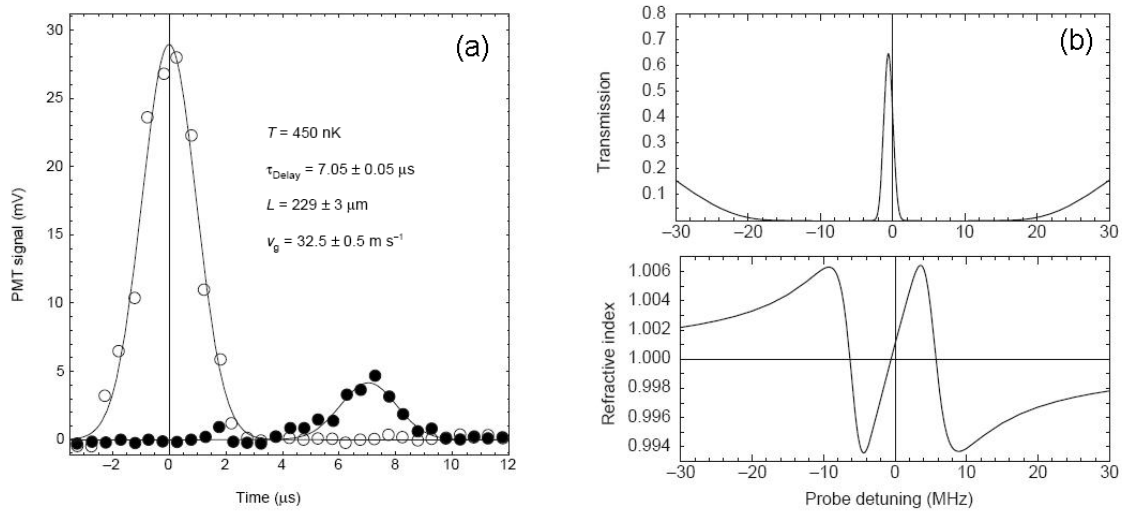

Figure A1.1. Pulses delay measured in [6]. The front pulse (open circles) is a reference pulse with no atoms in the cell. The other pulse (filled circles) is delayed by 7.05 μs with I_c = 12 mW/cm^2. (b) Calculated transmission and refractive index dispersion profiles for I_c = 52 mW/cm^2. The detuning is given in the linear frequency scale.

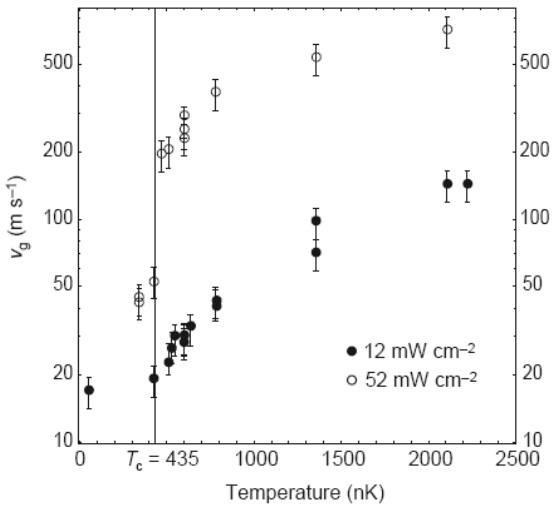

Figure A1.2. Dependency of the speed of light pulse on the vapour temperature in [6].

The same values can be calculated using equations (2.19 – 21) for the parameters of the experiment [6], which according to [4] are $\omega_p = 3.2.10^{15}$ rad/s, $\gamma_{31} = 3.1.10^7$ rad/s,

γ_{21} = 2.4.10^5 rad/s and M = 4.1.10^5 rad/s. The magnitudes of n_g, α_{min} and α_{max} obtained using theory (equations (2.19 – 21)) are given in Table A1.1 in brackets.

Table A1.1. Values of absorption and group index in [6]:experiment and theory.

I_c, mW/cm^2	n_g, x10^6	α_{min}, x10^3 m^{-1}	α_{max}, x10^5 m^{-1}
12	9.2 (27)	9 (21)	2.7 (8.8)
52	1.5 (5.7)	2 (4.5)	2.7 (8.8)

It is easy to see that the difference between the theory and the experiment is much higher than the claimed measurement accuracy of ~5% in [6].

It follows from Table A1.1 that the measured magnitudes of n_g, α_{min} and α_{max} are lower by a factor of 2-3 than these calculated. We note that if we introduce a common (see equations (2.19 – 21)) fitting parameter θ = 1/2.7 = 0.37, the difference between theoretically and experimentally estimated values is not more than 20% which is really good. It is only the magnitude of n_g at I_{c2} that manifests a difference more than 20%, being higher than the experimentally measured value by ~40%.

Also note that value of n_g at I_{c2} which follows form the Fig A1.1(b) is

$$n_g = \omega_p \left(\frac{dn}{d\omega} \right)_{\omega_p} = 3.2 \cdot 10^{15} \frac{0.012}{2\pi \cdot 8 \cdot 10^6} \approx 7.6 \cdot 10^5 \qquad \text{(A1.1)}$$

which is ~2 times lower than the experimentally observed one.

A similar level of inconsistency between the theory and experimental results can be found in [43]. In this work the delay was observed in a cell of hot Rubidium atoms under EIT conditions. The experimentally obtained delay characteristics are shown in Figure A1.3.

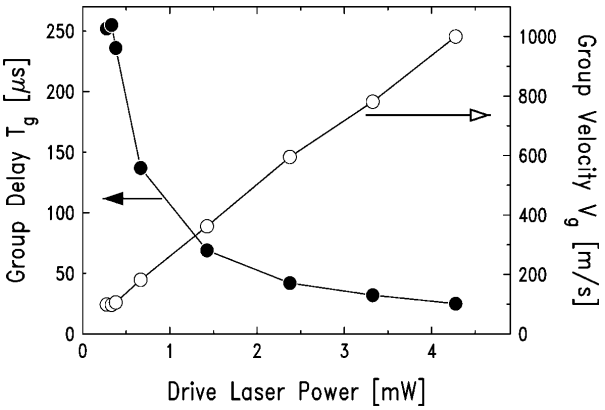

FigureA1.3. Observed group delay (solid circles) and averaged group velocity (open circles) vs the drive laser power [43].

Values of group velocity, v_g, from Figure A1.3 can be directly compared with the theoretical values calculated by the authors. For this purpose one only needs to find the magnitudes of the Rabi frequencies, Ω, corresponding to the drive laser power in Figure A1.3, since theoretical values of v_g are plotted against Rabi frequency. This is easily done knowing laser beam diameter (2 mm) and the relation $\Omega = 2\pi(1\cdot\text{MHz})(I_d)^{1/2}$ (I_d is in mW/cm^2) given in the paper. Figure A1.4 shows the theoretical curve of v_g vs $(\Omega/\gamma_r)^2$ reproduced from [43] together with experimental dependency from Figure A1.3 re-plotted against $(\Omega/\gamma_r)^2$, $\gamma_r = 2\pi(3\text{ MHz})$ as specified in [43].

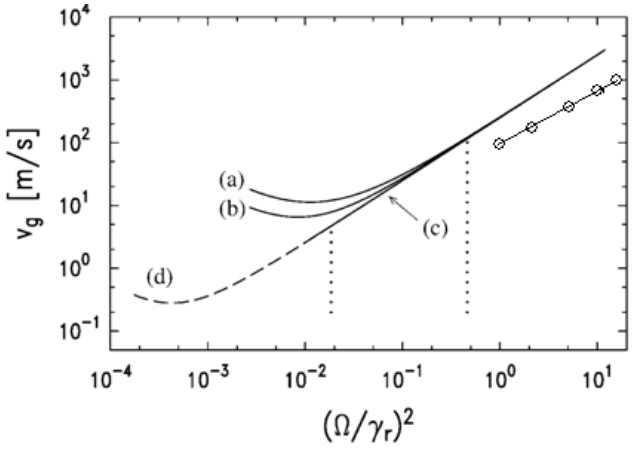

Figure A1.4. Calculated (thicker solid and dashed lines) and the reproduced from Figure A1.3 experimental (open circles and thin solid line) group velocity, v_g, vs drive laser power, which is represented here through the square of the Rabi frequency. Curves (a), (b), and (c) are calculated with Lorentzian, Gaussian, and no Doppler averaging, respectively [43].

The difference between the two is well pronounced. Actually the authors have noted that the experimental data is for the average velocity in the cell: in fact v_g has to be lower toward the output end of the cell because of the reduction of drive laser power due to absorption. According to this note the difference has to increase at lower drive laser powers. However the data in Figure A1.4 shows exactly the opposite effect: the difference is minimal, by a factor ~2.5, at the lowest power and increases to ~4 at the highest power in the experimental range.

Next we consider the work by Kasapi et al [5], who were the first to observe the actual pulse delays via EIT. Figure A1.5 shows delays of a probe optical pulse at λ = 283 nm with a FWHM duration of 12 ns observed in [5] in a 10 cm long cell filled with Pb vapour. The density of atomic vapour, N, was $(1.6\div2)\cdot10^{14}$ cm^{-3} and transmission of the cell in the absence of coupling filed is estimated to be $exp(-6000)$, which corresponds to $\alpha_{max} = 6.10^4$ m^{-1}.

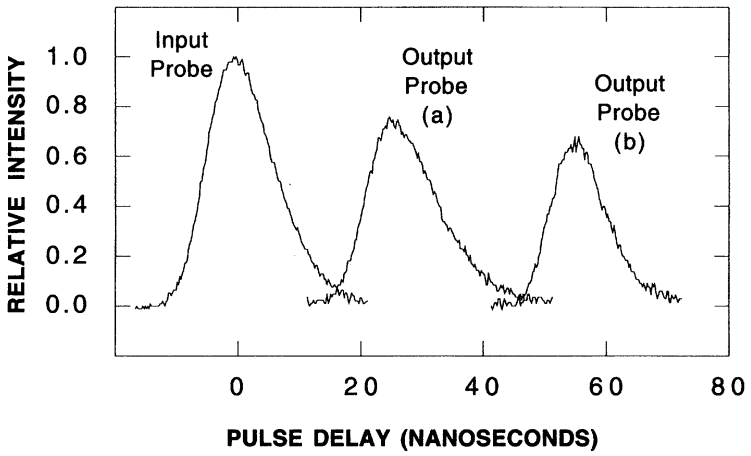

Figure A1.5. Delays (a) and (b) were obtained at different Rabi frequencies, Ω_c, induced by the coupling laser signal, which were 0.19±0.01 cm^{-1} and 0.13±0.02 cm^{-1} respectively. The observed delays are inversely proportional to the square of Rabi frequencies in agreement with the theory [4, 6] . Pulse (b) is delayed for 55 ns, which corresponds to the group velocity c/165, its power and energy transmissions are 65% and 55% respectively, after [5].

If we use equations (2.19 – 21) and the values of n_g = 165 (value for pulse (b) in Figure A1. 5) and corresponding to it Ω_c = 0.13±0.02 cm^{-1} we immediately get M = (1.6±0.25)10^4 rad/s. Using this value of M and the values of $\gamma_{31} = 1.9.10^8$ rad/s and γ_{21} = 10^7 rad/s which are given in [5] we get α_{min} = 5.6±0.5 m^{-1} and α_{max} = (1.2±0.1)10^4 m^{-1} The first of these is reasonably consistent, while the second one is essentially inconsistent with the experimental data presented in [5], which are α_{min} = 4.3 m^{-1} (corresponds to the power transmission of 65%) and $\alpha_{max} = 6.10^4$ m^{-1} respectively (see Table A1.2). It is easy to see that a similar kind of "agreement" between the theory (in brackets) in [4] and the experiment in this work takes place for α_{min} and α_{max} at other Ω_c (0.19±0.01 cm^{-1} and 0.4 cm^{-1} (see Figure A1.6)).

Table A1.2 Values of absorption and group index in [5]: experiment and theory**.**

Ω_c, cm^{-1}	n_g	α_{min}, m^{-1}	α_{max}, x10^4 m^{-1}
0.13±0.02	165	4.3 (5.6±0.5)	6 (1.2±0.1)
0.19±0.01	85	2.9 (2.9)	6 (1.2±0.1)
0.4		2.9 (0.8)	6 (1.5±0.1)

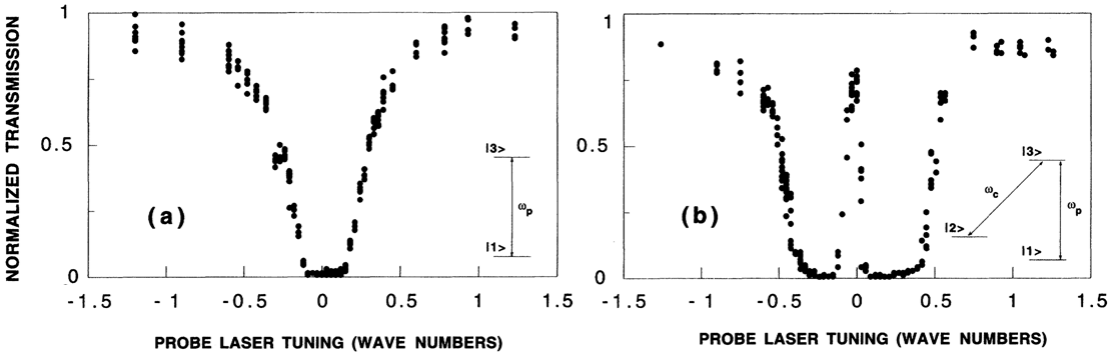

Figure A1.6. Transmission spectra of the vapour cell obtained in [5] at $N = 2\ 10^{14}$ cm^{-3}, $\Omega_c = 0$ (a) and $\Omega_c = 0.4$ cm^{-1}. The FWHM linewidth of the absorption coefficient profile (b), which gives the transmission curve shown on Figure A1.6 (a), is $1.9 \cdot 10^8$ rad/s [5].

Analysis of these papers ([5, 6, 43]) shows that one can find some discrepancies when comparing experimental data with the theory used for it explanation, which leave a doubt in to what extent the observed delays can be attributed solely to the group delay effect.

An example of the experiment where the group delay effect most probably dominates and the agreement between the theory and experiment is good is the work by [58]. In this work the authors made use of the dispersion of refractive index in the frequency range between two 3 GHz-spaced absorbing D_2 resonances in Rubidium 85 vapour. A delay of the 2 ns FWHM duration pulse vs the cell transmission was obtained in a 10 (and 40) cm glass cell with the vapour as shown in Figure A1.7 [58].

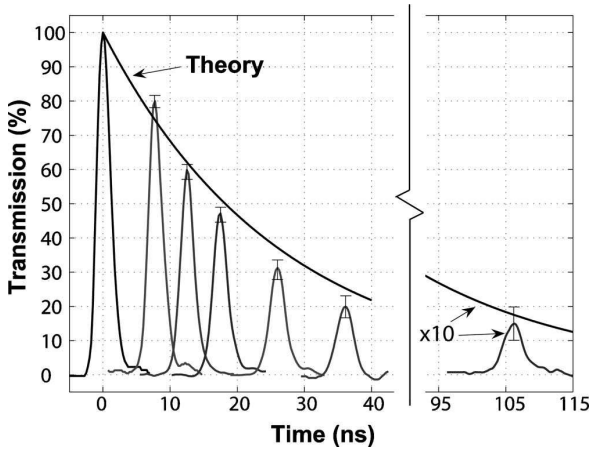

Figure A1.7 Pulse delays observed in [58]**.**

The experimentally measured delay in Figure A1.7 follows the theoretical curve, which, according to [58], is described by the equation

$$t_g = \frac{L}{\upsilon_g} \approx \frac{\alpha_m L}{2\gamma}, \tag{A1.2}$$

where α_m is the absorption coefficient in the center between resonances, L length of the medium and 2γ is FWHM of a resonance. In this experiment the radiation wavelength is detuned from both atomic resonances involved in the interaction, and, because of this, the effect of their saturation is suppressed, and so pulse reshaping does not contribute to overall pulse delay.

By contrast there are a number of works where the interpretation of experimental results in terms of group velocity is really doubtful, for example, the work by Turukhin, [59]. This is one of the first works which reported observation of ultra "slow light" in a solid. In this study the authors claim to exploit the phenomenon of EIT in the 3 mm crystal of Pr:YSO (Pr doped Y_2SiO_5). Figure A1.8 shows the observed pulse delays. The probe pulse has a square shape and pulse duration is 70 μs.

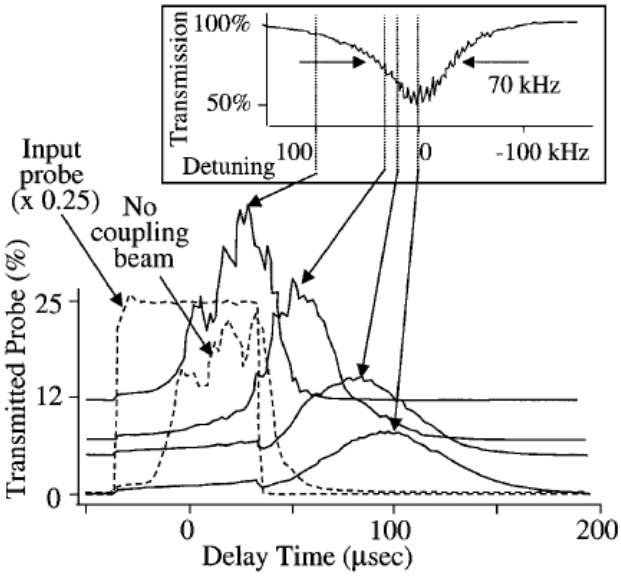

Figure A1.8. Delayed probe pulses at various detuning from the center of the EIT resonance [59].

There are however serious inconsistencies in this figure, which is a primary experimental results of their work, and its interpretation. The transmission spectrum presented corresponds to a normal rather than an inversed absorption resonance. As such the authors should observe an advancement of the probe pulse, i.e. the fast light effect rather than "slow light". Since the authors observe a delay, it is logical to suppose that the position of "100% Transmission" in the insert graph is a misprint. If

we then believe that at zero detuning the delay of the transmitted pulse is due to the group velocity effect then, according to the dispersion curves shown in Figure 2.1, the group velocity must be equal to the phase velocity in the medium at the detuning of ~HWHM from the center of absorption spectrum, and at higher detuning the fast light effect should be observed. As such the results presented are in an obvious contradiction with the basics of the "slow and fast" light phenomenon [4].

Also one can see another inconsistency: the maximal value of transmission for the delayed pulses at different detuning from the resonance shown in Figure A1.8 does not correspond to the value of transmission (absorption) indicated for corresponding detuning. We note that the shape of the transmitted pulse with no coupling beam explicitly shows the effect of the absorption saturation in the sample.

Another example of work which raises severe doubts about the nature of observed delays is the study by Bigellow et al [8]. The authors observed retardation of both Gaussian-shaped and amplitude modulated light pulses in a 7.25-cm-long ruby crystal at room temperature. The delay was attributed to decreased group velocities arising due to rapid spectral variation of the refractive index which was associated with the spectral hole created by the periodic modulation of the ground state population at the beat frequency between the pump and the probe fields applied to the material sample. (This effect is called coherent population oscillations (CPO)).

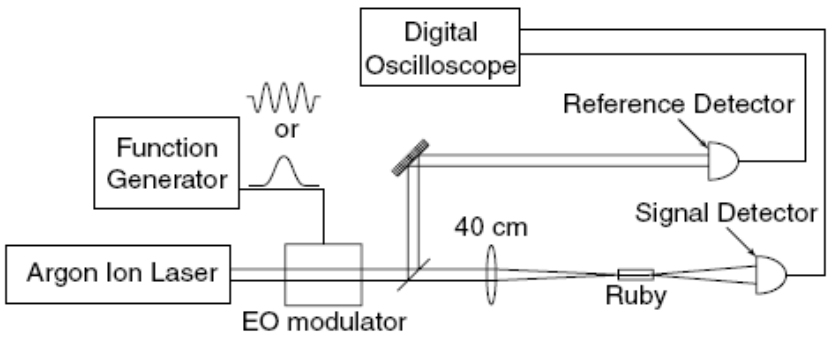

FigureA1.9. Experimental setup used for observation of "slow light" in [8].

The schematic of experimental setup they used is shown on the Figure A1.9. A CW single-line argon-ion laser operating at λ = 515 nm was taken as a pump source. (It is important to note here that conventionally the linewidth of an argon-ion laser emission in the regime of a single-line multimode emission is of several GHz and the narrowest published linewidth in a single-mode regime is ≥ 1 kHz). The EO modulator

driven by a function generator was used to place sinusoidal amplitude modulation on the CW emission or produce long (multi ms) pulses with almost no background intensity. A test beam, together with a reference beam, was detected and the signals were stored at a digital oscilloscope.

The authors claim a measurement of 35.8 Hz HWHM of the induced spectral hole in the absorption spectrum of ruby (see page 3 in [8]). This means that the accuracy of measurement must be at least ~1 Hz. This raises the questions: i) how is such a high precision of measurement achieved with a laser source, the linewidth of which cannot be less than 1 kHz, and ii) how can a laser source, the linewidth of which cannot be less than 1 kHz, create a hole of 35.8 Hz HWHM.

Experimentally observed pulse delays are shown in Figure A1.10. It is not clear why the authors, while interpreting these results, completely ignored the fact that the magnitude of ground state recovery time T_1 = 4.5 ms is comparable to the duration of the delayed pulses. Instead they consider the effect of the intensity dependent absorption coefficient (which is described by their equation (7)) on the characteristics of the delay in the steady state approximation (see their equation (11)). This is definitely incorrect. The case has to be described by the transient theory of a saturating absorption [49, 53].

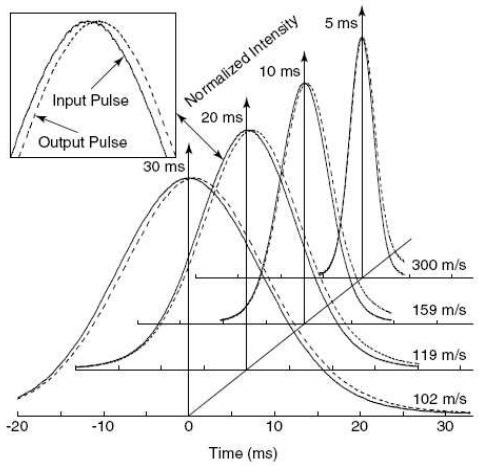

Figure A1.10. Pulse delays for different pulse durations experimentally observed in [8]**.**

An evidence for the fact that the observed delay is due to the transient absorption saturation is actually given in this work by the authors themselves. They note at the bottom of page 3 in [8] "*that it is not necessary to apply separate pump and probe waves to the ruby crystal in order to observe slow light effects. A single intense pulse of*

light is able to provide the saturation required to modify the group index to provide slow light propagation. These relatively intense pulses can be thought of as producing their own pump field and are thus self-delayed."

Actually, the work by [8] and some other studies which reported observation of "slow light" via CPO in a range of different media including alexandrite, bacteriorhodopsin, semiconductor quantum devices and erbium-doped optical fibres were re-examined in detail in recent works [60-62]. A direct quantitative comparison of results on "slow light" obtained via the CPO phenomena with the predictions of the theory of pulse propagation through the saturable absorber was made. It is shown that the results of "slow light" experiments are totally consistent with the latter and that the observed delays arise from time shifts caused by the finite relaxation time of the intensity dependent absorption.

Appendix 2: The procedure of obtaining equation (5.7) in Chapter 5

The dependency of the homogeneous spectral width, Γ_0, on the GeO_2 molar concentration, ρ, mol%, (equation (5.7) in Chapter 5) that we used in the analysis of our experimental results was obtained using data presented in the works of Dragic [113] and Nickles et al [114]. In both papers comprehensive studies of Brillouin gain spectra in doped silica fibres are presented. In particular, in [113] four fibres with ρ ranging from 3.9 to 31 mol % and in [114] eleven fibres were studied with ρ ranging from 2.6 to 17.7 wt %, (from ~1.5 to ~9.4 mol %). The procedure of extracting the dependencies we require was as follows.

Figure A2.1 shows the experimentally obtained in [113] and [114] values of the SBS bandwidth, Γ_{B_ex}, which are recalculated for our working wavelength of 1.06 μm and plotted against ρ in the units of molar %. It can be seen from Figure A2.1 that in the range of small concentrations $0 < \rho < 10$ mol% the experimental data from [113] and [114] coincide with a reasonable accuracy.

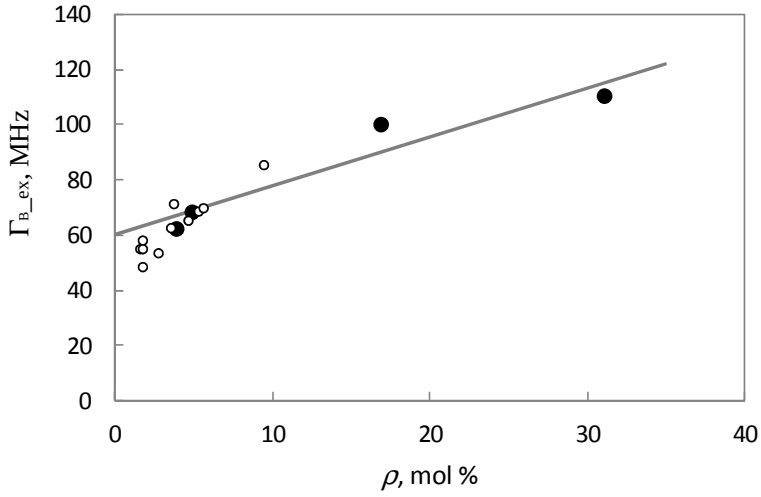

Figure A2.1. Experimentally measured SBS bandwidth (recalculated to λ = 1.06 μm) from [113] (black circles) and [114] (white circles). Solid line represents the linear fit to all data points.

A linear fit to the data shown on Figure A2.1 gives the following dependency of Γ_{B_ex} on ρ,

$$\Gamma_{B\_ex}(\rho) \approx (1.8\rho + 60)\,\text{MHz} \tag{A2.1}$$

where ρ is the concentration of GeO_2 in mol%.

It follows from equation (A2.1) that Γ_{B_ex} for pure silica ($\rho = 0$) is ~60 MHz while it has to be ~35 MHz [111]. Such obvious contradiction has called for more careful analysis of the data presented in [113] and the experimental procedures.

We then found that the experimentally measured SBS bandwidths in [113] inevitably contain contribution from the waveguide induced inhomogeneous broadening (WIIB). If one wish to retrieve the dependence of Γ_0 on ρ, this contribution has to be estimated and extracted from the dependency given by equation (A2.1).

As has been shown in [22, 23] the amount of WIIB is dependent on the *NA* of fibre. The corresponding dependence is given by equation (5.3) in Chapter 5. The data on SBS bandwidths in the tested fibres were accompanied by the data on their *NA* in Dragic's work only. This circumstance allowed us to examine the effect of WIIB in [113] directly. On doing so we found equation (5.3) to give an imaginary value of Γ_0 for NA > 0.17, which is obviously nonsense.

One detail of the experimental setup in [113] shown in Figure A 2.2 allowed us to resolve the problem.

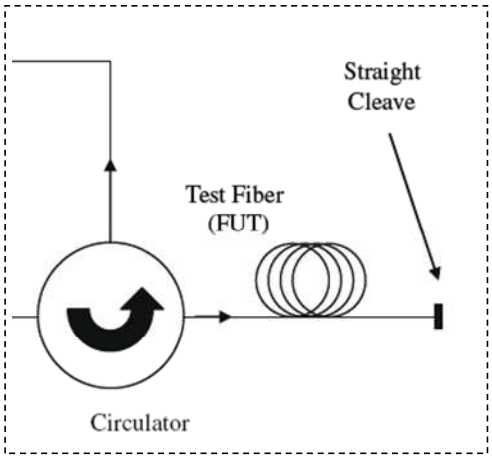

Figure A2.2. Fragment of the experimental setup used in [113].

The fibre under test (FUT) had its output end (with respect to the pump radiation) cleaved perpendicularly to the fibre axis and its input end was connected to the circulator, which was used to launch the pump radiation into the test fibre and to direct the scattered radiation into the detection system. The SBS gain spectra was obtained by optical heterodyne measurements. Spectra of the SBS amplified backscattered Stokes radiation which was seeded by the spontaneous Brillouin scattering were measured. According to [22, 23], these spectra must be inhomogeneously broadened due to the waveguiding effect in FUT. This means that the spectra must comprise the spectral contribution from all the spatial (angle) components allowed by the *NA* of the test fibre. However the circulator used in the setup can only transmit those angle components which are allowed by its own *NA*, which was 0.13 (SMF-28 fibre). Thus in the registered SBS spectrum the contribution of waveguide induced broadening was determined by the broadening allowed by the *NA* of the circulator. According to the equation (5.3) this contribution is $[\Omega_B \cdot NA^2/(2n_{co}^2)] \approx 2\pi 64$ MHz, when $NA = 0.13$, $n_{co} = 1.45$, and $\Omega_B = 2\pi 16$ GHz. Knowing this contribution, using equations (5.3) and (A2.1), and taking into account that the SBS bandwidth in pure silica is 35 MHz we obtained the dependency of Γ_0 on ρ,

$$\Gamma_0(\rho) = (2\rho + 35)\,\text{MHz}, \tag{A2.2}$$

which we use in our studies.

References

[1] T. Krauss, "Why do we need slow light?" *Nature Photonics*, vol. 2, pp. 448-450, 2008.

[2] R. W. Boyd, "Slow light now and then," *Nature Photonics*, vol. 2, pp. 454-455, 2008.

[3] A. E. Willner, B. Zhang, and L. Zhang, "Reconfigurable Signal Processing Using Slow-Light-Based Tunable Optical Delay Lines," in *Slow light, Science and applications*, J. B. Khurgin and R. S. Tucker, Eds.: CPC Press, Taylor and Francis Group, 2009, pp. 312-346.

[4] R. W. Boyd and D. J. Gauthier, ""Slow" and "fast" light," in *Progress in Optics*, E. Wolf, Ed.: Elsevier science B.V., 2002, pp. 497-530.

[5] A. Kasapi, M. Jain, G. Y. Yin, and S. E. Harris, "Electromagnetically Induced Transparency: Propagation Dynamics," *Physical Review Letters*, vol. 74, pp. 2447-2450, 1995.

[6] L. V. Hau, S. E. Harris, Z. Dutton, and C. H. Behroozi, "Light speed reduction to 17 metres per second in an ultracold atomic gas," *Nature*, vol. 397, pp. 594-598, 1999.

[7] D. Budker, D. F. Kimball, S. M. Rochester, and V. V. Yashchuk, "Nonlinear Magneto-optics and Reduced Group Velocity of Light in Atomic Vapor with Slow Ground State Relaxation," *Physical Review Letters*, vol. 83, pp. 1767-1770, 1999.

[8] M. S. Bigelow, N. N. Lepeshkin, and R. W. Boyd, "Observation of Ultraslow Light Propagation in a Ruby Crystal at Room Temperature," *Physical Review Letters*, vol. 90, pp. 113903 2003.

[9] M. S. Bigelow, N. N. Lepeshkin, and R. W. Boyd, "Superluminal and Slow Light Propagation in a Room-Temperature Solid," *Science*, vol. 301, pp. 200-202, 2003.

[10] E. Baldit, K. Bencheikh, P. Monnier, J. A. Levenson, and V. Rouget, "Ultraslow Light Propagation in an Inhomogeneously Broadened Rare-Earth Ion-Doped Crystal," *Physical Review Letters*, vol. 95, pp. 143601 2005.

[11] P. Palinginis, F. Sedgwick, S. Crankshaw, M. Moewe, and C. Chang-Hasnain, "Room temperature slow light in a quantum-well waveguide via coherent population oscillation," *Optics Express*, vol. 13, pp. 9909-9915, 2005.

[12] P. Wu and D. Rao, "Controllable Snail-Paced Light in Biological Bacteriorhodopsin Thin Film," *Physical Review Letters*, vol. 95, pp. 253601, 2005.

[13] A. Schweinsberg, N. N. Lepeshkin, M. S. Bigelow, R. W. Boyd, and S. Jarabo, "Observation of superluminal and slow light propagation in erbium-doped optical fiber," *Europhysics Letters*, vol. 73, pp. 218-224, 2006.

[14] D. J. Gauthier, A. L. Gaeta, and R. W. Boyd, "Slow Light: From Basics to Future Prospects," Photonis Spectra, 2006, pp. on-line article.

[15] S. Chang and S. L. Chuang, "Slow and Fast light in Semiconductors," in *Slow light, Science and applications*, J. B. Khurgin and R. S. Tucker, Eds.: CPC Press, Taylor and Francis Group, 2009, pp. 13-35.

[16] T. Baba, "Slow light in photonic crystals," *Nature Photonics*, vol. 2, pp. 465-473, 2008.

[17] T. F. Krauss, "Slow light in photonic crystal waveguides," *Journal of Physics D: Applied Physics*, vol. 40, pp. 2666-2670, 2007.

[18] T. Krauss, "Slow light in Photonic Crystal Waveguides," in *Slow light, Science and applications*, J. B. Khurgin and R. S. Tucker, Eds.: CPC Press, Taylor and Francis Group, 2009, pp. 59-75.

[19] K. Y. Song, M. Gonzalez Herraez, and L. Thevenaz, "Observation of pulse delaying and advancement in optical fibers using stimulated Brillouin scattering," *Optics Express*, vol. 13, pp. 82-88, 2005.

[20] J. Sharping, Y. Okawachi, and A. Gaeta, "Wide bandwidth slow light using a Raman fiber amplifier," *Optics Express*, vol. 13, pp. 6092-6098, 2005.

[21] J. B. Khurgin, "Slow light in various media: a tutorial," *Advances in Optics and Photonics*, vol. 2, pp. 287-318, 2010.

[22] V. I. Kovalev and R. G. Harrison, "Observation of Inhomogeneous Spectral Broadening of Stimulated Brillouin Scattering in an Optical Fiber," *Physical Review Letters*, vol. 85, pp. 1879-1882, 2000.

[23] V. I. Kovalev and R. Harrison, "Waveguide-induced inhomogeneous spectral broadening of stimulated Brillouin scattering in optical fiber," *Optics Letters*, vol. 27, pp. 2022-2024, 2002.

[24] V. I. Kovalev, R. G. Harrison, J. C. Knight, and N. E. Kotova, "Waveguide induced spectral bandwidth enhancement of slow light group index caused by stimulated Brillouin scattering in optical fiber." ,*Laser and Particle Beams*, vol. 26, pp. 320-323, 2008.

[25] A. A. Michelson, "On the velocity of light in carbon disulphide and the difference in velocity of red and blue light in the same.," *British Association Report*, pp. 654, 1884.

[26] J. D. Jackson, *Classical Electrodynamics*. New York: John Wiley & Sons,Inc, 1962.

[27] J. A. Stratton, *Electromagnetic theory*. New York and London: McGraw-Hill Book Company, 1941.

[28] M. B. Vinogradova, O. V. Rudenko, and A. P. Sukhorukov, *Wave Theory*, 2nd ed. Moscow: Nauka, 1979.

[29] O. Kocharovskaya, Y. Rostovtsev, and M. O. Scully, "Stopping Light via Hot Atoms," *Physical Review Letters*, vol. 86, pp. 628-631, 2001.

[30] L. D. Landau and E. M. Lifshtz, *Electrodynamics of continuous media*, vol. 8. Reading: Addison-Wesley Publishing Company, Inc, 1960.

[31] J. A. Carruthers and T. Bieber, "Pulse Velocity in a Self-Locked He-Ne Laser," *Journal of Applied Physics*, vol. 40, pp. 426-428, 1969.

[32] A. Frova, M. A. Duguay, C. G. B. Garrett, and S. L. McCall, "Pulse Delay Effects in the He-Ne Laser Mode-Locked by a Ne Absorption Cell," *Journal of Applied Physics*, vol. 40, pp. 3969-3972, 1969.

[33] L. Casperson and A. Yariv, "Pulse Propagation in a High-Gain Medium," *Physical Review Letters*, vol. 26, pp. 293-295, 1971.

[34] S. Chu and S. Wong, "Linear Pulse Propagation in an Absorbing Medium," *Physical Review Letters*, vol. 48, pp. 738-741, 1982.

[35] J. B. Khurgin and R. S. Tucker, *Slow light, Science and applications*. Boca Raton: CPC Press, Taylor and Francis Group, 2009.

[36] S. E. Harris, J. E. Field, and A. Imamoglu, "Nonlinear optical processes using electromagnetically induced transparency," *Physical Review Letters*, vol. 64, pp. 1107-1110, 1990.

[37] S. L. McCall and E. L. Hahn, "Self-Induced Transparency by Pulsed Coherent Light," *Physical Review Letters*, vol. 18, pp. 908-911, 1967.

[38] S. E. Harris, J. E. Field, and A. Kasapi, "Dispersive properties of electromagnetically induced transparency," *Physical Review A*, vol. 46, pp. R29, 1992.

[39] M. O. Scully, "Enhancement of the index of refraction via quantum coherence," *Physical Review Letters*, vol. 67, pp. 1855-1858, 1991.

[40] S. P. Tewari and G. S. Agarwal, "Control of Phase Matching and Nonlinear Generation in Dense Media by Resonant Fields," *Physical Review Letters*, vol. 56, pp. 1811-1814, 1986.

[41] M. Xiao, Y.-q. Li, S.-z. Jin, and J. Gea-Banacloche, "Measurement of Dispersive Properties of Electromagnetically Induced Transparency in Rubidium Atoms," *Physical Review Letters*, vol. 74, pp. 666-669, 1995.

[42] R. M. Camacho and J. C. Howell, "Slow ligth in atomic Vapors," in *Slow light, Science and applications*, J. B. Khurgin and R. S. Tucker, Eds.: CPC Press, Taylor and Francis Group, 2009, pp. 3-12.

[43] M. M. Kash, V. A. Sautenkov, A. S. Zibrov, L. Hollberg, G. R. Welch, M. D. Lukin, Y. Rostovtsev, E. S. Fry, and M. O. Scully, "Ultraslow Group Velocity and Enhanced Nonlinear Optical Effects in a Coherently Driven Hot Atomic Gas," *Physical Review Letters*, vol. 82, pp. 5229-5232, 1999.

[44] P. Kafalas, J. I. Masters, and E. M. E. Murray, "Photosensitive Liquid used as a Nondestructive Passive Q-Switch in a Ruby Laser," *Journal of Applied Physics*, vol. 35, pp. 2349-2350, 1964.

[45] P. P. Sorokin, J. J. Luzzi, J. R. Lankard, and G. D. Pettit, "Ruby Laser Q-Switching Elements Using Phthalocyanine Molecules in Solution," *IBM Journal of Research and Development*, vol. 8, pp. 182-184, 1964.

[46] A. J. DeMaria, D. A. Stetser, and H. Heynau, "Self mode-locking of lasers with saturable absorbers," vol. 8, pp. 174-176, 1966.

[47] O. R. Wood and S. E. Schwarz, "Passive mode locking of a CO2 laser," *Applied Physics Letters*, vol. 12, pp. 263-265, 1968.

[48] D. A. B. Miller, R. G. Harrison, A. M. Johnston, C. T. Seaton, and S. D. Smith, "Degenerate four-wave mixing in InSb at 5K," *Optics Communications*, vol. 32, pp. 478-480, 1980.

[49] L. M. Frantz and J. S. Nodvik, "Theory of Pulse Propagation in a Laser Amplifier," *Journal of Applied Physics*, vol. 34, pp. 2346-2349, 1963.

[50] N. G. Basov, R. V. Ambartsumyan, V. S. Zuev, P. G. Kryukov, and V. S. Letokhov, "Propagation velocity of an intense light pulse in a medium with inverted population," *Sov. Phys. Doklady*, vol. 10, pp. 1039-1040, 1966.

[51] F. Gires and F. Combaud, "Saturation de l'absorption optique de certaines solutions de phtalocyanines," *J. Phys. France*, vol. 26, pp. 325-330, 1965.

[52] V. I. Kovalev, Ruskin, and Suvorov, "Nonlinear absorption of randomly pulsating CO 2 laser radiation in narrow-gap semiconductors," *Soviet Journal of Quantum Electronics*, vol. 21, pp. 1346-1348, 1991.

[53] A. C. Selden, "Pulse transmission through a saturable absorber," *British Journal of Applied Physics*, vol. 18, pp. 743-748, 1967.

[54] A. C. Selden, "Analysis of the saturable absorber transmission equation," *Journal of Physics D: Applied Physics*, vol. 3, pp. 1935-1943, 1970.

[55] A. C. Selden, "Nonlinear transmission of an optical signal," *Electronics Letters*, vol. 7, pp. 287-288, 1971.

[56] V. I. Kovalev, "Maximum attainable efficiency of a cubic nonlinear response of matter," *Quantum Electronics*, vol. 27, pp. 732-734, 1997.

[57] S. E. Harris and L. V. Hau, "Nonlinear Optics at Low Light Levels," *Physical Review Letters*, vol. 82, pp. 4611-4614, 1999.

[58] R. M. Camacho, M. V. Pack, and J. C. Howell, "Low-distortion slow light using two absorption resonances," *Physical Review A*, vol. 73, pp. 063812 (1-4), 2006.

[59] A. V. Turukhin, V. S. Sudarshanam, M. S. Shahriar, J. A. Musser, B. S. Ham, and P. R. Hemmer, "Observation of Ultraslow and Stored Light Pulses in a Solid," *Physical Review Letters*, vol. 88, pp. 023602 (1-4), 2001.

[60] A. C. Selden, "Slow light and saturable absorption," *Optics and Spectroscopy*, vol. 106, pp. 881-888, 2009.

[61] V. Zapasskii and G. Kozlov, "A saturable absorber, coherent population oscillations, and slow light," *Optics and Spectroscopy*, vol. 100, pp. 419-424, 2006.

[62] V. S. Zapasskii and G. G. Kozlov, "On two models of light pulse delay in saturable absorber," *Optics and Spectroscopy*, vol. 109, pp. 407-412, 2010.

[63] D. Gauthier, *Physics and Applications of "Slow" Light," 2nd Annual Summer School, Fitzpatrick Center for Photonics and Communication Systems*. Duke University, Durham, NC,July 27, 2004.

[64] Y. Okawachi, M. S. Bigelow, J. E. Sharping, Z. Zhu, A. Schweinsberg, D. J. Gauthier, R. W. Boyd, and A. L. Gaeta, "Tunable All-Optical Delays via Brillouin Slow Light in an Optical Fiber," *Physical Review Letters*, vol. 94, pp. 153902 (1-4), 2005.

[65] B. Y. Zeldovich, "Time of establishment of stationary regime of stimulated light scattering," *Journal of Experimental and Theoretical Physics Letters*, vol. 15, pp. 158-159, 1972.

[66] R. Y. Chiao, C. H. Townes, and B. P. Stoicheff, "Stimulated Brillouin Scattering and Coherent Generation of Intense Hypersonic Waves," *Physical Review Letters*, vol. 12, pp. 592-595, 1964.

[67] Y. R. Shen and N. Bloembergen, "Theory of Stimulated Brillouin and Raman Scattering," *Physical Review*, vol. 137, pp. A1787–A1805, 1965.

[68] B. Y. Zeldovich, N. F. Pilipetsky, and V. V. Shkunov, *Principles of Phase Conjugation*, vol. 42. Berlin: Springer-Verlag Berlin Heidelberg, 1985.

[69] R. W. Boyd, "Stimulated Brillouin and Stimulated Rayleigh Scattering," in *Nonlinear Optics*, R. W. Boyd, Ed., Second ed, 2003.

[70] Z. Zhu, Daniel J. Gauthier, Y. Okawachi, Jay E. Sharping, Alexander L. Gaeta, Robert W. Boyd, and Alan E. Willner, "Numerical study of all-optical slow-light delays via stimulated Brillouin scattering in an optical fiber," *Journal of Optical Society of America B*, vol. 22, pp. 2378-2384, 2005.

[71] L. Thevenaz, "Slow and fast light in optical fibres," *Nature Photonics*, vol. 2, pp. 474-481, 2008.

[72] G. P. Agrawal, *Nonlinear fiber optics*. London: Academic Press, Inc, 1989.

[73] R. D. L. Kronig, "On the theory of dispersion of X-rays," *Journal of Optical Society of America*, vol. 12, pp. 547-556, 1926.

[74] M. Gonzalez-Herraez, K. Y. Song, and L. Thevenaz, "Arbitrary-bandwidth Brillouin slow light in optical fibers," *Optics Express*, vol. 14, pp. 1395-1400, 2006.

[75] M. Gonzalez-Herraez, K. Y. Song, and L. Thevenaz, "Optically controlled slow and fast light in optical fibers using stimulated Brillouin scattering," *Applied Physics Letters*, vol. 87, pp. 081113, 2005.

[76] A. Minardo, R. Bernini, and L. Zeni, "Low distortion Brillouin slow light in optical fibers using AM modulation," *Optics Express*, vol. 14, pp. 5866-5876, 2006.

[77] T. Schneider, M. Junker, and K.-U. Lauterbach, "Potential ultra wide slow-light bandwidthenhancement," *Optics Express*, vol. 14, pp. 11082-11087, 2006.

[78] T. Schneider, M. Junker, K. U. Lauterbach, and R. Henker, "Distortion reduction in cascaded slow light delays," *Electronics Letters*, vol. 42, pp. 1110-1111, 2006.

[79] K. Y. Song, K. S. Abedin, K. Hotate, M. González Herráez, and L. Thévenaz, "Highly efficient Brillouin slow and fast light using As2Se3 chalcogenide fiber," *Optics Express*, vol. 14, pp. 5860-5865, 2006.

[80] K. Y. Song, M. Gonzalez-Herraez, and L. Thevenaz, "Long optically controlled delays in optical fibers," *Optics Letters*, vol. 30, pp. 1782-1784, 2005.

[81] K. Y. Song and K. Hotate, "25 GHz bandwidth Brillouin slow light in optical fibers," *Optics Letters*, vol. 32, pp. 217-219, 2007.

[82] Z. Zhu, A. M. C. Dawes, D. J. Gauthier, L. Zhang, and A. E. Willner, "Broadband SBS Slow Light in an Optical Fiber," *Journal of Lightwave Technology*, vol. 25, pp. 201-206, 2007.

[83] Z. M. Zhu and D. J. Gauthier, "Nearly transparent SBS slow light in an optical fiber," *Optics Express*, vol. 14, pp. 7238-7245, 2006.

[84] N. Yoshizawa and T. Imai, "Stimulated Brillouin scattering suppression by means of applying strain distribution to fiber with cabling," *Journal of Lightwave Technology*, vol. 11, pp. 1518-1522, 1993.

[85] V. I. Kovalev, R. G. Harrison, J. C. Knight, and N. E. Kotova, "Slow light in optical fiber using stimulated Brillouin scattering," *Procedings of SPIE*, vol. 7024, pp. 702415 2008.

[86] J. C. Knight, J. Arriaga, T. A. Birks, A. Ortigosa-Blanch, W. J. Wadsworth, and P. S. J. Russell, "Anomalous dispersion in photonic crystal fiber," *Photonics Technology Letters, IEEE*, vol. 12, pp. 807-809, 2000.

[87] V. I. Kovalev and R. G. Harrison, "Temporally stable continuous-wave phase conjugation by stimulated Brillouin scattering in optical fiber with cavity feedback," *Optics Letters*, vol. 30, pp. 1375-1377, 2005.

[88] S. Chin, M. Gonzalez-Herraez, and L. Thevenaz, "Zero-gain slow & fast light propagation in an optical fiber," *Optics Express*, vol. 14, pp. 10684-10692, 2006.

[89] K. Y. Song, M. Gonzalez Herraez, and L. Thevenaz, "Gain-assisted pulse advancement using single and double Brillouin gain peaks in optical fibers," *Opt. Express*, vol. 13, pp. 9758-9765, 2005.

[90] M. D. Stenner, "Distortion management in slow-light pulse delay," *Optics Express*, vol. 13, pp. 9995-10002, 2005.

[91] V. S. Starunov and I. L. Fabelinskiy, "Stimulated Mandel'shtamâ-Brillouin scattering and stimulated entropy (temperature) scattering of light," *Soviet Physics Uspekhi*, vol. 12, pp. 463, 1970.

[92] R. G. Smith, "Optical Power Handling Capacity of Low Loss Optical Fibers as Determined by Stimulated Raman and Brillouin Scattering," *Applied Optics*, vol. 11, pp. 2489-2494, 1972.

[93] T. Schneider, R. Henker, K.-U. Lauterbach, and M. Junker, "Distortion reduction in Slow Light systems based on stimulated Brillouin scattering," *Optics Express*, vol. 16, pp. 8280-8285, 2008.

[94] Z. Shi, R. Pant, Z. Zhu, M. D. Stenner, M. A. Neifeld, D. J. Gauthier, and R. W. Boyd, "Design of a tunable time-delay element using multiple gain lines for increased fractional delay with high data fidelity," *Optics Letters*, vol. 32, pp. 1986-1988, 2007.

[95] L. Yi, Y. Jaouen, W. Hu, y. Su, and S. Bigo, "Improved slow-light performance of 10 Gb/sNRZ, PSBT and DPSK signals in fiberbroadband SBS," *Optics Express*, vol. 15, pp. 16972-16979, 2007.

[96] L. Yi, Y. Jaouën, W. Hu, J. Zhou, Y. Su, and E. Pincemin, "Simultaneous demodulation and slow light of differential phase-shift keying signals using stimulated-Brillouin-scattering-based optical filtering in fiber," *Optics Letters*, vol. 32, pp. 3182-3184, 2007.

[97] C. Yu, T. Luo, L. Zhang, and A. E. Willner, "Data pulse distortion induced by a slow-light tunable delay line in optical fiber," *Optics Letters*, vol. 32, pp. 20-22, 2007.

[98] B. Zhang, L. Yan, I. Fazal, L. Zhang, A. E. Willner, Z. Zhu, and D. J. Gauthier, "Slow light on Gbit/s differential-phase-shift-keying signals," *Optics Express*, vol. 15, pp. 1878-1883, 2007.

[99] A. A. Kharkevich, *Spectra and Analysis (in Russian)*, Fourth ed. Moscow: State publishing house of Physics and Mathematics literature, 1962.

[100] G. A. Korn and T. M. Korn, *Manual of mathematics*. New York: McGraw-Hill, 1967.

[101] I. N. Bronshtein and K. A. Semendyayev, *A guide book to mathematics* Zurich: Verlag Harri Deutsch, 1973.

[102] H. Goldstein, *Classical Mechanics*. Reading: Addison -Wesley Publishing Company, Inc, 1969.

[103] M. Born and E. Wolf, *Principles of Optics*. Oxford: Pergamon Press, 1964.

[104] S. A. Akhmanov, K. N. Drabovich, A. P. Sukhorukov, and A. S. Chirkin, "Stimulated Raman scattering in a field of ultrashort light pulses," *Soviet Physics Journal of Experimental and Theoreical Physics*, vol. 32, pp. 266–273, 1971.

[105] R. L. Carman, F. Shimizu, C. S. Wang, and N. Bloembergen, "Theory of Stokes Pulse Shapes in Transient Stimulated Raman Scattering," *Physical Review A*, vol. 2, pp. 60-72, 1970.

[106] N. Kroll, "Excitation of Hypersonic Vibrations by Means of Photoelastic Coupling of High-Intensity Light Waves to Elastic Waves," *Journal of Applied Physics*, vol. 36, pp. 34-43, 1965.

[107] I. M. Bel'dyugin, V. F. Efimkov, S. I. Mikhailov, and I. G. Zubarev, "Amplification of weak Stokes signals in the transient regime of stimulated Brillouin scattering," *Journal of Russian Laser Research*, vol. 26, pp. 1-12, 2005.

[108] C. Tang, "Saturation and Spectral Characteristics of the Stokes Emission in the Stimulated Brillouin Process," *J. Appl. Phys.*, vol. 37, pp. 2945-2955, 1966.

[109] D. Pohl and W. Kaiser, "Time-Resolved Investigations of Stimulated Brillouin Scattering in Transparent and Absorbing Media: Determination of Phonon Lifetimes," *Physical Review B*, vol. 1, pp. 31-43, 1970.

[110] V. I. Kovalev and R. G. Harrison, "Threshold for stimulated Brillouin scattering in optical fiber," *Optics Express*, vol. 15, pp. 17625-17630, 2007.

[111] D. A. Pinnow, "Guide lines for the selection of acoustooptic materials," *IEEE Journal of Quantum Electronics*, vol. 6, pp. 223-238, 1970.

[112] V. P. Kalosha, L. Chen, and X. Bao, "Slow and fast light via SBS in optical fibers for short pulses and broadbandpump," *Optics Express*, vol. 14, pp. 12693-12703, 2006.

[113] P. D. Dragic, "Brillouin spectroscopy of Nd-Ge co-doped silica fibers," *Journal of Non-Crystalline Solids*, vol. 355, pp. 403-413, 2009.

[114] M. Nikles, L. Thevenaz, and P. A. Robert, "Brillouin gain spectrum characterization in single-mode optical fibers," *Journal of Lightwave Technology, ,* vol. 15, pp. 1842-1851, 1997.

[115] "Fibres and cables, optical, aircraft use -Test methods.,", British Standard vol. BS EN 3745-302:2002, 2002.

[116] P. M. Ripley, "Deterministic Dynamics of stimulated Brillouin Scattering in Optical fibres," in *Physics Department*, vol. PhD. Edinburgh: Heriot-Watt, 1995.

[117] B. S. Kawasaki, D. C. Johnson, Y. Fujii, and K. O. Hill, "Bandwidth-limited operation of a mode-locked Brillouin parametric oscillator," *Applied Physics Letters*, vol. 32, pp. 429-431, 1978.

[118] V. I. Kovalev and R. G. Harrison, "The dynamics of a SBS fibre laser: the nature of periodic spiking at harmonics of the fundamental oscillation frequency," *Optics Communications*, vol. 204, pp. 349-354, 2002.

[119] R. G. Harrison, J. S. Uppal, A. Johnstone, and J. V. Moloney, "Evidence of chaotic stimulated Brillouin scattering in optical fibers," *Physical Review Letters*, vol. 65, pp. 167-170, 1990.

[120] R. G. Harrison, D. Yu, W. Lu, and P. M. Ripley, "Chaotic stimulated Brillouin scattering: theory and experiment," *Physica D: Nonlinear Phenomena*, vol. 86, pp. 182-188, 1995.

[121] V. I. Kovalev and R. G. Harrison, "Means for easy and accurate measurement of the stimulated Brillouin scattering gain coefficient in optical fiber," *Optics Letters*, vol. 33, pp. 2434-2436, 2008.

[122] V. I. Kovalev and R. G. Harrison, "Abnormally low threshold gain of stimulated Brillouin scattering in long optical fiber with feedback," *Optics Express*, vol. 16, pp. 12272-12277, 2008.

[123] L. Kirkup, *Experimental methods: an introduction to the analysis and presentation of data*. Milton: Jacaranda Wiley, LTD, 1994.

[124] E. B. Aleksandrov and V. S. Zapasskii, "Chasing 'slow light'," *Physics-Uspekhi*, vol. 49, pp. 1067, 2006.